



Department of Geosciences

Connecting the late Neoproterozoic flysch sedimentation in the Gariep Belt (Namibia) with its potential source region in southern Dom Feliciano Belt (Uruguay) – a U-Pb detrital and protolith zircon study.

-
Ina Nordbø Gilberg

Master's thesis in geology, GEO-3900, May 2020





UiT The Arctic University of Norway

UiT The Arctic University of Norway

Faculty of Science and Technology

Department of Geosciences

GEO-3900

Master thesis in Hard Rock Geology

Connecting the late Neoproterozoic flysch sedimentation in the Gariep Belt (Namibia) with its potential source region in southern Dom Feliciano Belt (Uruguay) – a U-Pb detrital and protolith zircon study.

Submitted by: Ina Nordbø Gilberg

Primary supervisor: Prof. Jiří Konopásek

Co-supervisor: Prof. Maria de Fátima Bitencourt

Acknowledgements

This work was supported by the Norwegian Centre for International Cooperation in Education (SIU), the Norwegian Agency for International Cooperation and Quality Enhancement in Higher Education (Diku), and the Coordenação de Aperfeiçoamento de Pessoal de Nível Superior (CAPES) in Brazil through the grant projects no. UTF-2016-CAPES-SIU10024 and UTF-2018-CAPES-Diku-10004.

First, I would like to thank my supervisor Jiří Konopásek for excellent guidance, support and the occasional push needed to finish this thesis. Your help has been essential during this journey, I appreciate the opportunity of working with something I find interesting, and the opportunity of learning more on geochronology. I would also like to thank Jack Percival for your help in learning the procedures in the laboratories, and for always being available for any questions I might have,

To Maria de Fátima Bitencourt, Pedro Oyhantçabal, Jack Percival, Matheus Battisti and others, thank you for making the field trip to Uruguay such an amazing trip. I learned so much about South American geology. But also got to learn about a new culture, and the appreciation of mate.

I would also like to thank Jiří Sláma for his help with the LA-ICP-MS and CL imaging of my samples. You and your colleagues gave me a warm welcoming to Prague, and I enjoyed getting to see another professional research institute. To all the people working in the geological lab at UiT, but especially Trine Merete Dahl, thank you for the help given to me during the mount preparation.

A big thank you to my family and friends for your support and love while I followed my dream. It has been 10 difficult years, and nobody thought I would finish my bachelor's degree, even less a master's degree. Even though it is not a common group to give thanks to, my medical team have been a big reason I am where I am today, so you have my gratitude.

Lastly my co-students at the Department of Geosciences, thank you for 2 years filled with fun, heated discussions on geology, life and everything else. When I needed a break, or a second

opinion, there was always somebody to take a break with. And when I needed a break from geology, I had my co-students and teacher in my Latin course. Thank you for interesting conversations and a lot of laughs.

Tromsø, May 2020

Ina Gilberg

Abstract

The Dom Feliciano Belt in Uruguay represents a counterpart of the Gariep Belt in Namibia and these two belts are presently considered as relics of one orogen split by the Atlantic Ocean. In this study, two presumed flysch samples from the Marmora Terrane of the Gariep Belt in Namibia, and five samples from potential source areas in the Nico Perez Terrane of the Dom Feliciano Belt in Uruguay have been dated to determine the possible source regions for the flysch sedimentation on the Namibian side of the orogenic system.

Two granites from the Nico Perez Terrane show Neoproterozoic ages of c. 614 Ma, interpreted as the crystallization ages. These data are compatible with the magmatic activity found in the Dom Feliciano Belt from 634 – 564 Ma. A metavolcanic sample from the Zanja del Tigre Complex presents crystallization age of 1.45 Ga. One of the metasedimentary samples from the Nico Perez Terrane shows zircon ages with dominant Mesoproterozoic peak at ca. 1.45 Ga interpreted as an age of volcanic admixture, and minor amount of Paleoproterozoic and Archean zircon. interpreted as detrital grains. Another sample of metasedimentary rock shows only Paleoproterozoic to Archean zircon ages. The detrital zircon population is interpreted as a result of erosion of the surrounding geological units.

Two presumed samples of metamorphosed flysch sediments from the Marmora Terrane present very different detrital zircon age spectra. One of the samples shows mainly Meso- and Paleoproterozoic ages, with individual Archean ages. This sample is interpreted as possibly connected with sedimentation in the rifting stage of the orogenic cycle. The second sample has a detrital zircon age spectrum that is consistent with syn-orogenic nature of flysch sedimentation, and shows several peaks at c. 650 Ma, 750 Ma, 1.0 Ga and 1.85 Ga.

When comparing the zircon signature in the flysch sample with protolith ages found in the surrounding geological units (the Nico Perez Terrane, The Punta del Este Terrane, South-African sources and the Rio de la Plata Craton), it becomes clear that the flysch sediment is a result of erosion of the Punta del Este Terrane basement, which contains the only nearby source of the c. 650 Ma zircons, the c. 800-750 Ma zircons and inherited zircons dated at 1.2 – 1.0 Ga. The sample also shows the same detrital zircon pattern found by other workers in their studies of flysch sediments in the Dom Feliciano – Gariep Belt.

Contents

Acknowledgements	II
Abstract.....	IV
1 Introduction	1
1.1 Geological setting.....	2
1.1.1 The Dom Feliciano Belt (DFB)	4
1.1.2 1.2.4 The Gariep Belt (Africa).....	7
1.2 Flysch sediments on the African side of the Dom Feliciano-Kaoko-Gariep orogenic system	11
2 Methods.....	14
2.1 U-Pb dating	14
2.2 Field work.....	17
2.2.1 Samples Uruguay	17
2.2.2 Samples Namibia	18
2.3 Laboratory work.....	18
2.3.1 Mineral separation.....	18
2.3.2 Mount preparation	18
2.3.3 Cathodoluminescence (CL-imaging)	19
2.3.4 Dating; laser ablation (LA-ICP-MS)	19
2.4 Data processing	19
3 Results.....	21
3.1 Field work.....	21
3.2 Laboratory.....	22
3.3 Samples from Uruguay.....	24
3.3.1 Sample UF 12b.....	24

3.3.2	Sample LA 227	26
3.3.3	Sample UF 30	28
3.3.4	Sample UF 22	31
3.3.5	UF 24.....	35
3.4	Samples from Namibia	39
3.4.1	Sample NS 32	39
3.4.2	Sample NS 44	41
4	Discussion	44
4.1	Potential source areas	44
4.1.1	Cerro Olivo as potential source region for the flysch sedimentation in the Gariep Belt	44
4.1.2	Nico Perez Terrane as potential source region for the flysch sedimentation in the Gariep Belt.	45
4.1.3	Piedra Alta Terrane as potential source region	46
4.1.4	New Data	46
4.1.5	The African foreland units as a potential source.....	47
4.1.6	Potential source units for metasedimentary samples of the Zanja del Tigre Complex	48
4.1.7	Interpretation of origin of the presumed flysch samples	49
5	Conclucions	53
6	References	55
7	Appendix A	1

1 Introduction

The reconstruction of Rodinia and later on Gondwana is heavily discussed through many years (Basei et al., 2008; Bogdanova et al., 2009; Abre et al., 2020; Konopásek et al., 2020). Different approaches have been used to put their crustal units together; from correlation of pre-orogenic basement units (Oriolo et al., 2017), to the usage of paleomagnetic poles (Li et al., 2008) and, geochronological and isotopic data (Basei et al., 2005; Becker et al., 2006; Konopásek et al., 2017a) among other disciplines. To reconstruct Rodinia and Gondwana requires a multidisciplinary approach, and the ability to put together research from different disciplines. The two key areas of this study are the Dom Feliciano Belt (Figure 5) and the Gariep Belt (Figure 8), both of which are part of a larger collection of Neoproterozoic mobile belts originating during the Brasiliano-Pan African orogenic cycle leading to the assembly of Southwest Gondwana (Basei et al., 2008; Hueck et al., 2018).

Konopásek et al. (2017a) recognized a widespread syn-orogenic (flysch) sedimentation on the African side of the orogenic system, i.e. rocks representing a sequence of sediments from deep- to shallow-water, often clastic in nature, deposited in a rapidly forming basin in the foreland of a rising orogen. By analyzing two presumed flysch sediment samples from the Marmora Terrane in the Gariep Belt, Namibia, this thesis tries to correlate their detrital zircon record with proposed source areas in Uruguay. More specifically, the aim of this study is to compare the ages of detrital zircon of the flysch sediments with both known and newly obtained zircon protolith ages of rocks from two potential source areas in the southern Dom Feliciano Belt - the Nico Perez Terrane and the Punta del Este Terrane. The samples from the key areas were processed at UiT, detrital and protolith zircons were extracted and dated by the Laser Ablation-Inductively Coupled Plasma-Mass Spectrometry (LA-ICP-MS) method.

The ages of detrital zircon from the presumed flysch sediment samples were compared with the results published by Konopásek et al. (2017a). One of the samples provided zircon ages comparable with erosion of the developing Neoproterozoic orogenic front, and these ages were compared with possible source regions represented by the Nico Perez and Punta del Este terranes in the southern Dom Feliciano Belt. The detrital zircon age spectra of the other sample suggest pre-orogenic origin of the rock comparable with erosion of the Namaqua sector and the Congo/Kalahari cratonic basement.

1.1 Geological setting

Pre-collisional evolution of the eastern Nico Perez Terrane (Dom Feliciano Belt) in eastern Uruguay

The supercontinent of Rodinia was assembled during the Mesoproterozoic and early Proterozoic eras (Li et al., 2008). Through several orogenic events, all known crustal blocks were assembled in one supercontinent, with Laurentia forming the core (Bogdanova et al., 2009). The break-up of this supercontinent led to the assembly of Gondwanaland (Li et al., 2008). The placement of the crustal blocks around Laurentia, that is important

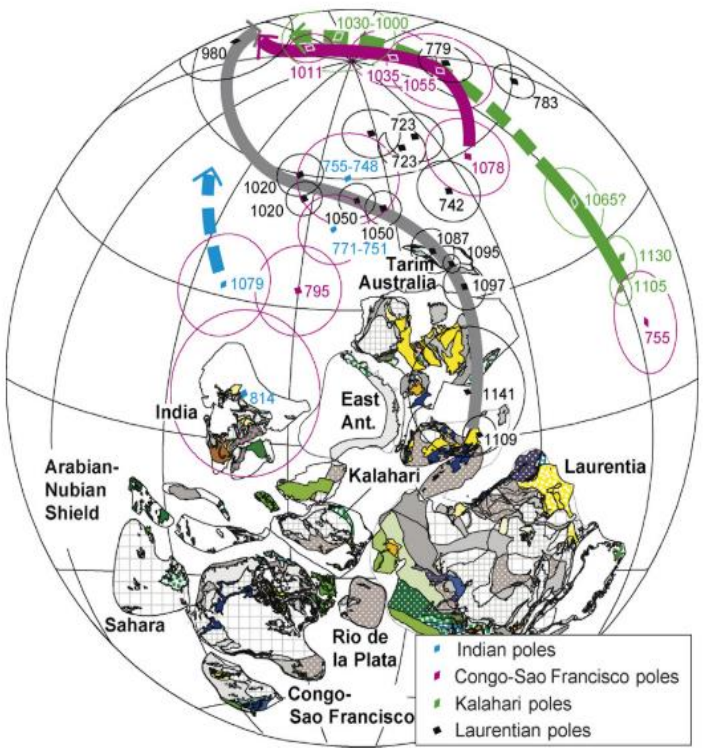


Figure 1: Simplified map of Rodinia with the paleomagnetic poles and positions of the Indian, Kalahari, Rio de la Plata and Congo cratons (Li et al., 2008)

for this thesis, differs from author to author (Li et al., 2008). Some researchers suggest that Rio de la Plata, Kalahari and Congo-São Francisco cratons were not part of Rodinia at all (Oriolo et al., 2017). Others like (Evans et al., 2016) include all blocks in Rodinia. Figure 1 shows Li et al. (2008) placement of Rio de la Plata, Congo – São Francisco and Kalahari in Rodinia. Paleomagnetic data for Congo – São Francisco show that it did not join Laurentia until c. 1010 Ma.

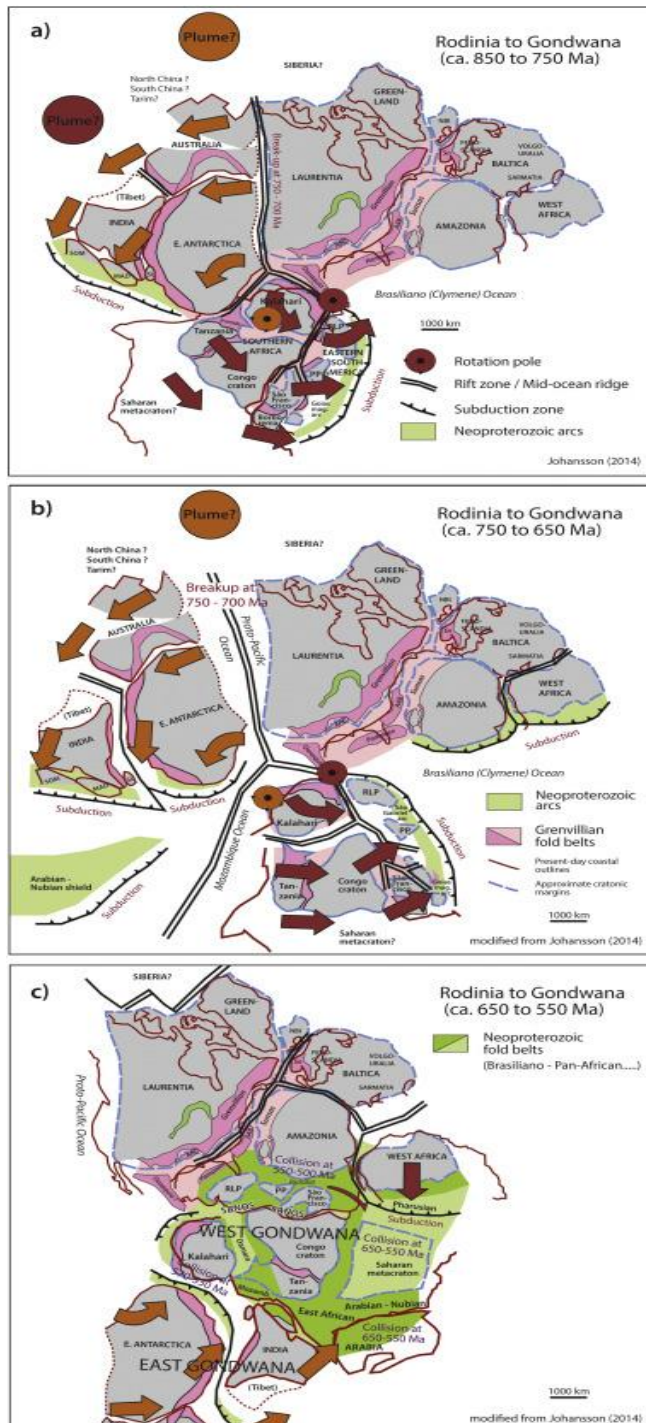


Figure 2: Map showing the transition from Rodinia to Gondwana. (Konopásek et al., 2020)

(Konopásek et al., 2017a; Konopásek et al., 2020) suggests that the Adamastor ocean was only a narrow ocean (max. 400 – 600 km wide with a spreading rate of 4cm/y) between the two cratons.

During rifting between 800 – 700 Ma (Figure 2), Rodinia started to fragment into smaller continental terranes (Li et al., 2008). The rifting between the Congo craton and the Kalahari and the Rio de La Plata craton can be seen in syn-tectonic rift related volcanism. Similar ages have been found on both sides of the Atlantic Ocean in Punta Del Este-Costal Terrane. On the African side Frimmel et al. (2001) Konopásek et al. (2014) and Konopásek et al. (2017b) have dated the rift-related volcanic rocks to 840-710 Ma. Similar ages were found by Oyhantçabal et al. (2009) and Lenz et al. (2011) in Uruguay and Brazil of South America. When Rodinia was breaking-up, the Adamastor rift between the Rio de la Plata and the Congo craton developed. From the late 60's a theory where the Adamastor rift evolved into a wide ocean has been widely accepted. Porada (1979) named the hypothetical ocean the proto-south Atlantic Ocean, while Hartnady (1985) proposed the name Adamastor ocean. Newer research

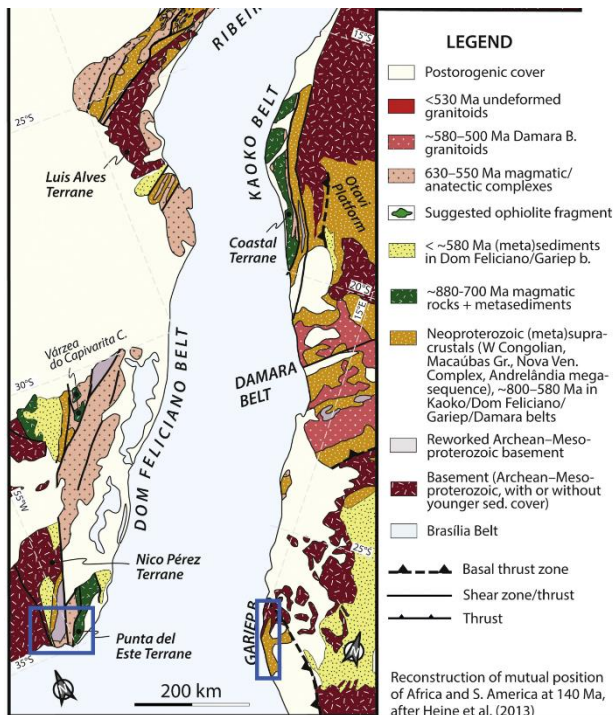


Figure 3: Geological map showing the Neoproterozoic mobile belts in South America and Africa. On the map the three sectors of the Dom Feliciano Belt can be seen; the Santa Catarina sector to the north, the Rio Grande do Sul in the middle, and the Uruguay sector to the south. The areas of study are shown in the boxes and they are shown in more detail in Figure 5 and 8. Modified from Konopásek et al. (2020)

south eastern Brazil to Uruguay, and has a width of up to 200 km (Figure 3(Hueck et al., 2018; Basei et al., 2008)). It is part of the Mantiqueira Province, represented by three mobile belts, the Araçai, Ribeira and Dom Feliciano belt. The Mantiqueira province originated during the Neoproterozoic Brasiliano-Pan African orogenic cycle, during the assembly of Southwest Gondwana (Basei et al., 2008; Hueck et al., 2018). The Neoproterozoic foreland units of the Dom Feliciano Belt are represented by the Luis Alvez Terrane in the north, small occurrences of basement rocks in the central sector and by the Nico Pérez Terrane in the south (Hueck et al., 2018). The Dom Feliciano Belt is divided geographically in three parts, the Santa Catarina-, Rio Grande do Sul- and Uruguay sectors (Figure 3), where the last sector is one of the focus areas of this thesis (Figure 4(Hueck et al., 2018)

The Dom Feliciano Belt in Uruguay can be further subdivided in two main domains - the western and the eastern domain, which are separated by the Sierra Ballena shear zone (SBZS;Figure 4). The western domain is in tectonic contact with the Nico Pérez Terrane basement and consists of metavolcano-sedimentary associations and granite intrusions of late Neoproterozoic (Ediacaran) age. The eastern domain is represented by the late

The beginning of amalgamation of Rio de la Plata, Kalahari and Congo – São Francisco cratons is constrained at c. 650 Ma, which makes it one of the earliest collisional events in the forming of south-west Gondwana (Oriolo et al., 2017). By 600 Ma, most of the western Gondwana continental blocks had joined together, but the formation of Gondwanaland was not completed until c. 530 Ma with the Malagasy Orogeny and the Pinjarra Orogen which connected India to Australia-East Antarctica (Li et al., 2008).

1.1.1 The Dom Feliciano Belt (DFB)

The Dom Feliciano belt (DFB) extends c. 1200 km along the Atlantic coast from

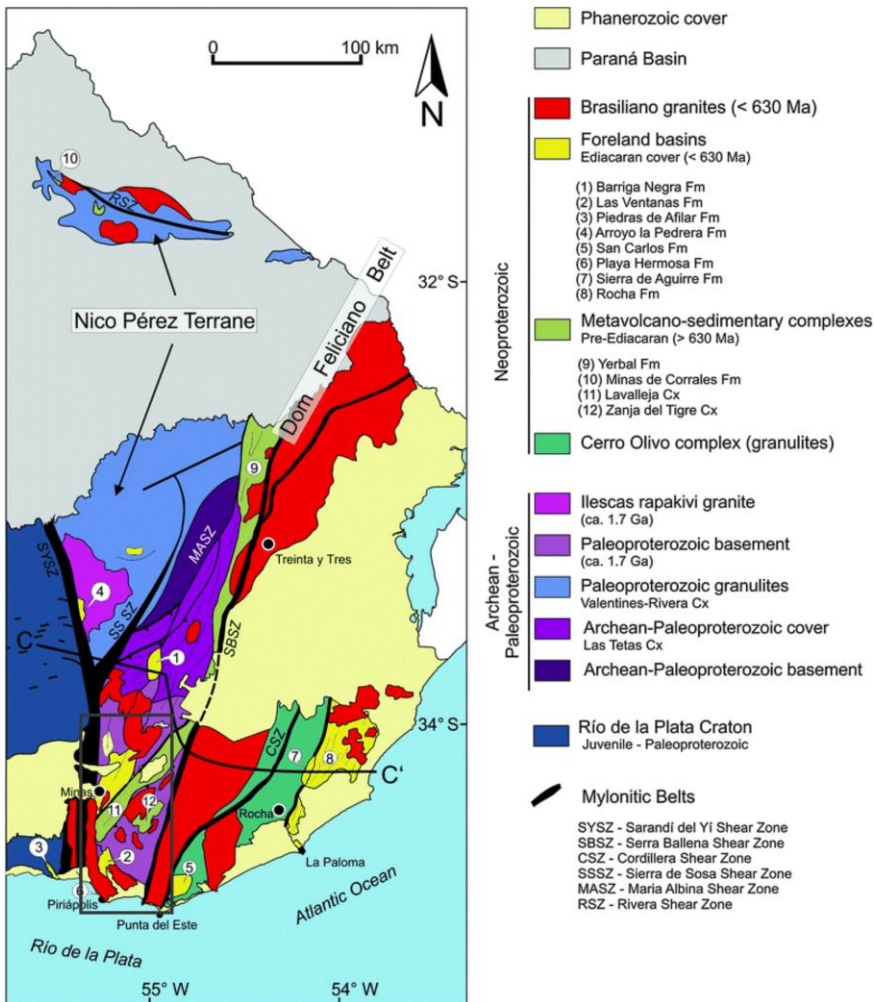


Figure 4: Geological map over the Uruguay Sector of the Dom Feliciano Belt. The black rectangle shows the focus area of this thesis.

Neoproterozoic Aiguá Batolith and the Punta del Este Terrane built of the early

Neoproterozoic Cerro Olivo Complex, and covered by the late Neoproterozoic Rocha- and Sierra de Aguirre formations (Figure 4) (Hueck et al., 2018; Basei et al., 2010)

The Nico Pérez Terrane (NPT) basement consists of Archean orthogneisses and Archean to Paleoproterozoic supracrustal rocks, Paleoproterozoic

orthogneisses and a Mesoproterozoic metavolcano-sedimentary cover (Oyhantçabal et al., 2018). All these units underwent reworking during the Pan-African/Brasiliano orogeny. The Archean–Mesoproterozoic basement is partly covered by Neoproterozoic sedimentary rocks of the Arrojo del Soldado Group. The Campanero Unit in the eastern part of the Nico Pérez

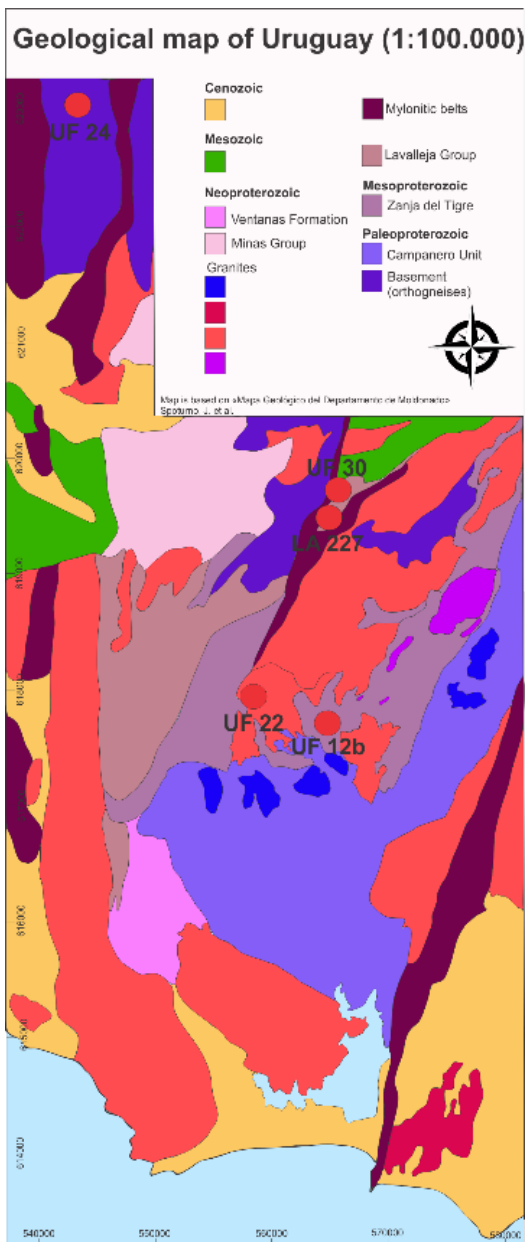


Figure 5: map of this thesis' focus area, modified after "Mapa Geológico del Departamento de Moldonado" (Spotorno et al.)

Terrane represents a basement inlier thrust on top of the Mesoproterozoic volcano-sedimentary units, and it is made of orthogneisses dated at 1750 Ma (Lara et al., 2020).

The oldest supracrustal succession in the belt is the Mesoproterozoic Zanja del Tigre Complex dated to 1400-1800 Ma (Figure 4)(Lara et al., 2020), and interpreted as a sedimentary cover of the Nico Pérez Terrane. The Lavalleja Group (Figure 4) includes metavolcano-sedimentary complexes of Neoproterozoic age (700-600 Ma)(Lara et al., 2020). The Lavalleja Group is up to 40 km wide and more than 250 km long (Hueck et al., 2018). Several granite bodies have intruded the western domain of the belt. These intrusions have been dated to 654-580 Ma.

The Aiguá Batolith (Figure 4) lies along the boundary between the western and eastern domains and consists of several plutons. U-Pb dating of the different plutons of the Aiguá Batolith show ages between 616 - 564 Ma (Hueck et al., 2018).

The eastern part of the belt has basement rocks exposed in the Cerro Olivo Complex, which consists of para- and ortho derived granulites and migmatites (Figure 4). The ortho-derived rocks have been dated at c. 880-770 Ma, with zircon xenocrysts showing ages between 1.3 - 1.0 Ga (Lenz et al., 2011). A metamorphic overgrowth in the magmatic zircons shows a metamorphic event at c. 650 Ma (Hueck et al., 2018). East of the Cerro Olivo Complex lies the Rocha Formation, which is described by Abre et al. (2020) as a turbiditic sequence of sandstones, wackestones and mudstones metamorphosed in greenschist facies and deposited in an active tectonic setting. The maximum age of this formation is constrained by the

youngest detrital zircons at c. 570 Ma (Abre et al., 2020), and the minimum age is set by the intrusion of the Santa Teresa granite, which is ca. 543 Ma (Hueck et al., 2018).

In Uruguay, three samples were collected from the Zanja del Tigre Complex (volcano-sedimentary sample LA 227, metarhyolite sample UF 30 and quartzite sample UF 12b). Two additional samples of granitic rocks (UF 22 and UF 24) were collected to characterize the syn-orogenic magmatism in the western domain. UF 22 was collected from an intrusion into the Lavalleja Group, while UF 24 was collected from an intrusion in the Nico Perez Terrane basement (Figure 5).

1.1.2 – 1.2.4 The Gariep Belt (Africa)

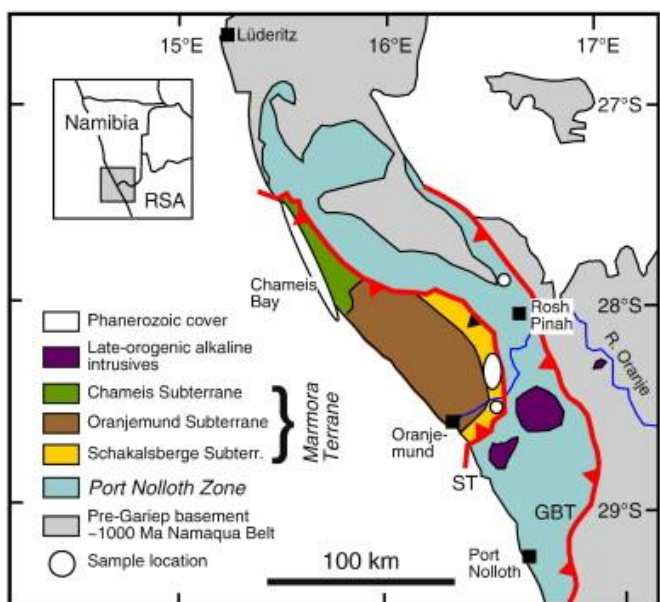


Figure 6: Overview map of the Gariep Belt (Will et al., 2014)

The Gariep Belt (Figure 3) is the African counterpart to the Dom Feliciano Belt. It stretches along the coast of southwest Namibia and northwest South Africa, where it forms most of the bedrock found in the coastal areas (Uwe, 1994). The width of the belt is up to 80 km, and it consists of two main tectonostratigraphic zones – the continental Port Nolloth Zone which is found to the east and the largely oceanic Marmora Terrane in the west,

which is considered as an allochthonous domain (Figure 6 ((Frimmel, 2018). The two zones of the Gariep Belt are divided by a major thrust fault called the Schakalsberge Thrust. The different rocks found in the Gariep Belt are the result of a series of tectonic events, from crustal thinning, continental rifting, opening of an oceanic basin, basin closure and continent-continent collision during the amalgamation of West Gondwana. In the sedimentary, volcanic and plutonic units one can follow the tectonic evolution from Rodinia to West Gondwana. All these represent pre-, - syn- or post orogenic deposits, based on lithological content, deformational and metamorphic history, areal distribution of each unit and on

geochronological data. Magmatic activity is recorded from pre-rift, rifting and post-orogenic, however there is no evidence of synorogenic magmatism (Frimmel, 2018; Uwe, 1994).

The Port Nolloth Zone (Figure 7) has a para-autochthonous relationship with its basement, which has been confirmed by sedimentological and geochemical evidence (Uwe, 1994). The basement of the Gariep belt has been dated to 1.4 – 1.2 Ga and 2.2 – 1.8 Ga. The early basin started as a continental rift basin filled with material eroded from nearby sources together

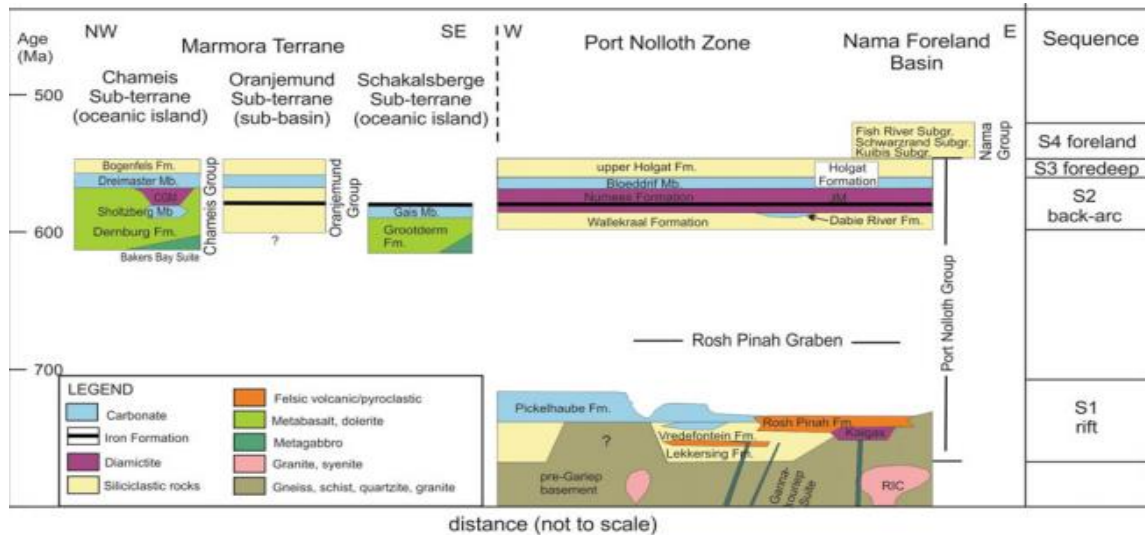


Figure 7: Lithostratigraphic overview of the Gariep Belt, from Frimmel (2018).

products of predominantly felsic volcanism. This lithological sequence is called the Stinkfontein subgroup (Figure 7) and represent continental rift deposits. 750 Ma dolerite dykes crosscut the whole subgroup. The Stinkfontein subgroup is further divided in two formations; the Lekkersing and Vredefontein formations (Figure 7). The Lekkersing formation is a 500 m thick unit with mainly medium-bedded quartz sandstones. While the Vredefontein formation is a 300m thick unit with dominantly medium-bedded feldspathic sandstone. The sedimentation of the Stinkfontein subgroup took place along a rising fault, with alluvial fans, alluvial planes and fan deltas. The felsic volcanism was concentrated on this developing fault. The loading of sediments led to subsidence towards the west, and thus facies with deep water deposits can be found to the west in the Stinkfontein sub-group. The Kaigas formation (Figure 7), a 150 m thick glaciogenic diamictite only locally developed along the eastern and north eastern margin of the former rift basin. The boarder between the Stinkfontein sub-group and the Kaigas formation is conform. The Kaigas formation is represented by layered diamictite and sand-, silt, and mudstones. Sedimentary features such as ripples, cross-bedding, flutes and others are common throughout the layers. The Kaigas formation is followed by the deposition of carbonate sediments and tempestite in the

Pickelhaube Formation (Figure 7). It rests both unconformably directly on the basement, and conformably on top of the Kaigas formation, and reaches 280 m in thickness. The composition varies from dolomitized limestones to a sequence with mudstone and marl. The Pickelhaube Formation was formed at a quieter submerged depositional environment, this can be seen in the scarcity of cross-bedding, absence of conglomerate, thin beddings and increasing content of Carbonates compared with the underlaying Stinkfontein Subgroup and the Kaigas formation (Frimmel, 2018). The Rosh Pinah Formation (Figure 7) with alternating layers of felsic volcanic and near-shore volcanoclastic deposits is contained in the Pickelhaube Formation. The repetitive sedimentary cycles conserved in the formation is an evidence of rapid deposition. The sedimentation then stopped for a long time, before breccias, conglomerates and other clastic deposits of different types was deposited in the overlaying Wallekraal Formation (Figure 7). Within this formation, the reef-facies Dabie River Formation is found (Figure 7). This carbonate formation differs from other carbonate-bearing successions in the subgroup by the presence of stromatolites, indicating a shallow marine deposition environment such as a barrier bar or shelf lagoon. Overlaying the Wallekraal formation is a massive diamictite unit called the Numes Formation (Figure 7). The Numes Formation is regarded as a glaciogenic unit, and it represents the youngest glaciogenic diamictite in the Port Nolloth Zone. This unit is topped by a cap of predominantly siliciclastic succession with arkose and greywacke, it is called the Holgat Formation (Figure 7), which is also the youngest unit of the Port Nolloth group. One unit in the Holgat Formation, the Bloeddrif Member (Figure 7), consists of carbonates, and is in its lower parts the cap carbonates of the Numees glaciation (Frimmel, 2018).

The Marmorra Terrane is subdivided into three sub-terrane or thrust sheets, which represent an oceanic island (Chameis), a sub-basin (Oranjemund) and an oceanic crust (Schakalsberge) (Uwe, 1994). The Schakalsberge sub-terrane consist mostly of mafic volcanic rocks and some mafic intrusive rocks, with carbonates (stromatolites and oolitic dolomite) on top. It has been interpreted as guyots and the carbonates ass reef structures at the top of them. The middle thrust sheet, the Oranjemund group, is made up of chlorite schist, and lacks the volcanic rocks found in the other two subgroups. The occasionally occurring mafic schist could have originated from erosion of nearby units. The Oranjemund sub-terrane represents syn-orogenic foredeep deposits. Above the schist of the Oranjemund group there is a thin chert layer, carbonates and a layer of arenite. The Chameis sub-terrane is divided into two formations - the Dernburg and the Bogenfels. The Dernburg Formation consists of volcanic rocks overlain

by carbonates. However, this formation also contains gabbros, and serpentinized ultramafic rocks. The Bogenfels Formation is made predominately of carbonates with turbiditic siliciclastic layers on top. It has strong similarities with the upper part of the Oranjemund Group, (Frimmel, 2018).

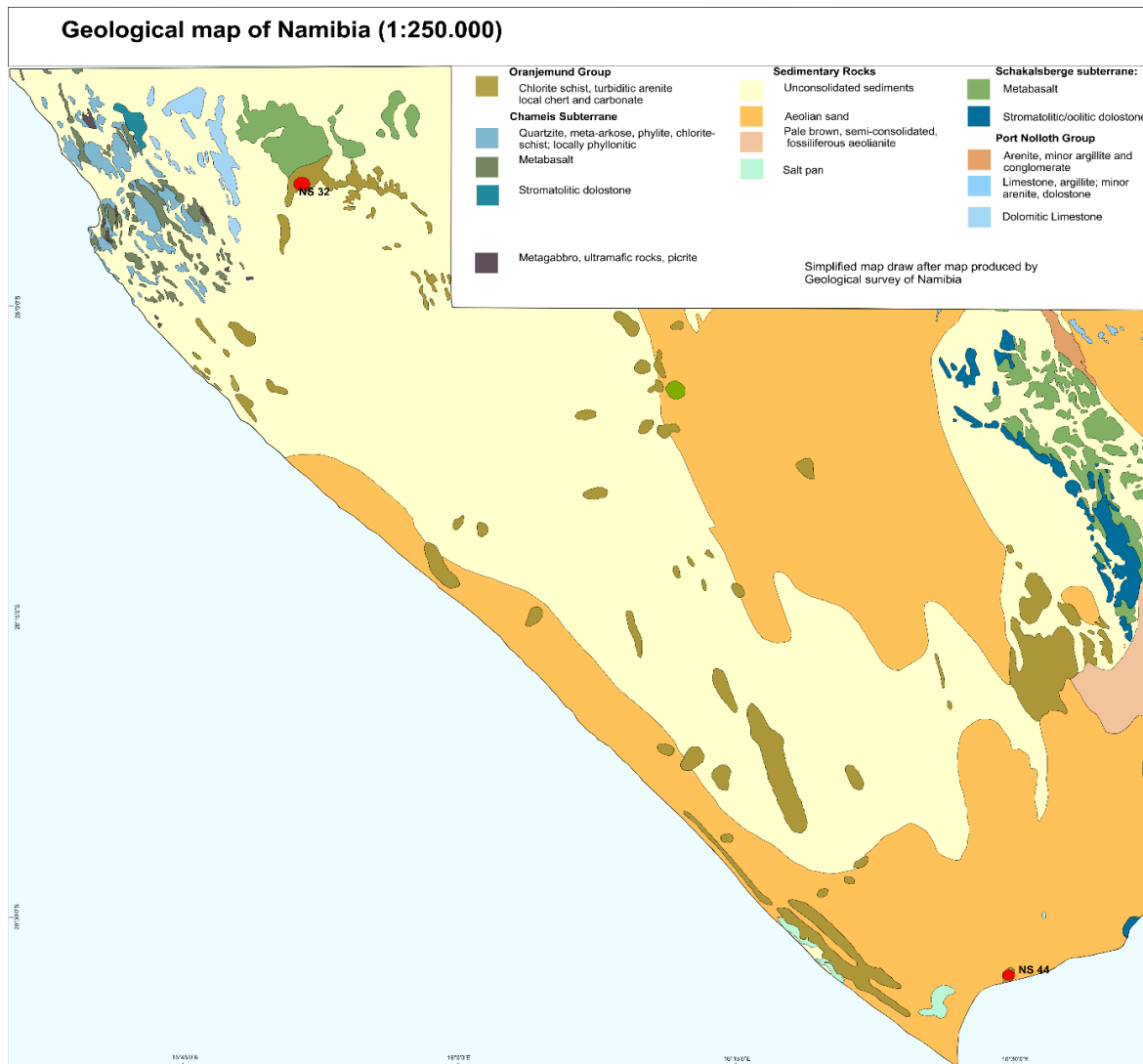


Figure 8: Geological map of this thesis area in the Gariep Belt. Map is modified after Geological map of Namibia, Geological survey of Namibia (1999).

The samples from Namibia were both collected from the Oranjemund Group in the Marmora Terrane, which based on the works of Basei et al. (2008) and Konopásek et al. (2017a) represents an early orogenic flysch unit in the Gariep Belt. NS 44 was collected from an outcrop close to the South-African border near the city of Oranjemund, and NS 32 from an outcrop further north along the coast (Figure 8).

1.2 Flysch sediments on the African side of the Dom Feliciano-Kaoko-Gariep orogenic system

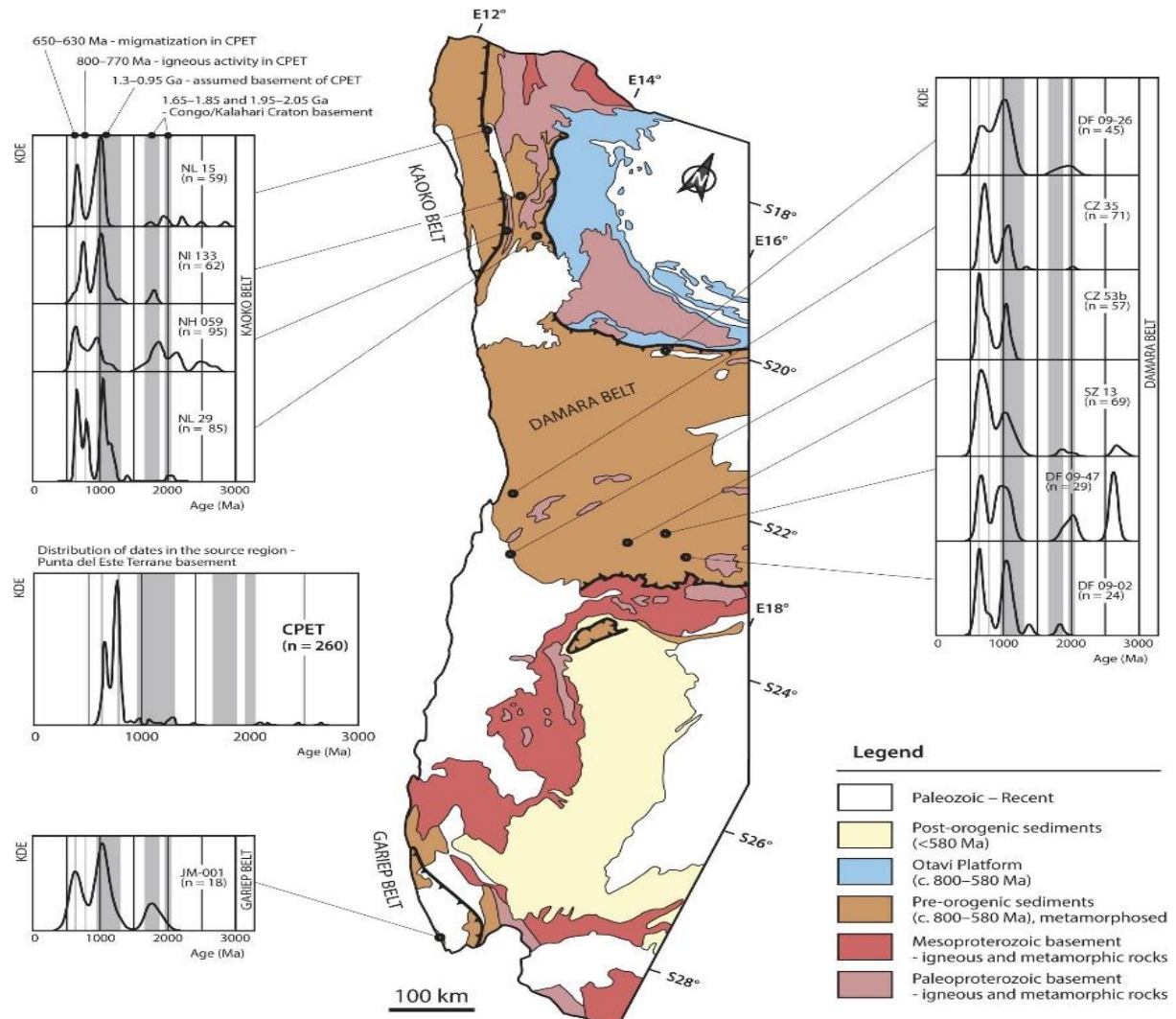


Figure 9: Map showing extent and age of sedimentation in the Gariep Belt. Detrital zircon kernel-density plot showing flysch sedimentation (Konopásek et al., 2017a).

Flysch sediment is a term used for a sequence of sedimentary rocks representing deep-water and turbidity flow deposits to shallow-water shales and sandstones, often detrital in origin. The flysch sequence can commonly be several thousands of meters thick, however the individual layers are thin, from cm to a few meters. The flysch sediments deposit when a basin is forming quickly in the foreland of an ongoing orogeny. The flysch sediments are characterized by a cyclic alteration of several lithological varieties of graded beds with finer grains towards the top. The deposition environment of flysch sediments is thought to be shallow to deep marine waters (Einsele, 2000).

Konopásek et al. (2017a) recognized regional extent of the flysch sediments (Figure 9) on the African side of the Dom Feliciano-Kaoko-Gariep orogenic system. The typical pattern of

detrital zircon ages from the flysch sediments consists of peaks in the intervals 1.85 – 1.65 and 2.05 – 1.95 Ga (Congo/Kalahari craton), 1.3 – 0.95 Ga (assumed basement of Punta del Este Terrane-Coastal Terrane (CPET)), 800 – 770 Ma (igneous activity in CPET) and 650 – 630 Ma (migmatization CPET).

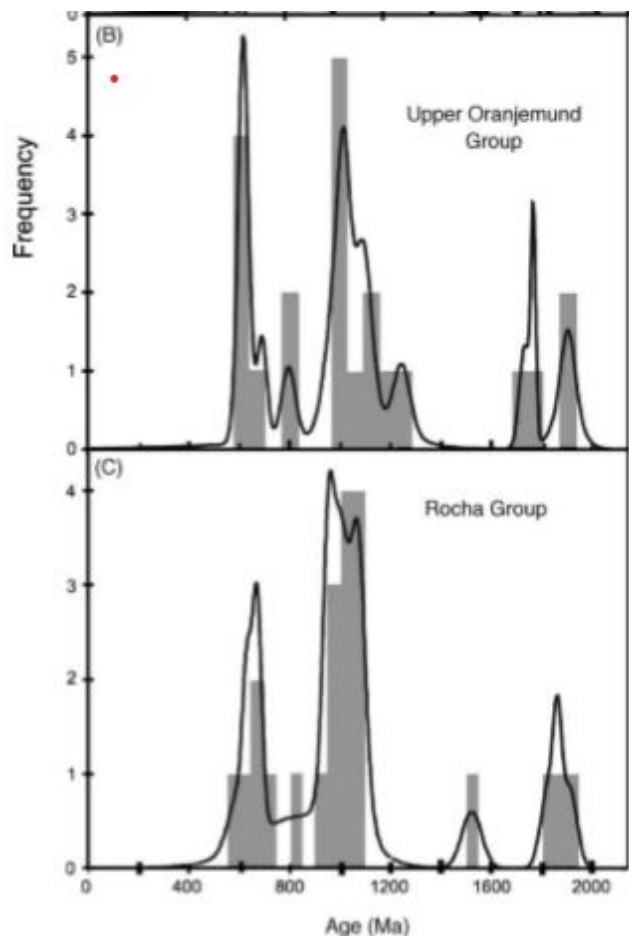


Figure 10: U-Pb detrital zircon dating of flysch samples, one from the Gariep-Oranjemund and one from the Rocha Group (Basei et al., 2005).

dominance of Paleoproterozoic 1.9 – 1.7 Ga ages. The source for the 1.9 - 1.7 Ga age data is more compatible with a source from southwestern Africa, i.e. the Congo/Kalahari craton basement, when compared to the South American Rio de la Plata Craton, where all the Paleoproterozoic units are older than 2.0 Ga. The zircon grains with ages around c. 800 Ma could have sources either from granites in the Punta del Este Terrane (762 Ma) or the pre-Gariep basement in South Africa (800 – 770 Ma). The 800 Ma zircon age is seen in both samples and found in the typical flysch sediment pattern. The source of the youngest zircon age population from around c. 600 Ma has only one potential source in the Florianópolis-Pelotas-Aiguá Batholith with intrusion ages c. 640 – 590 Ma. As both samples are lithological

Basei et al. (2005) dated one flysch sample from the Gariep-Oranjemund (JM-0001) in Africa and one from the Rocha Group (32710) in Uruguay (Figure 10). They found similarities in the age pattern of the two samples, despite the low number of dated zircon grains (ca. 20 grains/sample). This age pattern also corresponds with the typical flysch pattern described by Konopásek et al. (2017a). Both samples have a dominance of 1.2 – 1.0 Ga ages, which is the same as in the typical age pattern of flysch sediments. The authors suggested that the source for the age peak at 1.3 – 1.0 Ga is the Namaqua Metamorphic Complex on the African side and the basement of the Punta del Este Terrane for the South American sample (Basei et al., 2005). Both samples also display individual zircons with Meso- and Proterozoic ages, all under 2.0 Ga with the

similar and share comparable metamorphic and deformational history, they are considered by Basei et al. (2005) to be stratigraphic equivalents that represent the filling of the same basin (Gariep basin).

A new study by Abre et al. (2020) looked at two samples from the Rocha Group (Figure 11). The detrital zircon pattern seen in the two samples are comparable with the pattern found by Basei et al. (2005) and also with the typical flysch sediment pattern, as the zircon ages are concentrated at c. 600 Ma, c. 800, 1.0 Ga and 2.0 – 1.95 Ga. The authors put the most probable source of the youngest zircons (680 – 570 Ma) as the Neoproterozoic calc-alkaline

granitoids of the southern Dom Feliciano Belt, the c. 800 Ma zircon source as derived from the Cerro Olivo Complex. On the other hand, the authors do not consider any African source for this population. For the Mesoproterozoic population, mainly 1.2 – 1.0 Ga, the authors consider the Nama Group and the Western Kalahari Craton as a potential source area. Also, for the zircons of Paleoproterozoic and Archean ages, the Kalahari Craton is proposed as a potential source area.

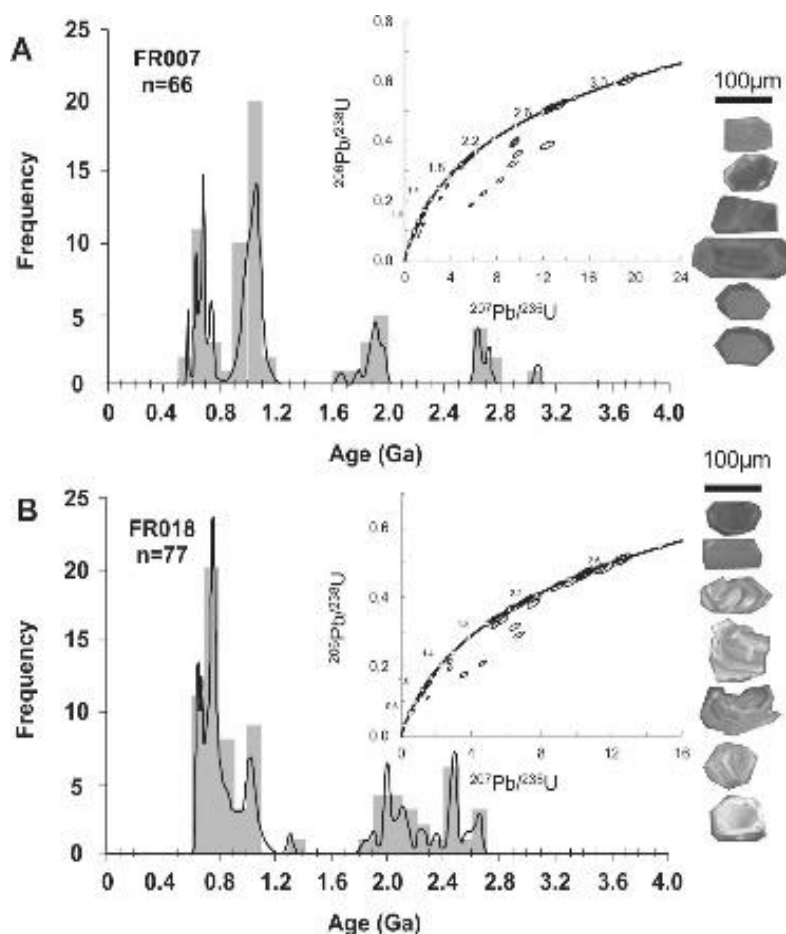


Figure 11: U-Pb dating of flysch samples from the Rocha Group (Abre et al., 2020).

2 Methods

2.1 U-Pb dating

Radioactivity is a spontaneous transformation that changes the number of protons and neutrons in the nucleus. This natural decay will continue until a stable isotope daughter is found. Radioactivity was discovered in 1896 by Henry Bequerel, but its importance to geology first became apparent in 1903. The discipline to date rocks and minerals was named isotope geology (Faure, 1998).

Radiogenic isotopes are the product of natural radioactivity (White, 2013). Two fundamental assumptions are the basis for all geological use of radiogenic isotopes.

1. Decay rate is only a function of the nuclide and time. Other parameters have no effect on the process.
2. *“Two isotopes of the same element are chemical identical and therefore that chemical processes cannot change, or fractionate, the ratio of two isotopes of the same elements. Neither of these assumptions holds in the absolute. Nevertheless, all available evidence indicates violations of these assumptions are entirely negligible.”* (White, 2013)

There are three forms of nuclear decay - alpha, beta and fission - and a decay chain usually consists of at least two of these decay types. All radioactive decay follows *the law of radioactivity*:

$$Eq\ (1): -\frac{dN}{dt} = \lambda N$$

, which was discovered by Rutherford and Soddy in 1902. Here, λ is the decay constant, the probability that a given atom would decay in some time dt . Rearrangement of this equation looks like this

$$Eq\ (2): A_t = A_0 * e^{-\lambda t}$$

The definition of half-life is the rearrangement of the law of radioactivity that gives

$$Eq\ (3): t_{\frac{1}{2}} = \frac{\ln 2}{\lambda} .$$

The number of daughters produced is the difference between the initial number of parents and their number remaining after time = t. A general expression for this is

$$\text{Eq (4): } D = D_0 + N(e^{\lambda t} - 1)$$

, where D_0 is daughters originally present, and D is the daughters after time = t. For geochronology equation 4 is rewritten as

$$\text{Eq (5): } R = R_0 + R_{P/D}(e^{\lambda t} - 1)$$

, where R_0 is initial ratio, and $R_{P/D}$ is the parent daughter ratio.

For U-Th-Pb there are three decay series that produce different isotopes of Pb. The fact that two U isotopes decays to two Pb isotopes that are chemically identical, makes U-Pb dating especially useful in geochronological work. U and Th does not decay directly to Pb, but it involves a series of decay steps (Figure 12).

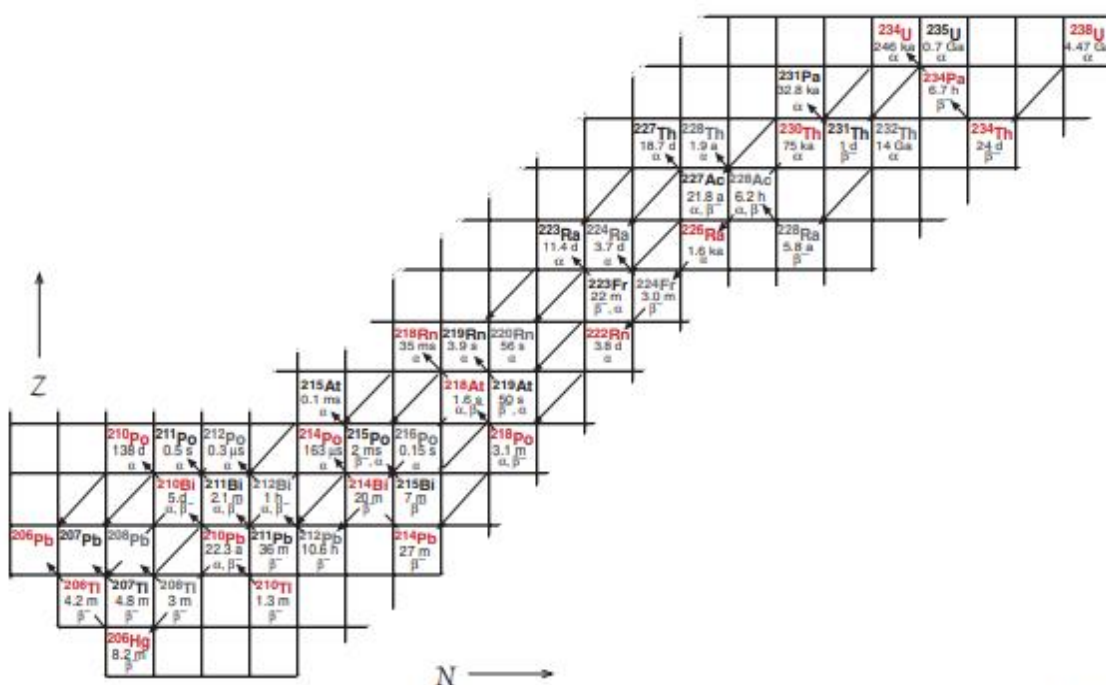


Figure 8.19. Part of the chart of the nuclides showing the series of decays that occur as ^{238}U , ^{235}U , and ^{232}Th are transformed to ^{206}Pb , ^{207}Pb , and ^{208}Pb respectively. Nuclides of the ^{238}U series are shown in red, the ^{232}Th series in gray, and the ^{235}U series in black.

Figure 12: An overview of the U-Th-Pb decay series (White, 2013).

The LA-ICP-MS analysis for this thesis measured ratios of ^{238}U , ^{235}U , ^{206}Pb , ^{207}Pb , ^{232}Th , ^{208}Pb . Half-life of each decay series is as follows: $^{238}\text{U} - ^{206}\text{Pb}$: 4.468 Ga, $^{235}\text{U} - ^{207}\text{Pb}$: 0.704 Ga, and $^{232}\text{Th} - ^{208}\text{Pb}$: 14.1 Ga

Geochronometry equations utilizing these measured isotopic ratios become:

$$\text{Eq (6): } \frac{^{206}\text{Pb}}{^{204}\text{Pb}} = \left(\frac{^{206}\text{Pb}}{^{204}\text{Pb}}\right)_0 + \frac{^{238}\text{U}}{^{204}\text{Pb}} (e^{\lambda_1 t - 1})$$

$$\text{Eq (7): } \frac{^{207}\text{Pb}}{^{204}\text{Pb}} = \left(\frac{^{207}\text{Pb}}{^{204}\text{Pb}}\right)_0 + \frac{^{235}\text{U}}{^{204}\text{Pb}} (e^{\lambda_2 t - 1})$$

$$\text{Eq (8): } \frac{^{208}\text{Pb}}{^{204}\text{Pb}} = \left(\frac{^{208}\text{Pb}}{^{204}\text{Pb}}\right)_0 + \frac{^{232}\text{Th}}{^{204}\text{Pb}} (e^{\lambda_3 t - 1})$$

In theory, these three decay schemes can yield the same age independently, if the system is completely closed with no loss or gain of U, Th and Pb. In most real-life cases the ages will not be the same and it is said that the analytical results are discordant. The discordance appears most of the time due to lead loss or loss of intermediate daughters. Another problem is radiation damage, a result of energy release during alpha decay, which destroys the lattice of the host mineral and can lead to lead loss. To be a good candidate for U-Pb dating, a mineral should be common and it should retain radiogenic Pb. Zircon is the best mineral for this method, as it meets both criteria better than e.g. monazite or apatite. While all of them are used, zircon is preferred in most cases.

In geochronology, data are plotted in a concordia diagram (Figure 13) which is a plot of $^{206}\text{Pb}^*/^{238}\text{U}$ vs. $^{207}\text{Pb}^*/^{235}\text{U}$, or in the Wetherill diagram which is a plot of $^{207}\text{Pb}/^{206}\text{Pb}$ vs. $^{238}\text{U}/^{206}\text{Pb}$. All ratios are proportional to time. The concordia cord is the locus of points where the ages (i.e. time) coincide. Ages that plot on this line are called concordant.

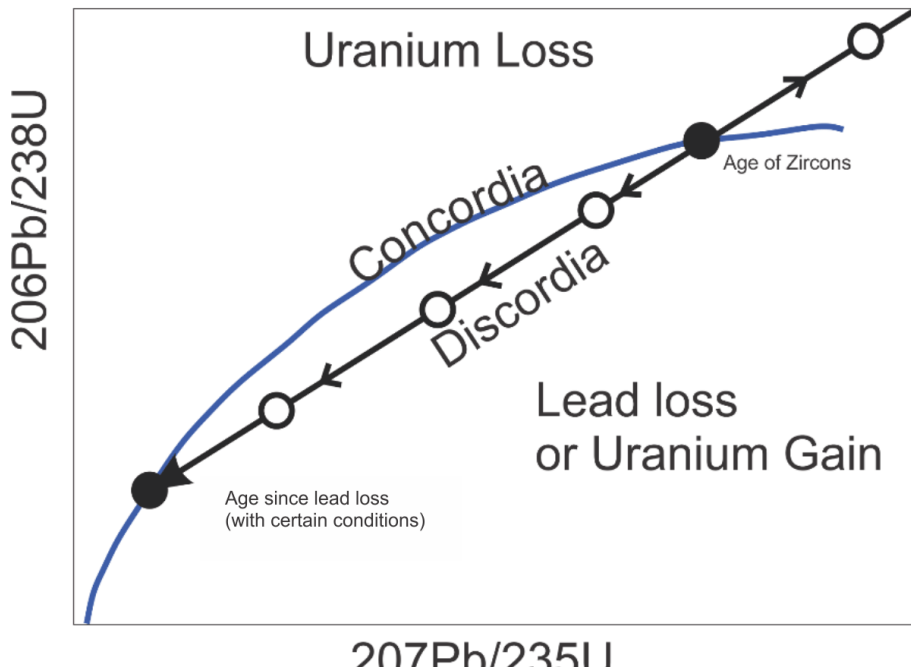


Figure 13: This picture shows the concordia diagram, and a simple example on how to read it. The diagram is modified from Allègre (2008).

Lead loss: both Pb isotopes (207 and 206) must be lost in proportion as they exist in the zircon as isotopes of the same element.

Metamorphic event can often cause a lead loss. If all lead was lost, the zircon would reset the clock, and its age will reflect the time

of the lead loss i.e. for example the metamorphic age. If the zircon loses just some amount of the total radiogenic lead, the ratios will plot under the concord line, and such data are called discordant. When a series of zircon samples are discordant, they generate a discordant line, named “Discordia” in Figure 13. The upper interception point between the Discordia and the Concordia (Figure 13: Age of Zircons) will reflect the original age of the zircon, while the lower interception point will reflect the age of the lead loss. To draw a discordia line, at least three discordant zircons are needed to get accurate interception points. All three decay routes give the same age if there is no lead loss (White, 2013; Faure, 1998).

2.2 Field work

2.2.1 Samples Uruguay

The fieldwork took place from December 3rd to December 12th in 2018 in Uruguay. It was conducted in the foreland part of the Dom Feliciano Belt represented by the Nico Perez Terrane basement overlain by volcano-sedimentary units of the Zanja del Tigre Complex and the Lavalleja Complex (Figure 5). A total of 8 samples was collected for geochronological study. The samples for geochronology weighted 2-3 kg and they were sent to Norway for further processing. Each location was photographed, marked with GPS coordinates (WGS 84), some field notes and basic structural measurements.

2.2.2 Samples Namibia

Two samples of assumed metamorphosed flysch sediments were studied in this work. They come from the Oranjemund Group of the Gariep Belt in southern Namibia (Figure 8) and were collected by supervisor Jiri Konopasek in the summer of 2019.

2.3 Laboratory work

2.3.1 Mineral separation

The first step in processing of the samples was washing them clean with a metal scrub to minimize the risk of contamination. Then a small piece of the sample was cut off with a diamond blade saw, this piece was further used to make a thin section. 2-3 kg of each sample were first split to smaller pieces manually with a sledge. The size was further reduced with a jaw crusher, which produced a gravel with particles around 10 mm large. A hammer mill with an aperture of 0.5 mm was used next, which left the sample very fine grained and ready for the next step.

From now, the goal was to separate heavy and light weight fractions of minerals. The Wilfley gravity shaking table was used to concentrate the heaviest grains of each sample. The shaking of the table under flowing water separates the grains into 3 fractions, heavy, middle and light grains. As zircon crystals are one of the heaviest minerals, only the heaviest fraction of each sample was processed further. The light and middle fraction were kept in case they are needed later on, but no further processing was done on them. After the gravity separation, the sample contained zircon, apatite, opaque minerals (magnetite etc.) and other heavy minerals together with some portion of light minerals (quartz, feldspar etc.). A hand magnet was then used to remove paramagnetic minerals. The rest of the weakly magnetic minerals was removed by using the Frantz isodynamic separator. Finally, the samples were loaded in diiodomethane (DIM), lithium heteropolytungstate (LST) or both, depending on the size and mineral content of the sample. LST has a density of 2.9 g/cm³ and DIM 3.325 g/cm³ (University of Bergen, 2019), and as zircons has a higher density than DIM and LST, it will sink to the bottom while lighter minerals remain afloat.

2.3.2 Mount preparation

Preparation of the mount starts with transferring the mineral concentrates to a petri dish, and observing them under a binocular microscope. Three samples were found to contain no or very few zircon grains and these were therefore not further prepared. The zircons were then

handpicked with a needle. Grains of different color, size and shape were chosen in samples for detrital zircon analysis in order to get the maximum possible variability of the zircon population. Also, metamict (non-transparent) grains were avoided, while transparent grains were chosen in order to avoid discordant analytic results. A double-sided tape has been attached to a glass plate, where the circular size of the mount was drawn and the zircon grains were then transferred onto the tape with a pipette. Approximately 200 grains were picked for each sample, however some were destroyed in the polishing phase. The zircon grains were finally mounted in epoxy and polished with a diamond paste.

2.3.3 Cathodoluminescence (CL-imaging)

Before the dating, CL-imaging of each sample was done to get an overview over the zircon internal structure. Before the images were taken, the mounts were coated with carbon. With the help of these images, the exact spots for the LA-ICP-MS analysis were chosen.

2.3.4 Dating; laser ablation (LA-ICP-MS)

The ELEMENT2 (Thermo-Fisher scientific) high-resolution magnetic sector field ICP-MS coupled with a separate ANALYTE EXCITE excimer 193 nm laser ablation system with an Aridus II desolvating nebulizer (Teledyne) were used for actual analysis of the zircon grains. The laser beams diameter was chosen to be 25 μm (Institute of Geology of the Czech Academy of Sciences, 2019).

Before the LA-ICP-MS analysis, the zircon mounts had to be cleansed of the carbon coating from the CL-imaging. The coating was removed by re-polishing the mount, and then the mount was cleaned from the relics of the polish paste. When done, the mount was inserted in a sample holder in the laser. The sample was observed and compared with the CL-images to find the best possible spots for the analysis. Inclusions and metamict zircons were avoided.

The analysis was done in sequences of 14 samples followed by 6 standards. The standards were the GJ1 (Jackson et al., 2004) with an age of 608.53 ± 0.4 Ma, the Plesovice (Sláma et al., 2008) with an age of 337.13 ± 0.37 and the 91500 (Wiedenbeck et al., 1995) with an age of 1065.4 ± 0.3 Ma.

2.4 Data processing

The data were processed in Igor Pro program of the Iolite software. The program was used to reduce the data and to remove background noise by subtracting the baseline from the total signal. After this, the data were transferred to Excel for analysis and plotting. With the add-on

software Isoplot 4.15 (Ludwig, 2012), the U-Pb ages were presented in concordia diagrams. The discordance of the $^{206}\text{Pb}/^{238}\text{U}$ and $^{207}\text{Pb}/^{206}\text{Pb}$ ages were calculated by the following equations, respectively:

$$\text{Eq (9): } ^{206}\text{Pb}/^{238}\text{U} = (1 - (^{206}\text{Pb}/^{238}\text{U} / ^{207}\text{Pb}/^{206}\text{Pb})) * 100$$

$$\text{Eq (10): } ^{207}\text{Pb}/^{206}\text{Pb} = (1 - (^{206}\text{Pb}/^{238}\text{U} / ^{207}\text{Pb}/^{235}\text{U})) * 100$$

The Isoplot 4.15 software was then used to calculate interception points of discordias, and the concordia age of concordant clusters. For the detrital zircon samples and inherited zircons, the software DensityPlotter (Vermeesch, 2012) was used to create histograms and Kernel Density estimates to display the age distribution. The histogram bin width was chosen to be 30 Ma. For the data below 1.0 Ga Ma the $^{206}\text{Pb}/^{238}\text{U}$ ages were used, whereas the $^{207}\text{Pb}/^{206}\text{Pb}$ ages were used for the data above 1.0 Ga.

3 Results

3.1 Field work

All the locations for the samples collected for this thesis are shown in Figure 5 for the Uruguayan samples, and in Figure 8 for the Namibian samples. All samples were taken from in situ outcrops (Figure 14 and Figure 15). All the outcrops that were sampled were affected by weathering, and a sledge was used to get down to fresher rock.

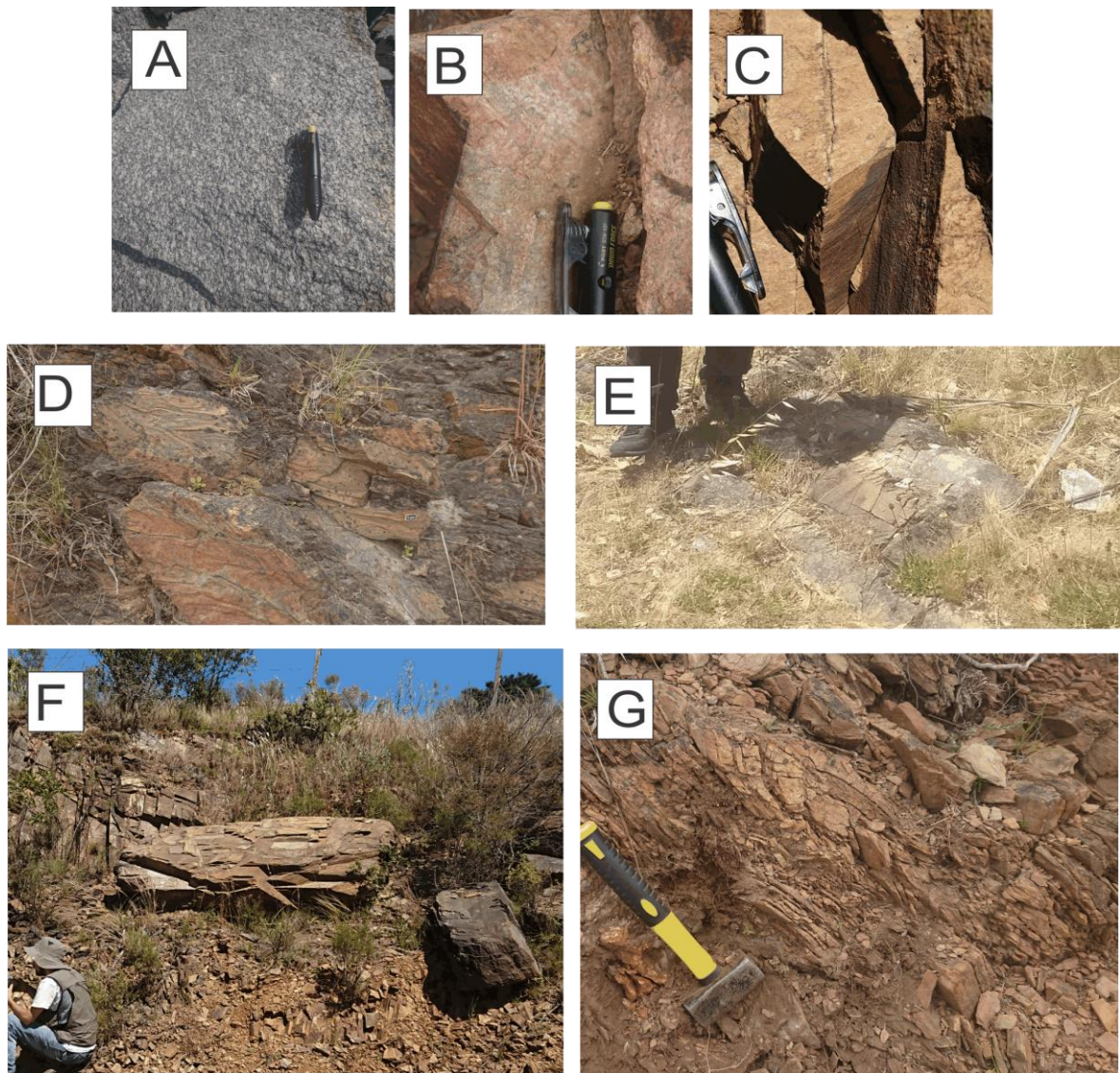
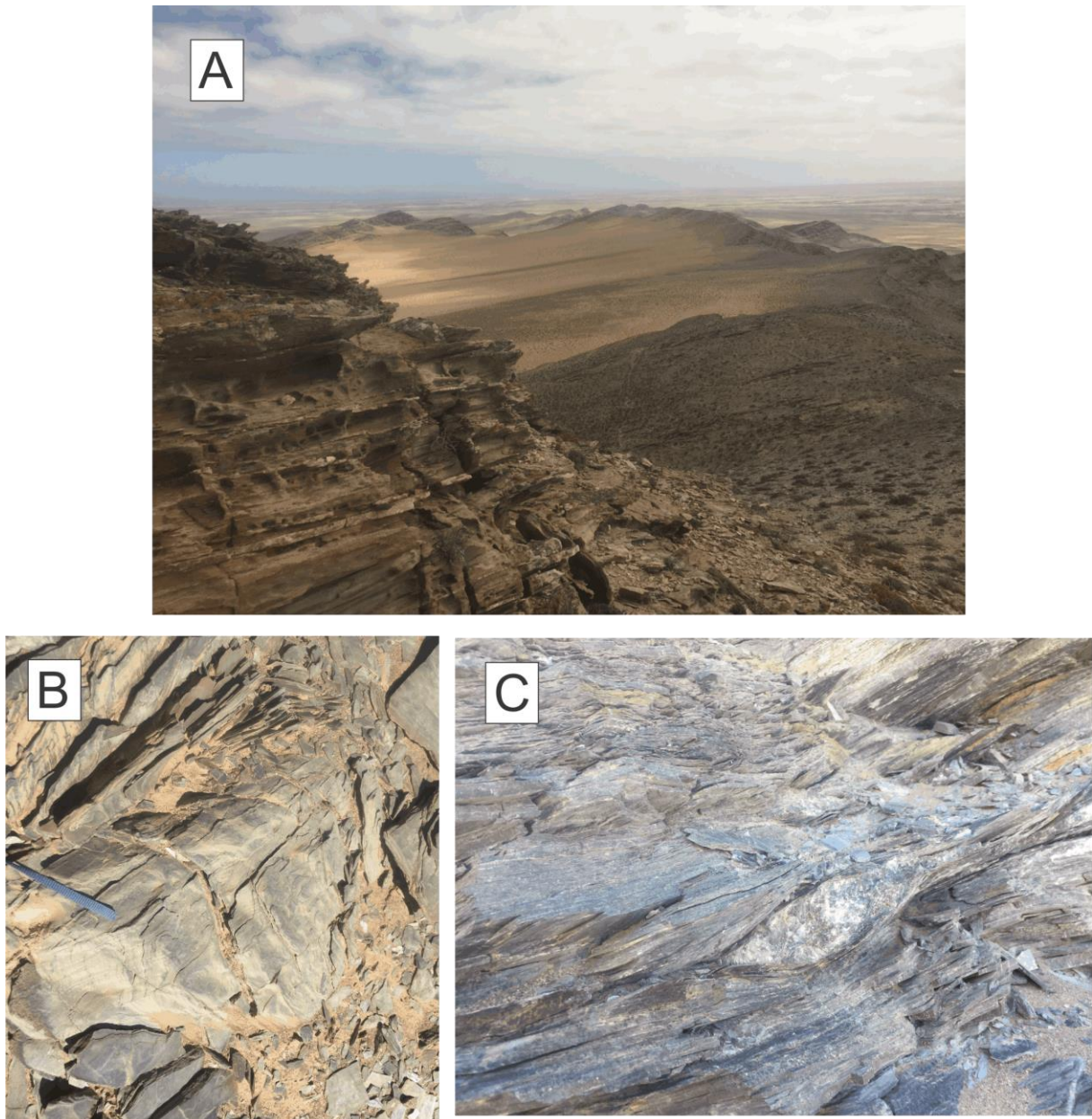


Figure 14: Photographs of the outcrops where the Uruguayan samples were collected. A: sample UF 24, B: sample UF 22, C: sample UF 30, D: sample UF 12b, E: sample LA 227, F: sample UF 30, G: sample UF 12b. Photo E courtesy of Jack Percival, University of Tromsø, Norway



*Figure 15: Photographs of the Namibian outcrops where the samples were collected. **A:** sample NS 32, **B:** sample NS 44 **C:** sample NS 44. All three photos courtesy of Cess Passchier, University of Mainz, Germany.*

3.2 Laboratory

All geochronological data from the Laser Ablation-Inductively Coupled Plasma-Mass Spectrometry (LA-ICP-MS) and the calculated ages are given in appendix A. The samples UD 17, UF 17 and UF 32 did not contain any zircons and have thus not been dated. The sample UF 12a was also not dated, as second sample from the same locality (UF 12b) contained enough zircons. The remaining seven samples were dated, and thin section photographs, cathodoluminescence (CL) images, histograms and Concordia diagrams were

produces. These are presented in the following sections. Corfu (2003) was used in the identification of the different textures in the zircons.

Table 1: All samples collected for this thesis, showing if they were dated or not.

Sample Name	Dated or not
UF 12a	Not dated (duplicate sample)
UF 12b	Dated
UF 17	Not enough zircons
UD 17	Not enough zircons
UF 22	Dated
UF 24	Dated
UF 30	Dated
UF 32	Not enough zircons
LA 227	Dated
NS 32	Dated
NS 44	Dated

3.3 Samples from Uruguay

3.3.1 Sample UF 12b

Sample UF 12b (-34.55480, -55.08887) comes from the Zanja del Tigre Complex (Figure 5) and it is a medium grained, low-grade metamorphosed sedimentary rock.



Figure 16: A photograph of UF 12b, showing folding and parasitic folds.

In hand sample, UF 12b has a matte brown-grey color with black to dark brown bands marking the foliation. The whole outcrop was heavily folded with larger folds and parasitic folds within (Figure 16).

The outcrop has quartz veins going through, and parallel to the foliation bands.

The sample mainly contains quartz, plagioclase and elongated white mica and biotite. In lesser amounts, it contains the minerals zircon, rutile and opaque minerals (Figure 17 and Figure 18). The zircons range in size from 40 to 130 μm in length and 40 to 80 μm in width. The shapes of the zircon grains range from ovoid to oval, with some showing prismatic habits. Numerous grains are fragments of larger grains. The cathodoluminescence (CL) images (Figure 19) reveal that most zircons have oscillatory zoning, and a large portion of the grains has distinct xenocrystic cores. A small number of the zircons have sector zoning or show signs of multiple cores. A large portion of the crystals has fractures, and a few grains have inclusions.

Analysis of 140 zircon grains yielded 123 concordant U-Pb ages, and the resulting age spectrum is presented in Figure 20. The spectrum has several peaks at 2.05, 2.15 Ga, 2.7 Ga,

2.9 Ga and 3.2 Ga with the largest peak at 2.15 Ga. The zircons ages are concentrated in two groups from c. 2.2 – 2.0 Ga and from 3.3 – 2.6 Ga, and there are no data below 1.95 Ga.

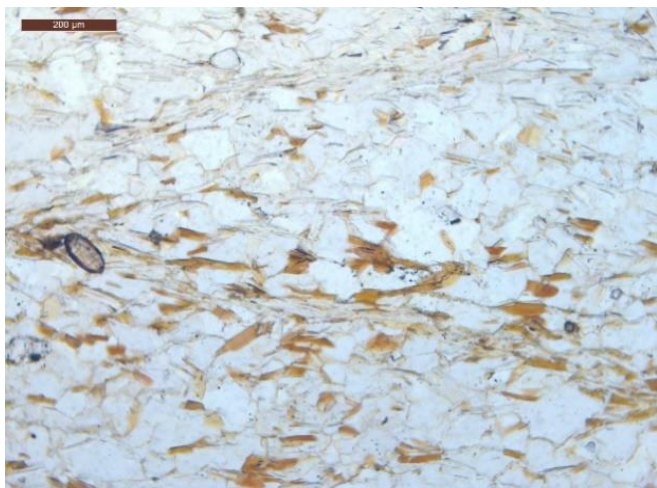


Figure 17: Thin section photograph in cross polarized light of the sample UF 12b (ppl) and magnification 100x

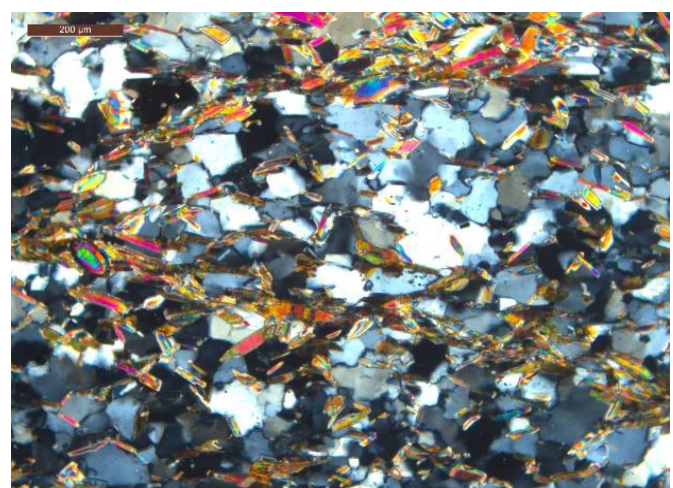


Figure 18: Thin section photograph in cross polarized light of the sample UF 12b (xpl) and magnification 100x

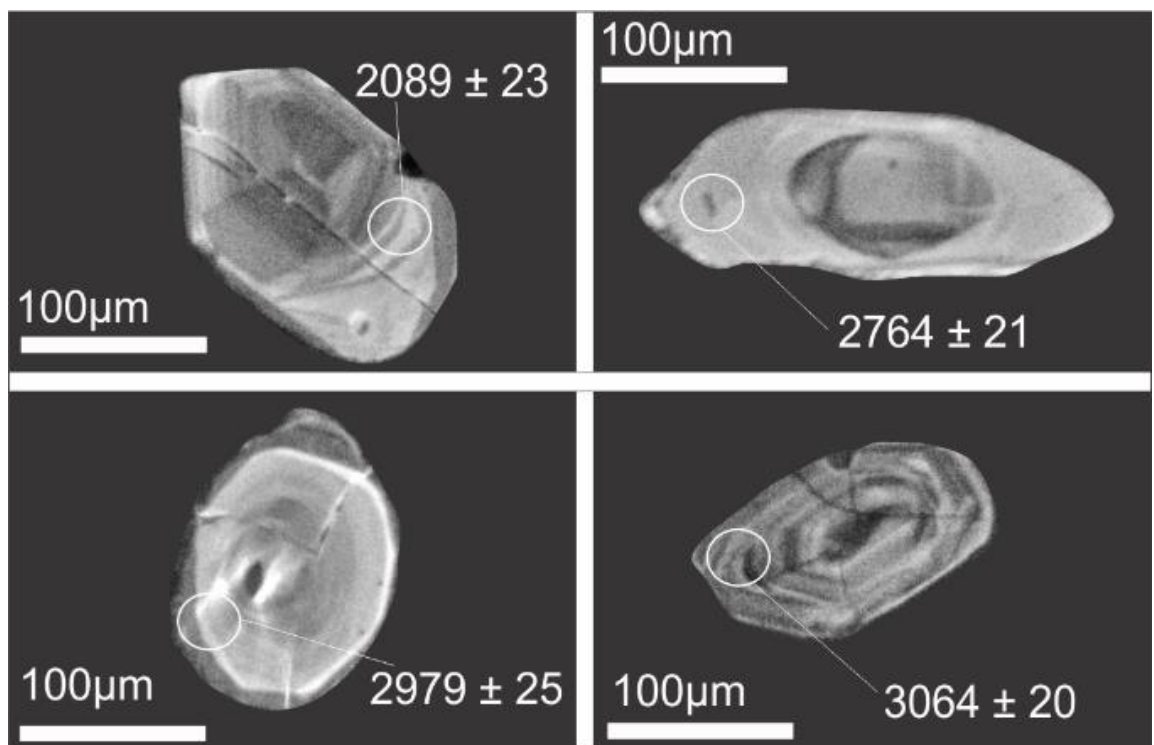


Figure 19: Cathodoluminescence images of representative detrital zircon grains from sample UF 12b. The circles represent the analysis spots for each grain, and the numbers to the yielded age.

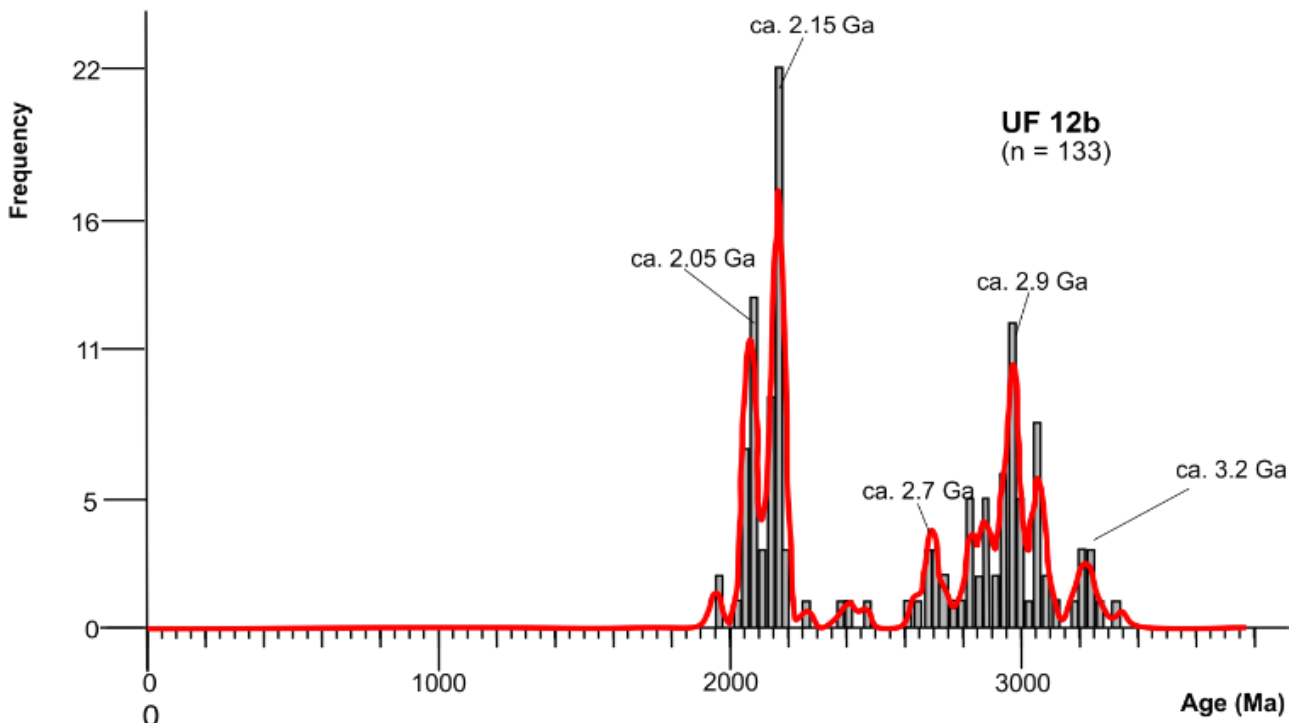


Figure 20: Kernel density plot and histogram of detrital zircon age data from the sample UF 12b. The sample shows a bimodal distribution with peaks at 2.05 Ga, 2.15 Ga, 2.7 Ga, 2.9 Ga and 3.2 Ga.

3.3.2 Sample LA 227

Sample LA 227 (-34.3701, -55.08716) comes from the Lavalleja Complex (Figure 5) and it is interpreted as a fine-grained metamorphic sedimentary rock with volcanic admixture. In hand sample the rock has a light grey color with darker bands marking the foliation. It has a mineral assemblage of white mica, quartz, plagioclase, K-feldspar and accessory amount of zircon, rutile, titanite and opaque minerals (Figure 21 and Figure 22). The zircons range in size from 90 to 200 μm in length and 60 to 120 μm in width. The shapes of the zircon grains range between elongated, ovoid and oval, with the elongated grains being more prismatic and showing some crystal faces. CL-images (Figure 23) show oscillatory zoning in most grains with complex cores, but a minor number of the zircons show sector zoning, no zoning at all or very little zoning. Both inclusions and fractures are present in a large number of the zircons.

Analysis of 140 zircon grains yielded 125 concordant U-Pb ages. The corresponding age spectrum is presented in Figure 24 and shows no ages below c. 1.4 Ga. This sample has one

major peak at c. 1.45 Ga, but individual data can be seen around 1.7 Ga, 2.2 – 2.0 Ga and 3.2 – 2.7 Ga.

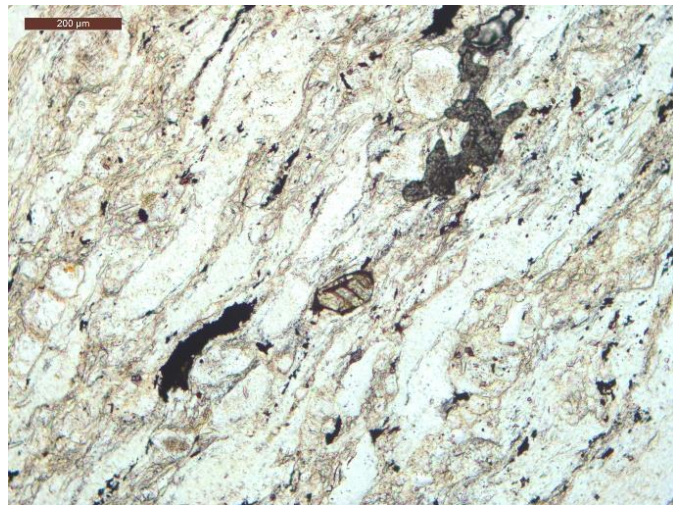


Figure 21: Thin section photograph of the sample LA 227 in plain polarized light (ppl) and magnification 100x.

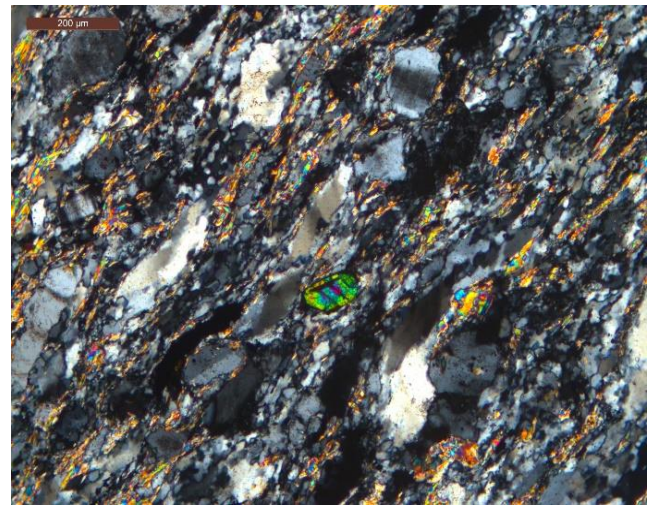


Figure 22: Thin section photograph of the sample LA 227 in plain polarized light (xpl) and magnification 100x.

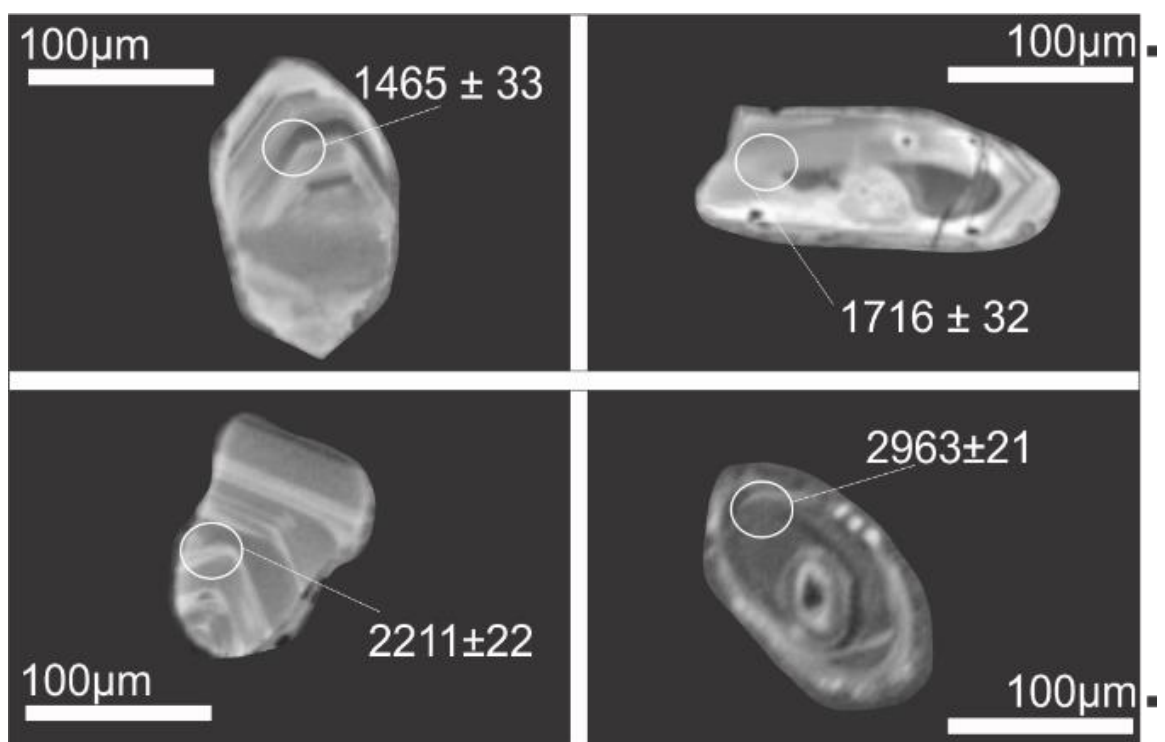


Figure 23: Cathodoluminescence images of representative detrital zircon grains from sample LA 227. The circles represent the analysis spots for each grain, and the numbers to the yielded age.

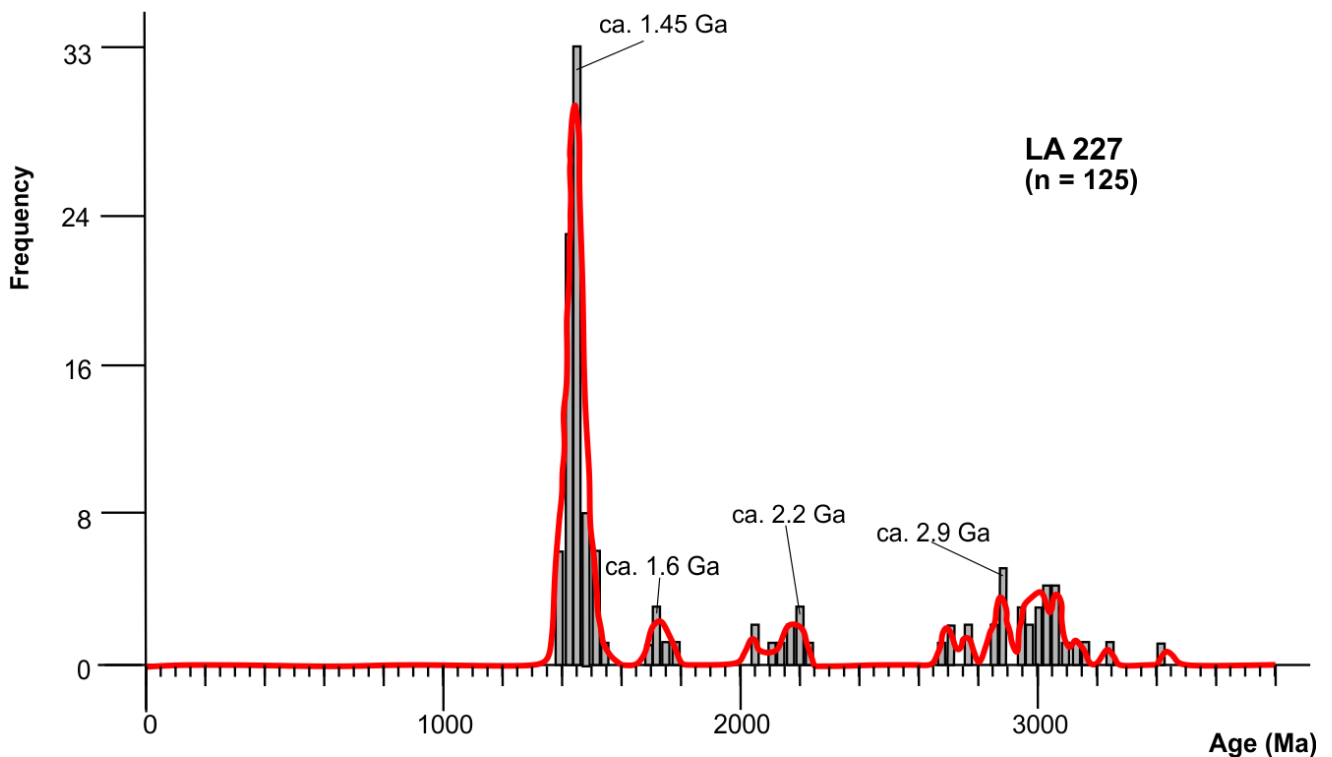


Figure 24: Kernel density plot and histogram of detrital zircon age data from the sample LA 227. The sample show one major peak at 1.45 Ga, and has minor peaks at 1.6 Ga, 2.2 Ga and 2.9 Ga.

3.3.3 Sample UF 30

Sample UF 30 (-34.36051 -55.08436) comes from the Zanja del Tigre Complex (Figure 5) and is a felsic metavolcanic rock interpreted as metarhyolite. UF 30 is a dark grey with dark foliation bands of recrystallized minerals representing the foliation, and elongated pink feldspars. In situ, the rock looked brown and matte due to weathering. It has a mineral assemblage of white mica, quartz, plagioclase/K-feldspar and accessory amount of zircon, rutile, titanite and opaque minerals (Figure 25 and Figure 26). The zircon grains of sample UF 30 ranges from around 30 to 100 μm in width, and from 50 to 200 μm in length. Most zircons are however fragments of larger grains. The shapes ranges from elongated to circular, the elongated crystals show some prismatic habit but have for the most part rounded edges. CL images (Figure 27) of the sample reveal that most zircons have oscillatory zoning, with one or two having sector zoning. Some zircon grains show little or no zoning at all. The majority of the zircons have xenocrystic cores, some quite complex. Fractures are common and visible in numerous zircon grains, while inclusions occur but are less common.

The zircon yield for UF 30 was low, and only 41 zircon grains were separated from this rock. Figure 28 show concordia diagram with the 31 concordant data points. Five analyses yielded dates below 1.45 Ga, which are considered as contamination and will not be discussed further. Four analyses gave dates above 1.45 Ga. The calculated concordia age of the cluster around 1.45 Ga is shown in Figure 29 and yielded the age of 1457 ± 2.5 Ma, which is considered as a protolith age of the metarhyolite. The four ages above 1.45 are considered to inherited grains and these are presented in a histogram in Figure 30.

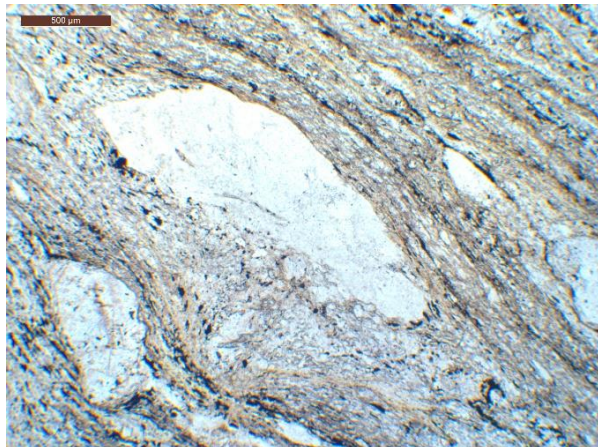


Figure 25: Thin section photograph of the sample UF 30 in plain polarized light (ppl) and magnification 40x

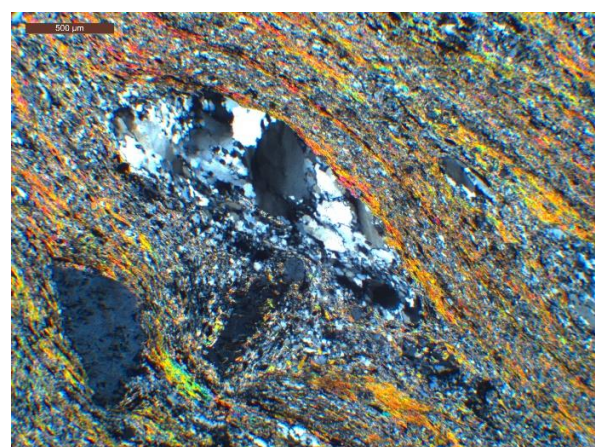


Figure 26: Thin section photograph of the sample UF 30 in plain polarized light (xpl) and magnification 40x

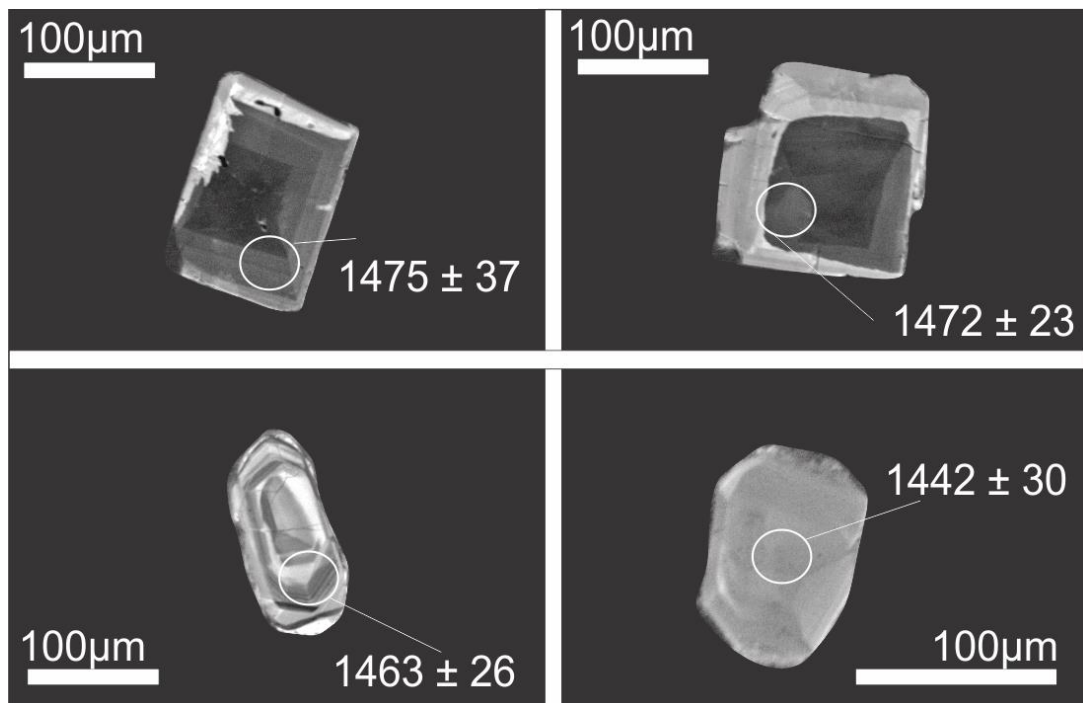


Figure 27: Cathodoluminescence images of representative detrital zircon grains from sample UF 30. The circles represent the analysis spots for each grain, and the numbers to the yielded age.

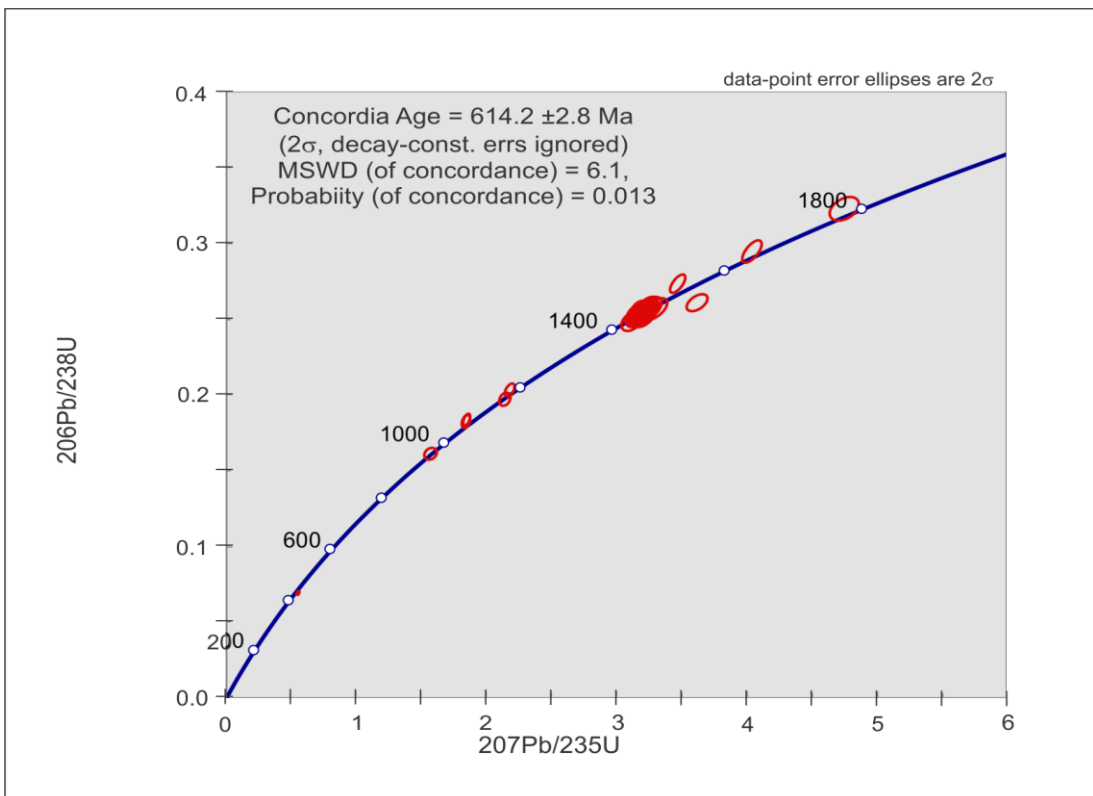


Figure 28: Concordia diagram showing the age spectrum for the sample UF 30,

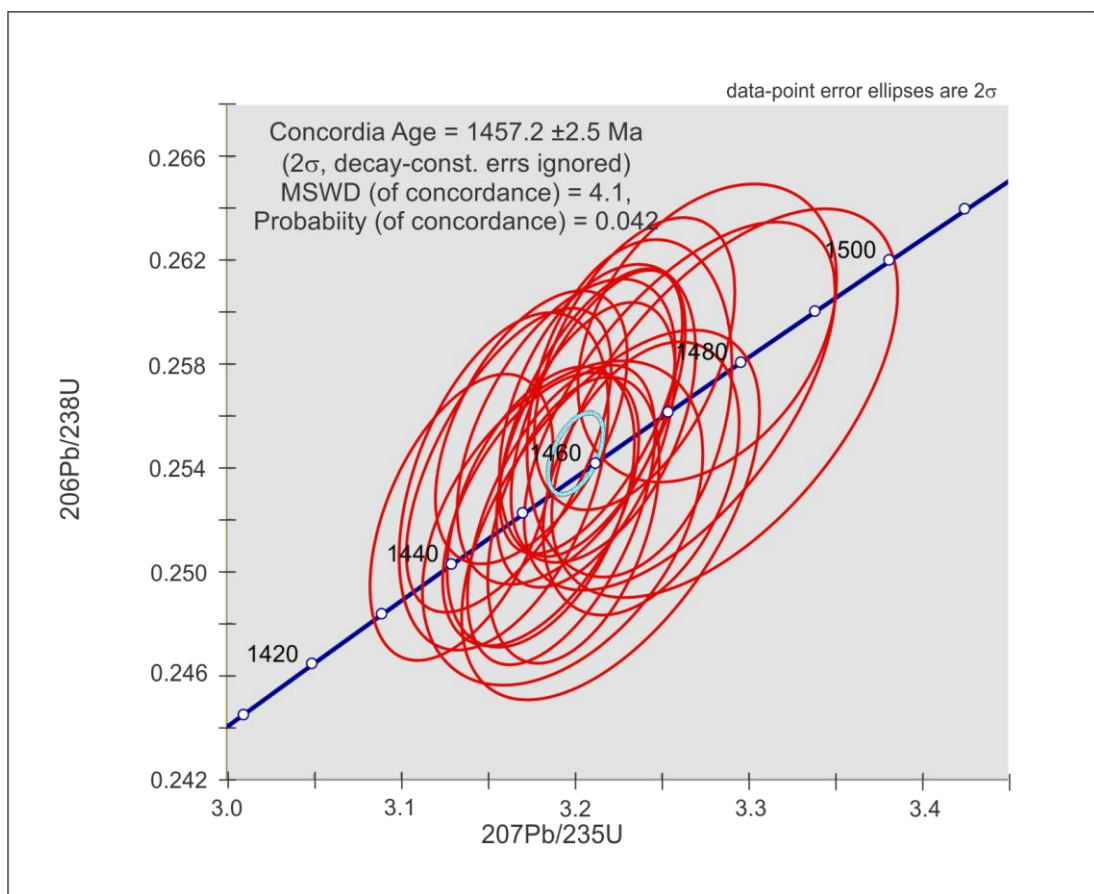


Figure 29: Cluster of ages around 1457 Ma for sample UF 30. Calculated cordia age is c. 1460 Ma.

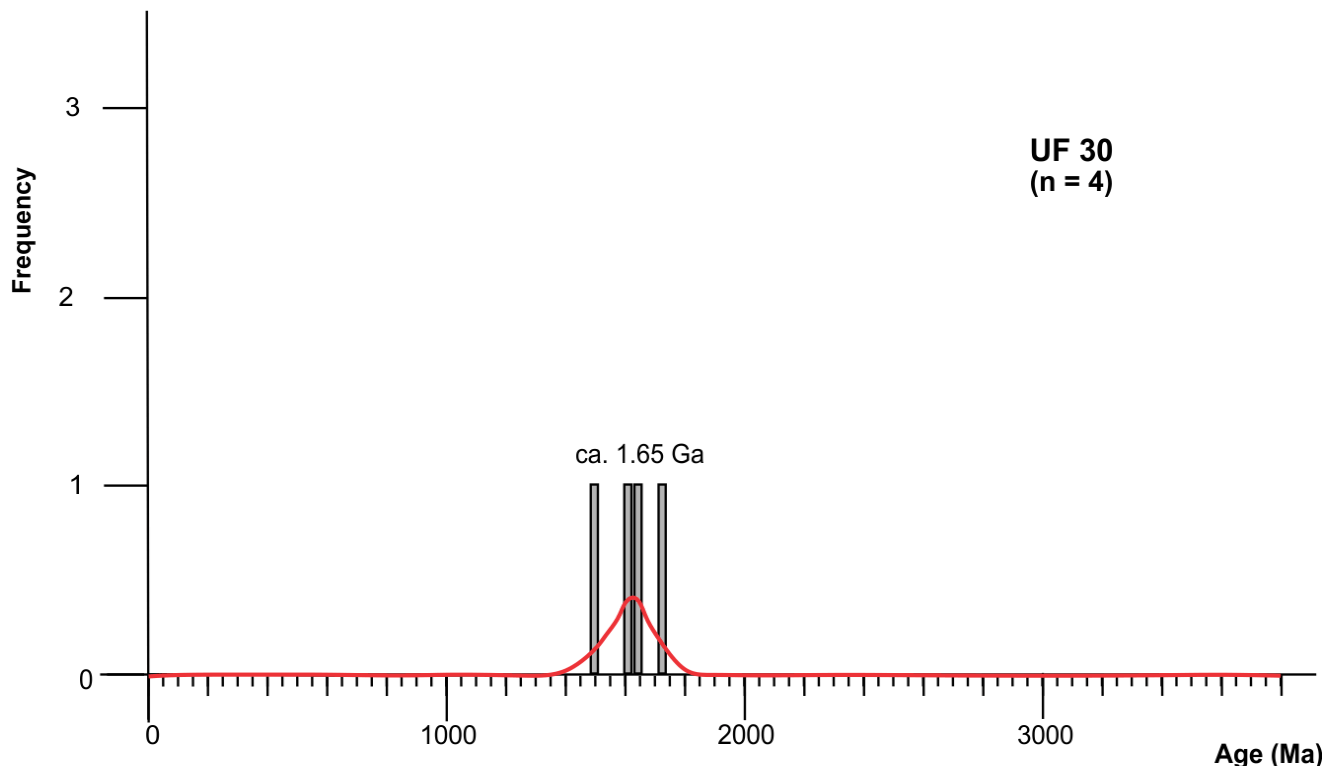


Figure 30: Histogram and Kernel-density plot for xenocrystic zircon ages for sample UF 30.

3.3.4 Sample UF 22

Sample UF 22 (-34.53078 -55.16303) represents a granite intrusion into the Zanja del Tigre Complex (Figure 5). The granite UF 22 looks in situ as a very light rock. However, on the fresh surfaces the color gets more pink. This granite has higher proportion of mafic minerals, compared with the other granite sample UF 24. It consists of mainly the minerals quartz, plagioclase, K-feldspar, chloritized biotite, apatite and minor amounts of zircon, rutile, titanite (Figure 31 and Figure 32). The zircon grains range in size from 110 to 270 μm in length and 60 to 150 μm in width. Most of the zircon grains have elongated shape with prismatic habit; a few grains have oval shape with rounded edges. CL images (Figure 33) reveal that the zircons in this sample all have zoning, mostly of oscillatory type. The vast majority of grains have xenocrystic cores and few of them are quite complex. Fractures are common and occurs in a high number of the grains, while inclusion are rarer but still present in some zircon grains.

Analyses of 70 zircon grains yielded 70 U-Pb ages and the resulting concordia diagram is shown in Figure 34. The youngest dates are shown in Figure 35 and this is considered the magmatic age of the rock. The last figure (Figure 38) shows the age spectrum for zircons older than the magmatic age, these probably represents xenocrystic zircons which were trapped in the magma during melting of the source rock. From Figure 35 the cluster of younger zircons can be seen, in Figure 36 the data that are linearly arranged next to it. The

linearly arranged data is interpreted as the zircons having variable amount of common lead. When putting a discordia through the linear data a lower intercept age is found at 611 ± 3 Ma. A concordia age can be calculated from the cluster of concordant or nearly-concordant data. Using the data with discordance of $\leq 2\%$, the resulting concordia age is 614 ± 3 Ma (Figure 37). This is the same, within error, as the lower intercept age.

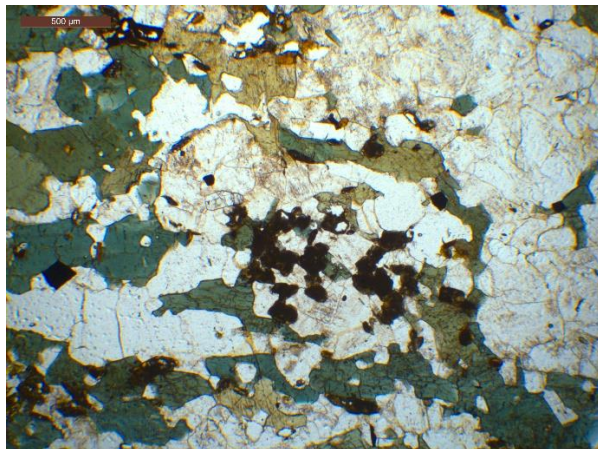


Figure 31: Thin section photograph of the sample UF 22 in plain polarized light (ppl) and magnification 40x.

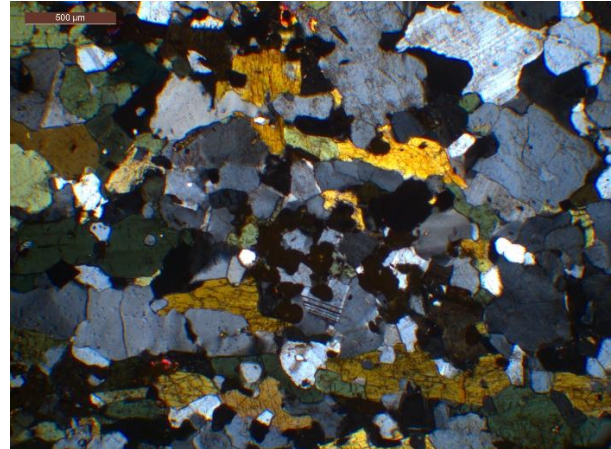


Figure 32: Thin section photograph of the sample UF 22 in cross polarized light (xpl) and magnification 40x.

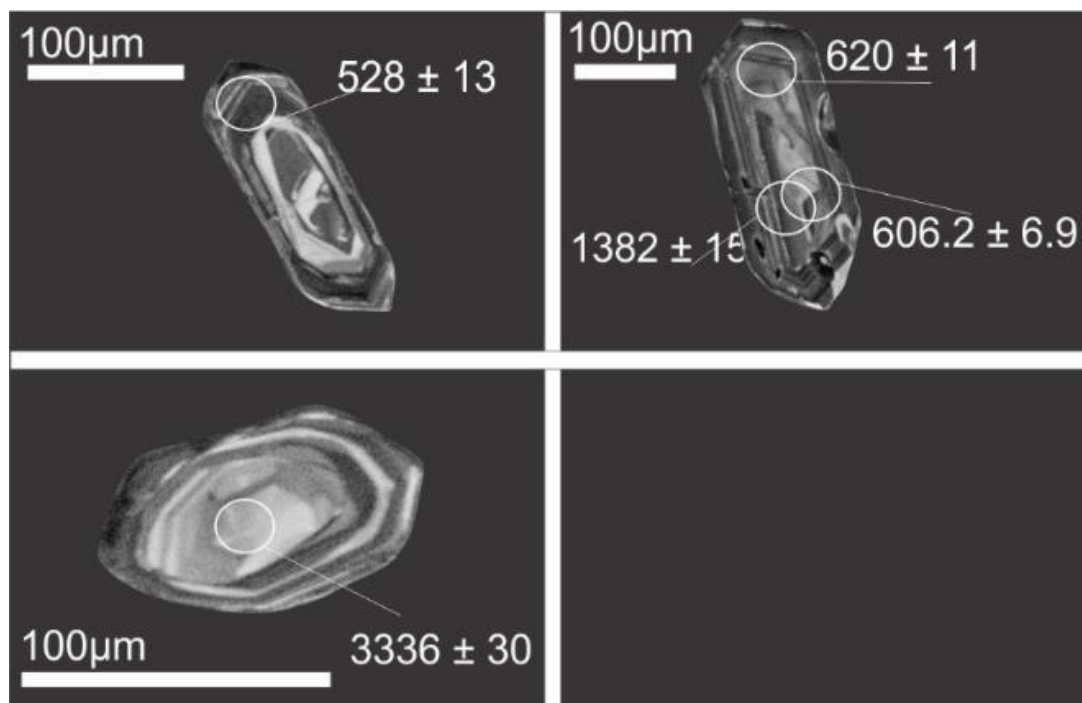


Figure 33: Cathodoluminescence images of representative detrital zircon grains from sample UF 22. The circles represent the analysis spots for each grain, and the numbers to the yielded age.

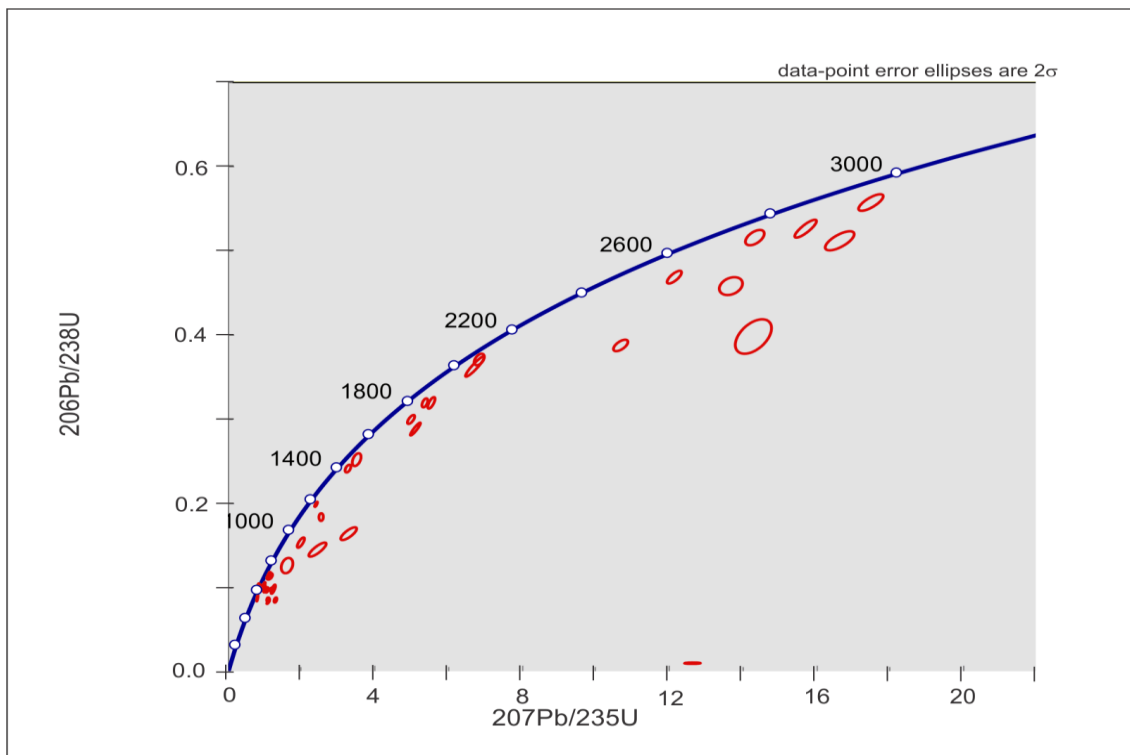


Figure 34: Concordia diagram of sample UF 22 showing the whole age spectrum.

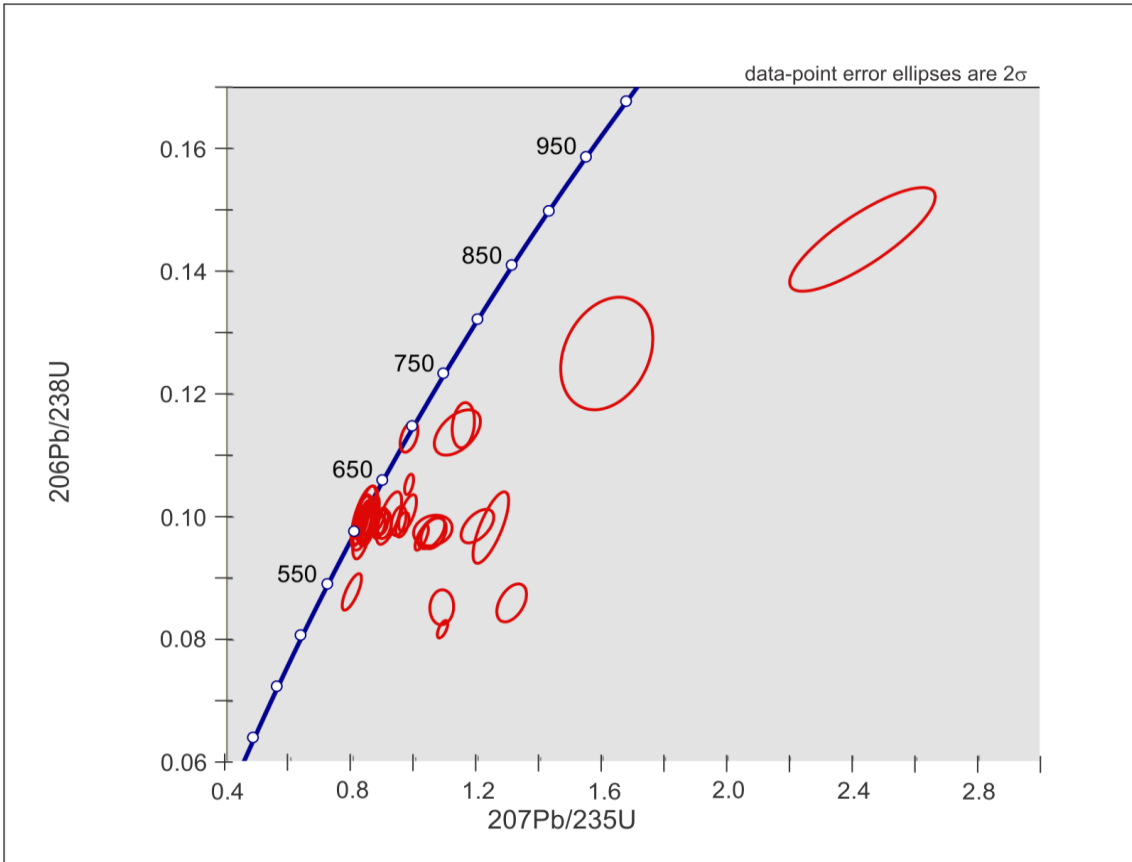


Figure 35: Concordia diagram of sample UF 22 showing the young population of ages.

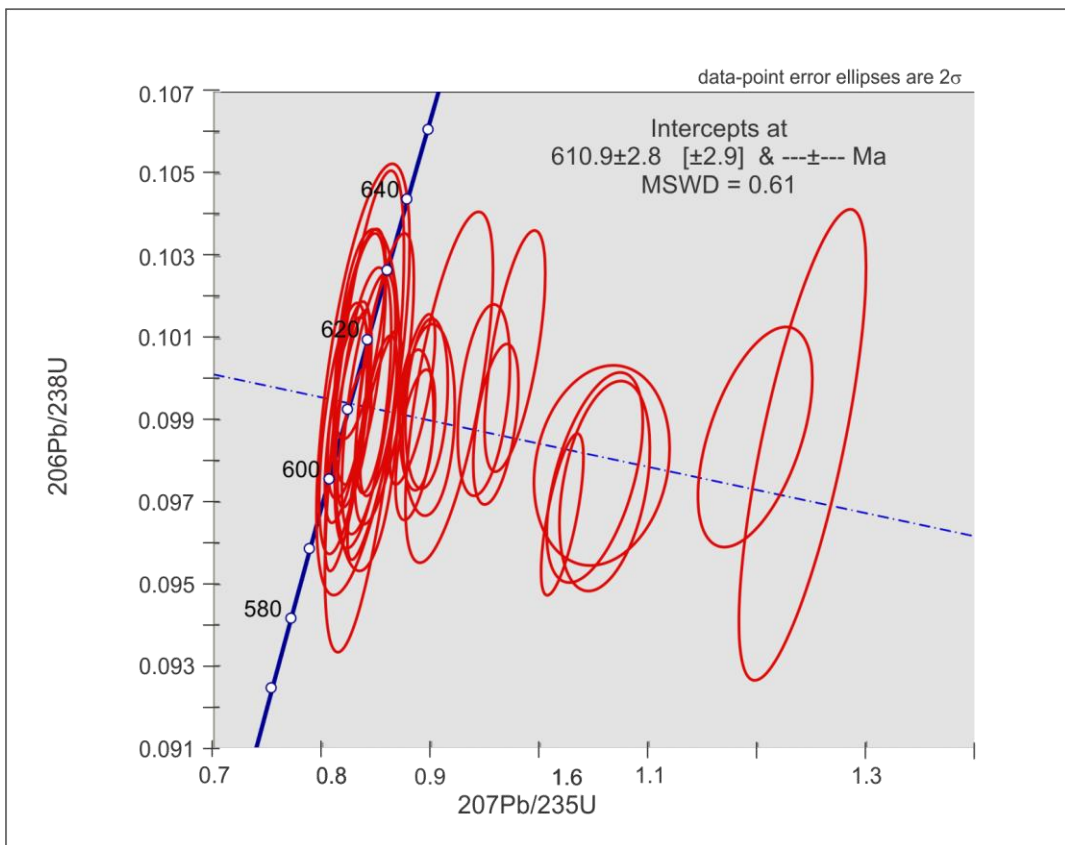


Figure 36: Calculated intercept age of sample UF 22, c. 610.9 ± 2.8 Ma

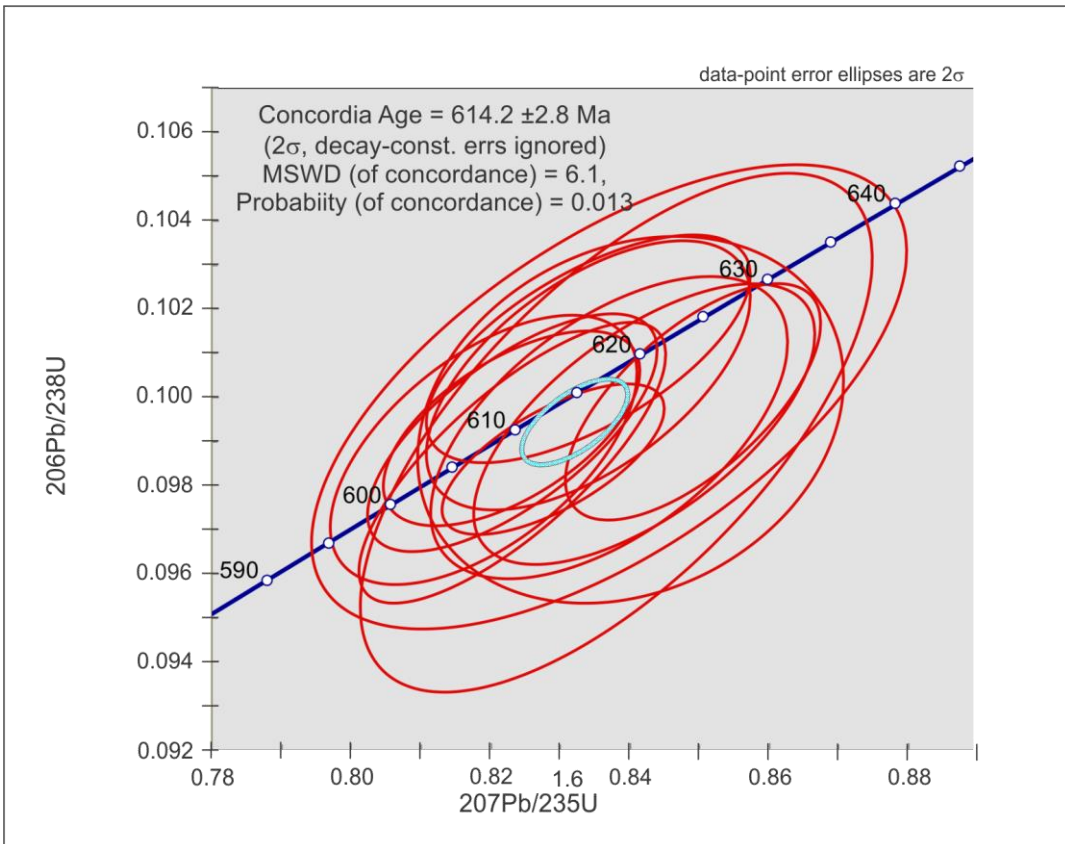


Figure 37: Calculated concordia age of sample UF 22, 614.2 ± 2.8

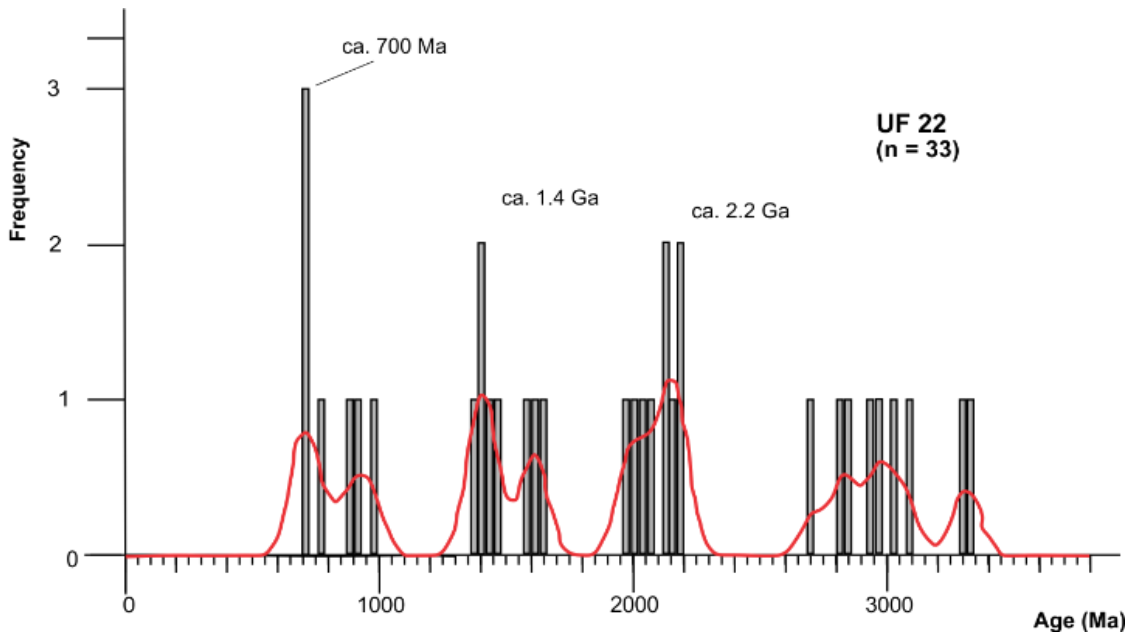


Figure 38: Kernel-density and histogram of inherited zircons in sample Uf 22. It shows peaks at c. 700 Ma, 1.4 Ga and 2.2 Ga

3.3.5 UF 24

Sample UF 24 (-34.05531 -55.33584) is a granite associated with granitic gneisses and migmatites of the basement of the Nico Perez Terrane (Figure 5). This granite has pink color both in situ and in a hand sample. There is no obvious foliation in this granite. It is much lighter in color than UF 22 and has less mafic minerals. The sample consists mainly of quartz, plagioclase and K-feldspar with minor amounts of chloritized biotite, zircon and opaque minerals (Figure 39 and Figure 40). The sizes of the zircons range from 80 to 250 μm in length and 30 to 150 μm in width. A large portion of the zircon grains reveals prismatic habit. Sharp crystal faces can be clearly seen on the CL images (Figure 41), especially for the elongated crystals, whereas the smaller grains are more rounded or oval with less prominent crystal faces. The CL images also reveal that all zircons have zoning, most of them oscillatory zoning, but a few zircons have only a faint trace of zoning. Most of the zircons have a xenocrystic core and a large portion of the zircons are fragments of larger crystals. There are few crystals with inclusions, and many of the grains have fractures.

Analysis of 24 zircon grains yielded 24 ages which is represented in a concordia diagram (Figure 42) and in Figure 43 the cluster of younger ages and the linearly arranged data next to it. The linear data is interpreted as caused by the zircons having variable amounts of common lead.

These data are considered as representing the magmatic age of the rock. The younger cluster is considered the magmatic age of the rock, and the zircons older than c. 650 are probably inherited zircons, trapped in the magma during melting of the source rock. These older zircons are presented in Figure 46 as an age spectrum. Figure 45 shows the calculation of the Discordia put through the linear data; this gives a lower intercept age at 614.8 ± 3.3 Ma. The calculation of a Concordia age with $\leq 2\%$ discordance is shown in Figure 44, the calculation gives a Concordia age of 615.7 ± 3.4 Ma which is equal (within error) to the intercept age.

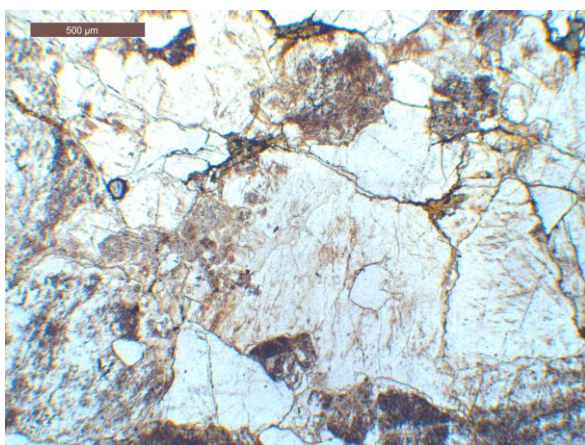


Figure 39: Thin section photograph of the sample UF 24 in plain polarized light (ppl) and magnification 40x.

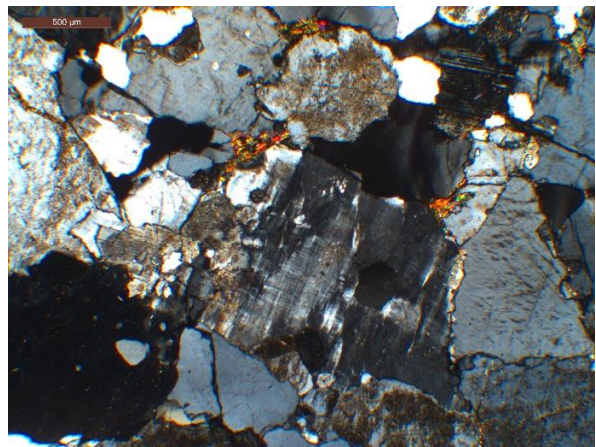


Figure 40: Thin section photograph of the sample UF 24 in cross polarized light (xpl) and magnification 40x.

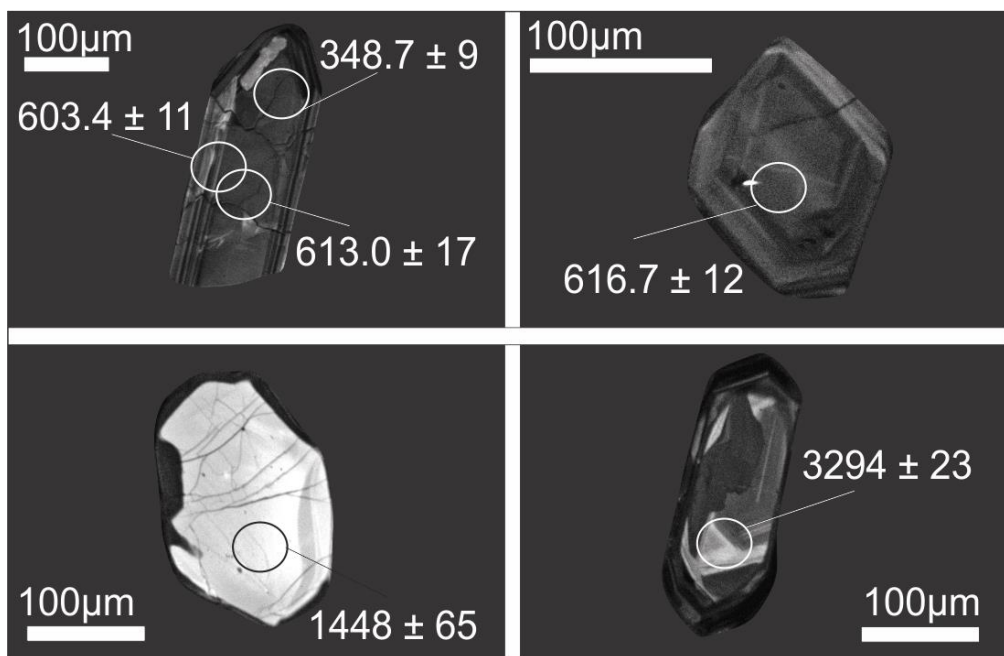


Figure 41: Cathodoluminescence images of representative detrital zircon grains from sample UF 24. The circles represent the analysis spots for each grain, and the numbers to the yielded age.

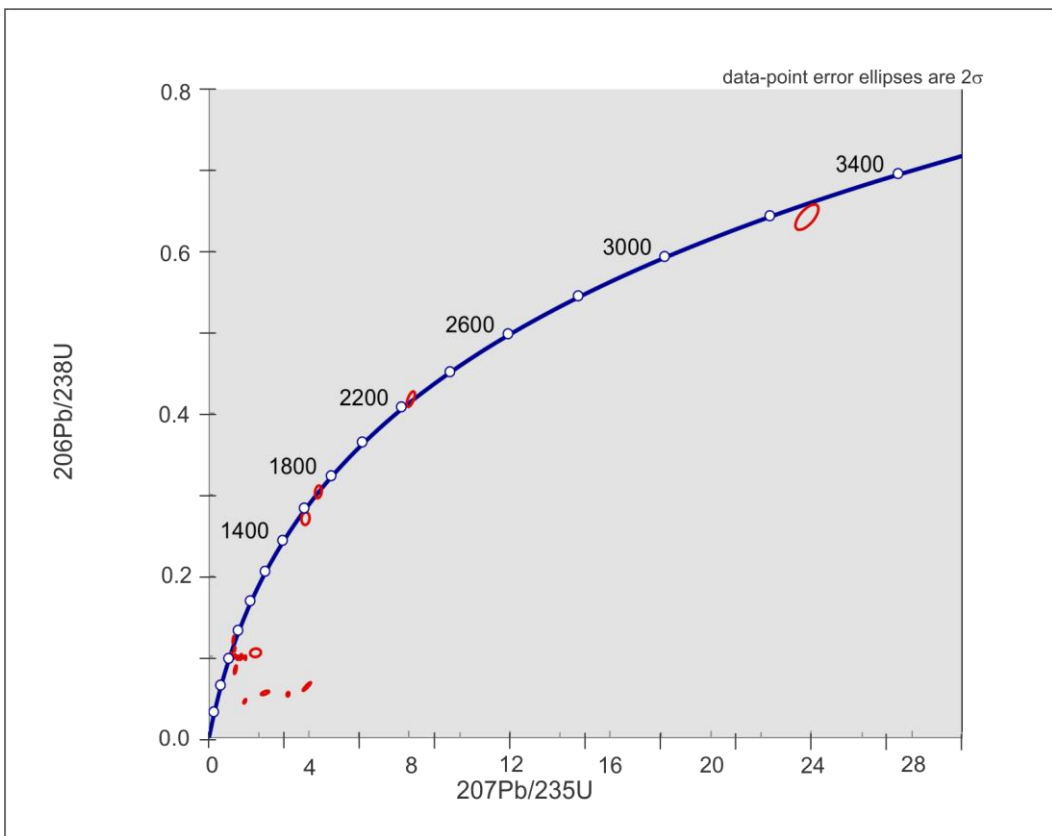


Figure 42: Concordia diagram of sample UF 24 showing the whole age spectrum.

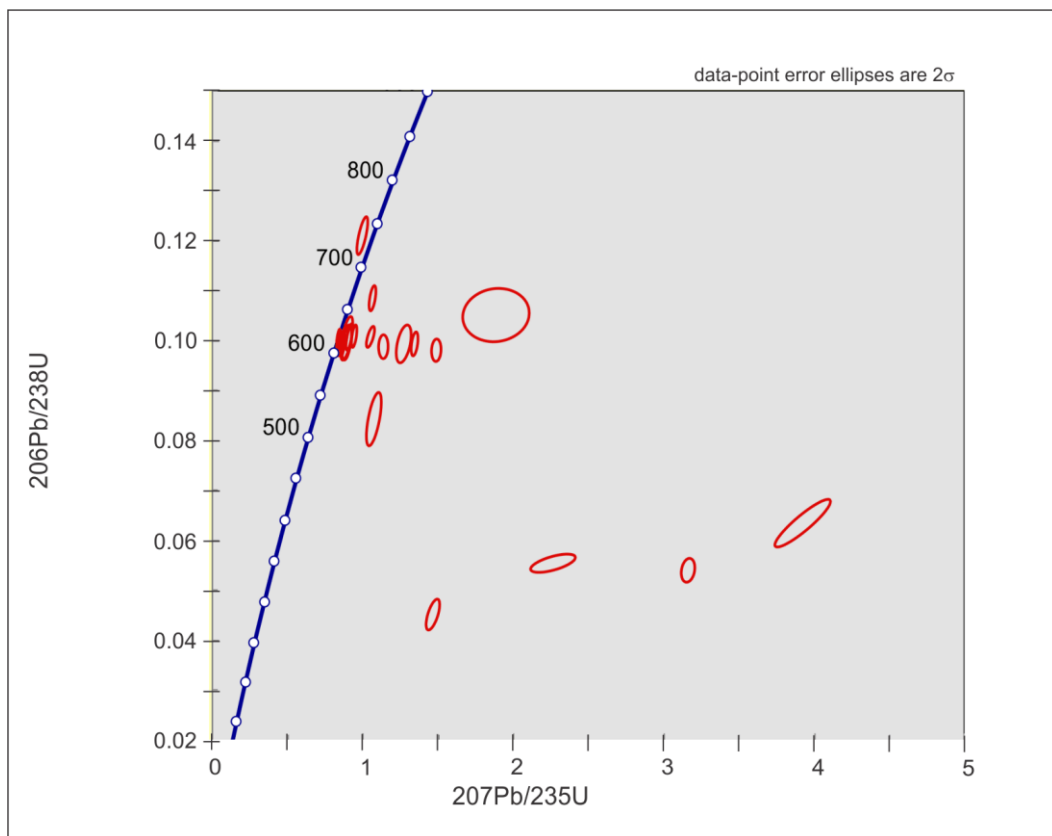


Figure 43: Concordia diagram of sample UF 24 showing the younger data.

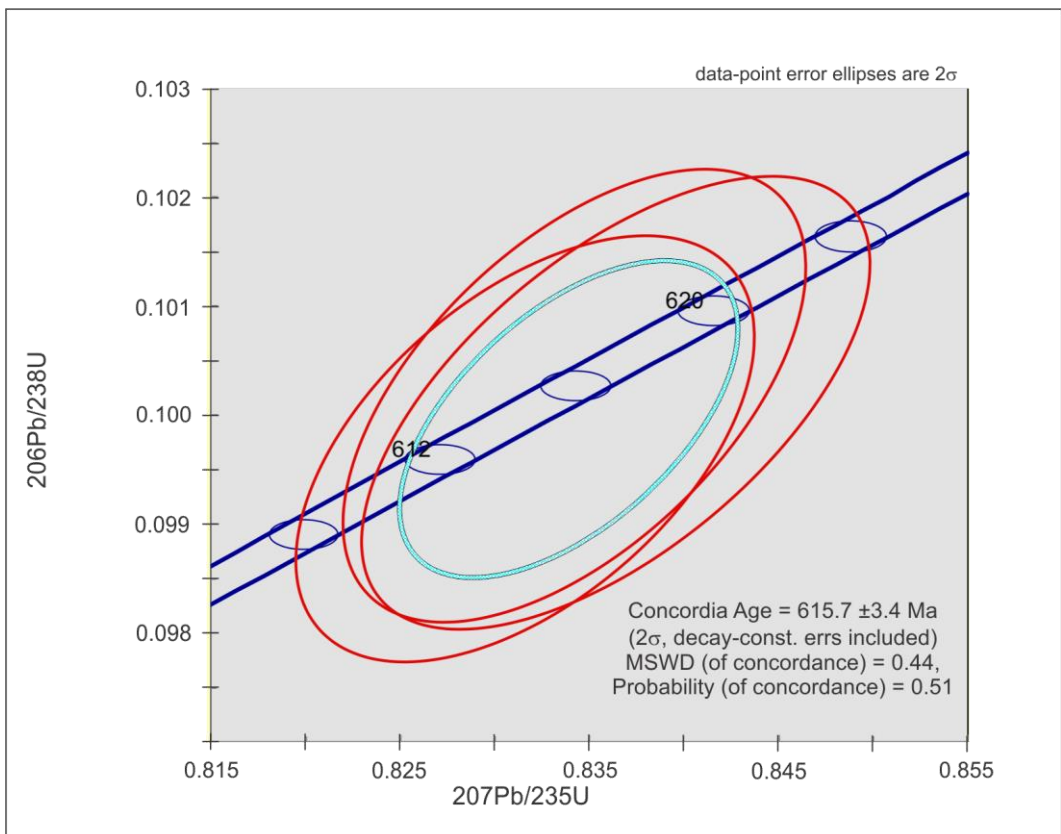


Figure 44: Calculated concordia age for sample UF 24, 615.7 ± 3.4 Ma.

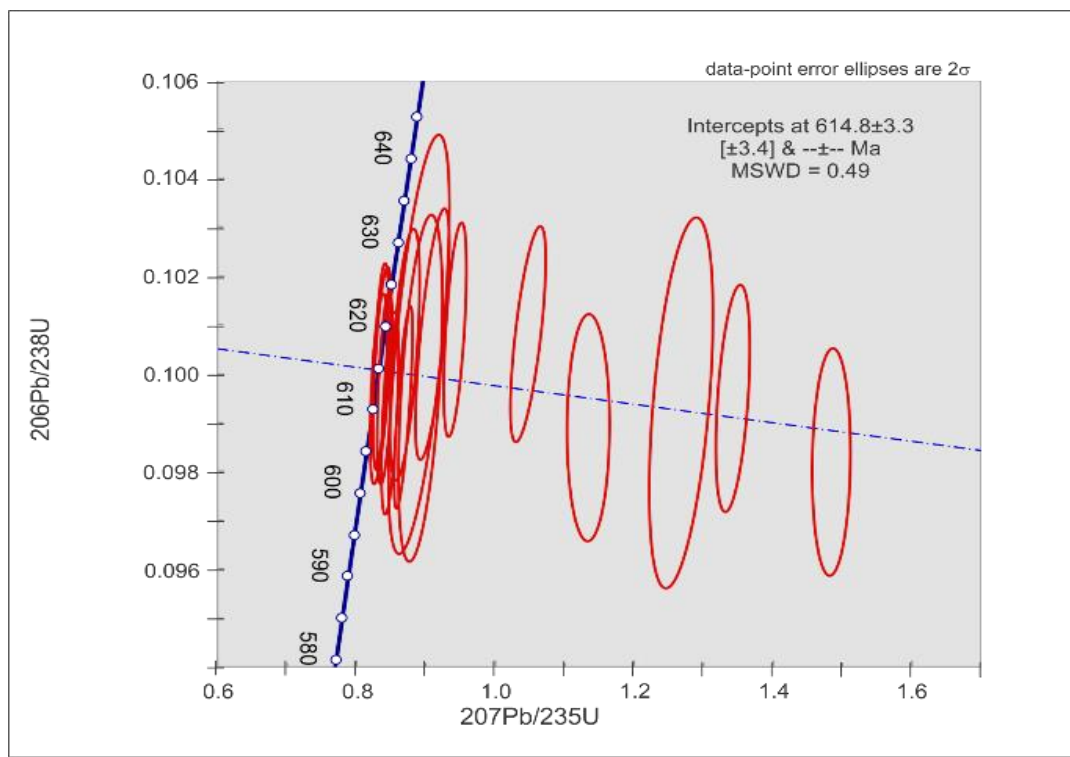


Figure 45: Concordia diagram with linear array of younger ages for sample UF 24, and calculated intercept age 614.8 ± 3.3 Ma.

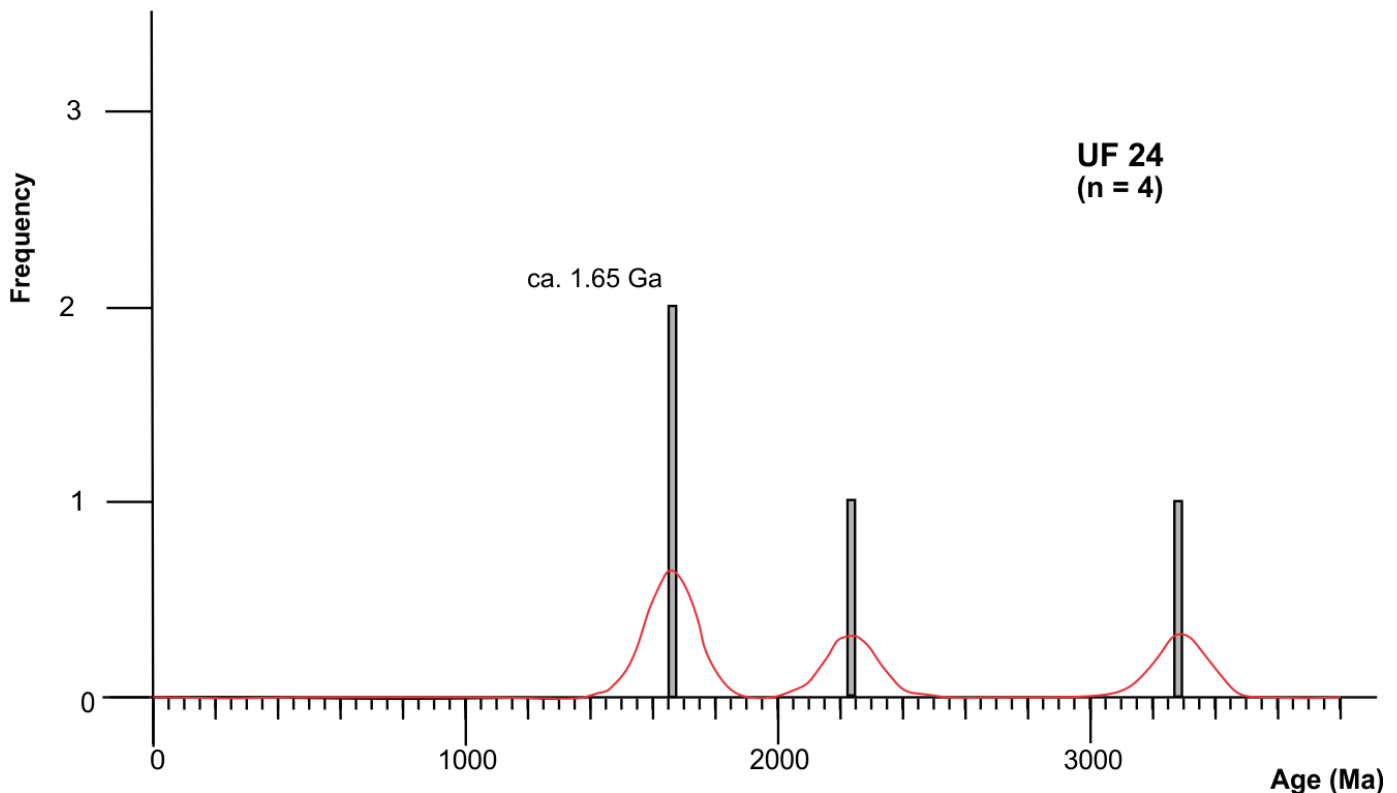


Figure 46: Inherited zircon data for sample UF 24

3.4 Samples from Namibia

3.4.1 Sample NS 32

Sample NS 32 (-27.904600, 15.93905) comes from the Marmora Terrane in the Gariep Belt (Figure 8) and it is a medium-grained metamorphosed sedimentary rock. It has a grey color with visible white quartz and mafic minerals in a hand sample. In the microscope, it has a mineral assemblage of quartz, plagioclase, biotite, chlorite, white mica, opaque minerals and an accessory amount of zircon and titanite (Figure 47 and Figure 48). The zircon ranges in size from 100 to 250 μm in length and 50 to 100 μm in width. The majority of the grains are prismatic, but a few grains are ovoid to oval. In this sample, numerous grains are fragments of larger crystals. CL images (Figure 49) of the sample have shown a large portion of zircons with oscillatory zoning, while a few have sector zoning. A large portion of the zircons has texturally distinguishable cores, and quite a few of them are very complex, some with multiple cores. A few zircons show very faint zoning, or no zoning at all. In this sample, inclusions in zircon grains are common, while fractures occur in a minor number of the zircons.

Analysis of 126 zircon grains yielded 104 concordant U-Pb ages and the resulting age spectrum is presented in Figure 50 the sample has shown no dates below c. 900 Ma. The sample shows the majority of data distributed between 1.0 and 1.4 Ga with one major peak at 1.1 Ga and another one at c. 1.2 Ga. Individual zircon dates can be seen nearly continuously from c. 900 Ma to 3.0 Ga with one peak at 2.05 Ga.

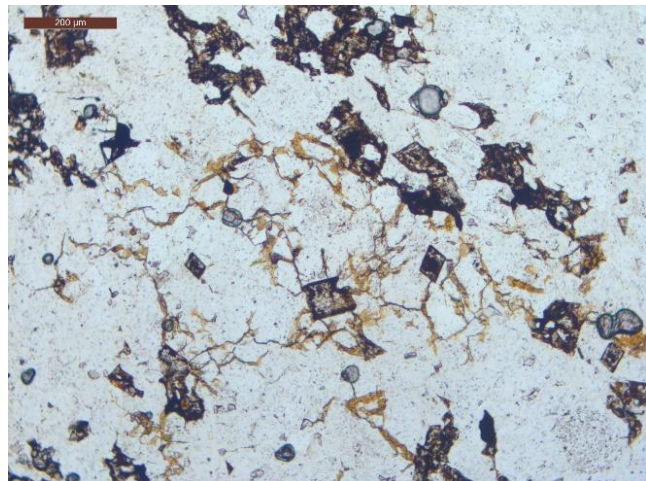


Figure 47: Thin section photograph of the sample NS 32 in cross polarized light (ppl) and magnification 100x.

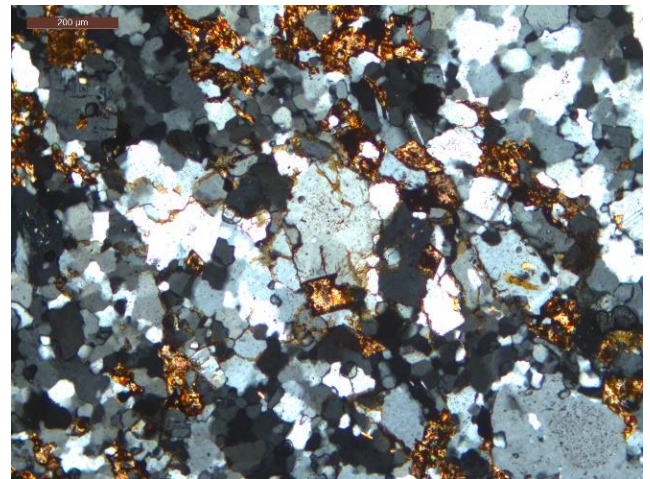


Figure 48: Thin section photograph of the sample NS 32 in plain polarized light (xpl) and magnification 100x.

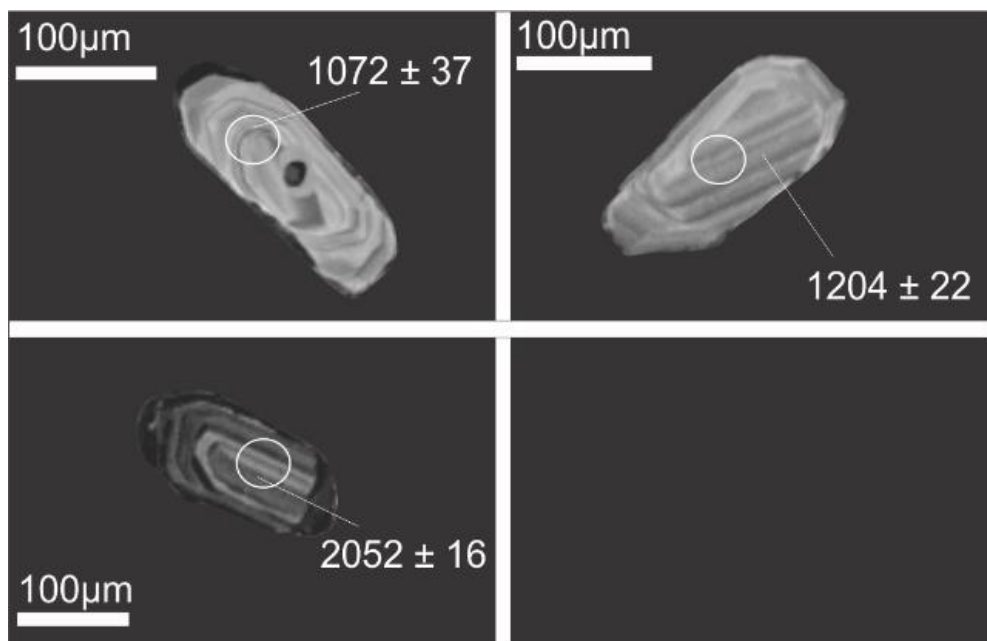


Figure 49: Cathodoluminescence images of representative detrital zircon grains from sample NS 32. The circles represent the analysis spots for each grain, and the numbers to the yielded age.

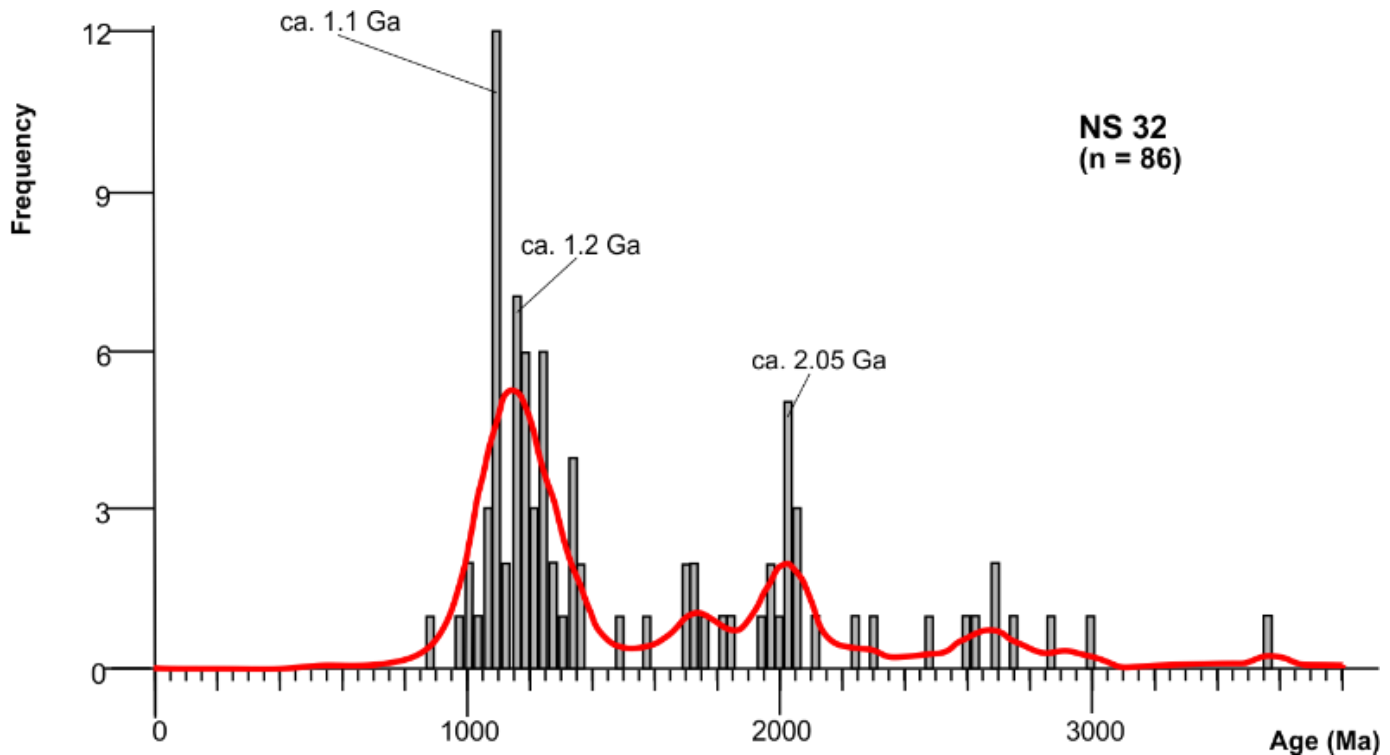


Figure 50: Histogram and Kernel-density plot of detrital zircon sample NS 32. The graph shows two peaks, one major at c. 1.1 Ga and a smaller peak at 2.05 Ga.

3.4.2 Sample NS 44

Sample NS 44 (-28.5575833 16.5014333) also comes from the Marmora Terrane (Figure 8) and is a fine-grained metamorphosed sedimentary rock. It has a matte grey shine, and foliation is visible as dark banding. The sample consists mostly of white mica, quartz, plagioclase and K-feldspar, but has minor amounts of biotite, chlorite, garnet and opaque minerals, as well as accessory amount of zircon and rutile (Figure 51 and Figure 52). The size of the zircon grains ranges from 100 to 220 μm in length and 50 to 100 μm in width. A large portion of the grains reveal shapes that vary from elongated to oval, with a minor portion of the elongated grains having a rectangular shape. The rest of the elongated crystals show prismatic habit, many of the grains are fragments of larger crystals. Most of the zircons have oscillatory zoning with some showing a very complex core or even multiple cores, very few grains show little to no zoning at all. The CL images (Figure 53) show that while some grains have inclusions and fractures, that both are less common than in sample NS 32.

Analysis of 139 zircon grains yielded 122 concordant U-Pb ages and the resulting age spectrum is presented in Figure 54. The data show peaks at c. 650 Ma, c. 750 Ma, c. 1.0 Ga,

1.85 Ga and a smaller peak at c. 2.6 Ga. Individual zircon dates can be seen from c. 1.1 Ga to c. 1.8 Ga.

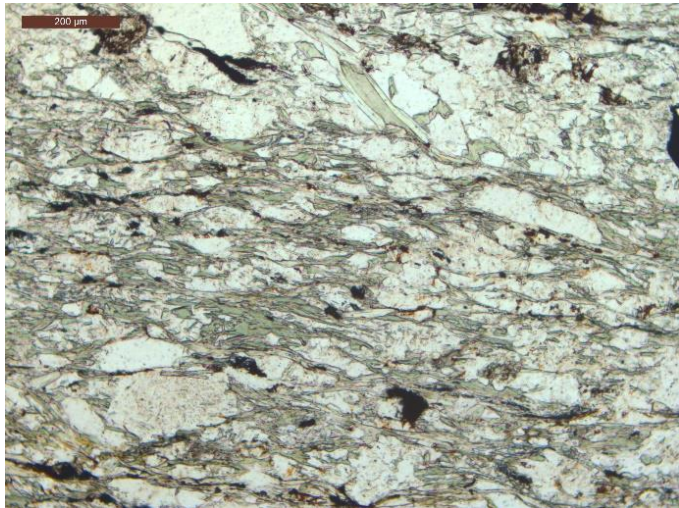


Figure 51: Thin section photograph of the sample NS 44 in cross polarized light (ppl) and magnification 100x.

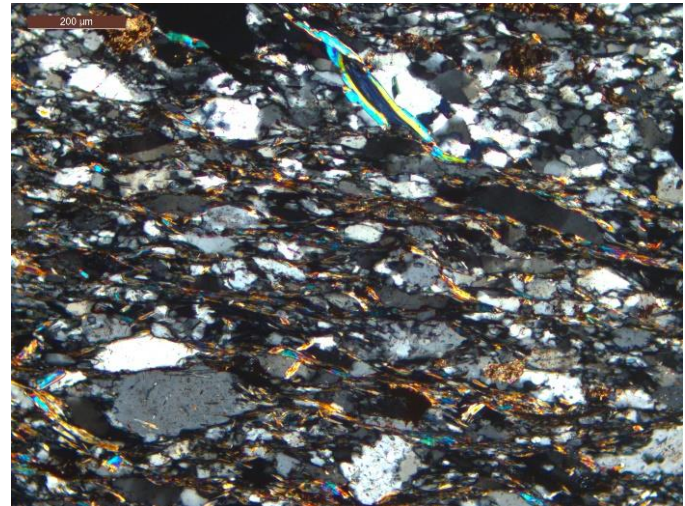


Figure 52: Thin section photograph of the sample NS 44 in plain polarized light (xpl) and magnification 100x.

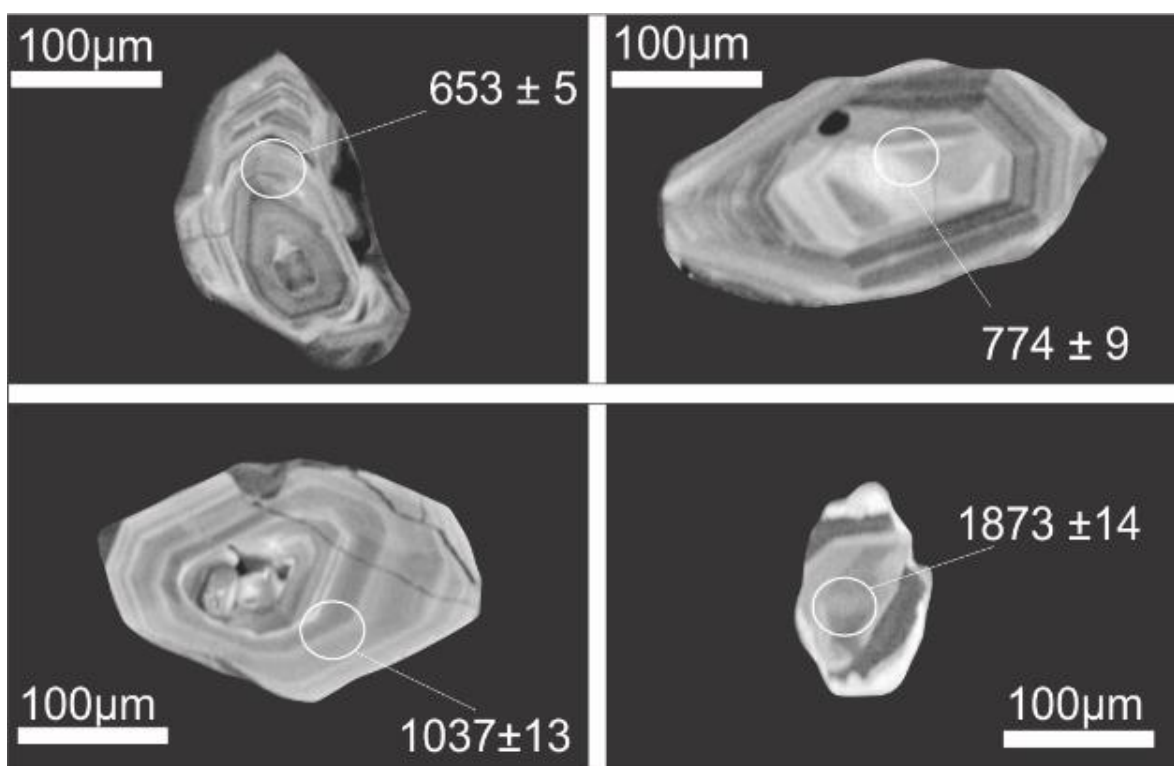


Figure 53: Cathodoluminescence images of representative detrital zircon grains from sample NS 44. The circles represent the analysis spots for each grain, and the numbers to the yielded age.

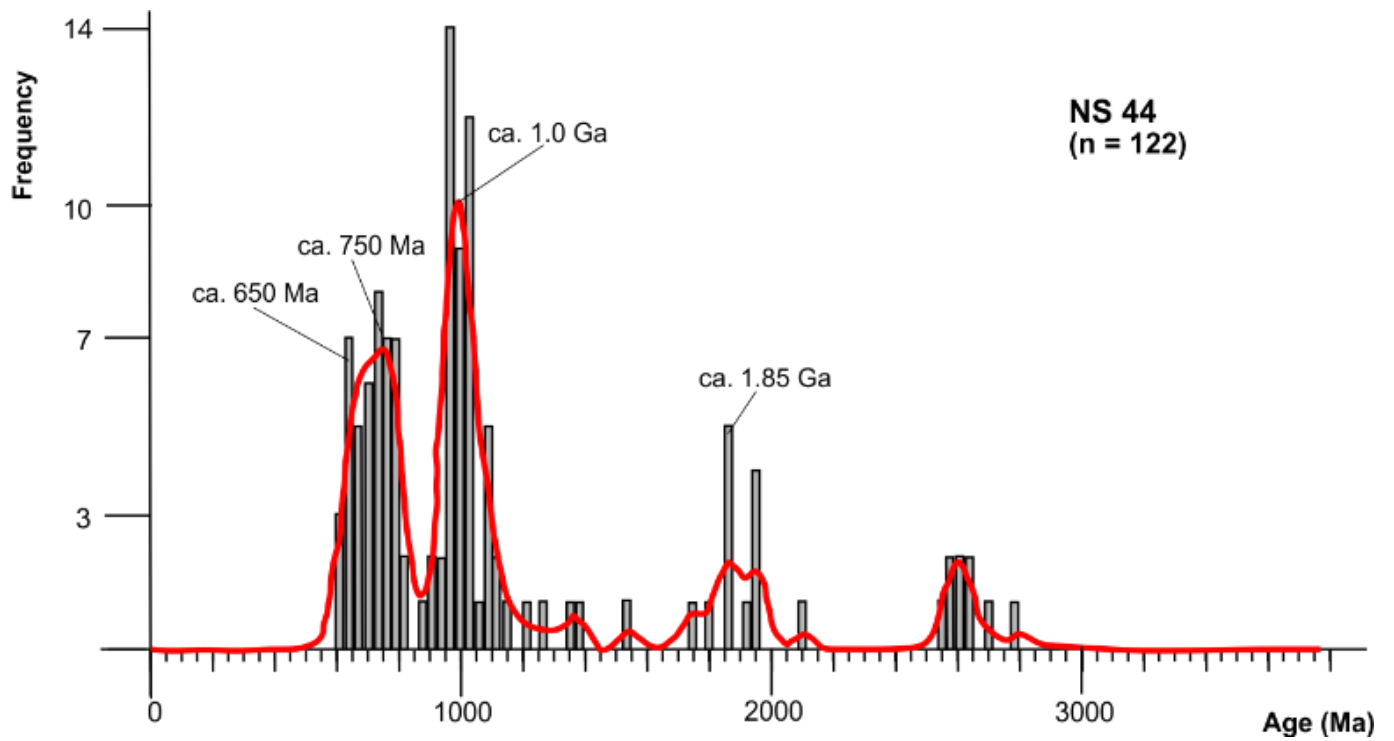


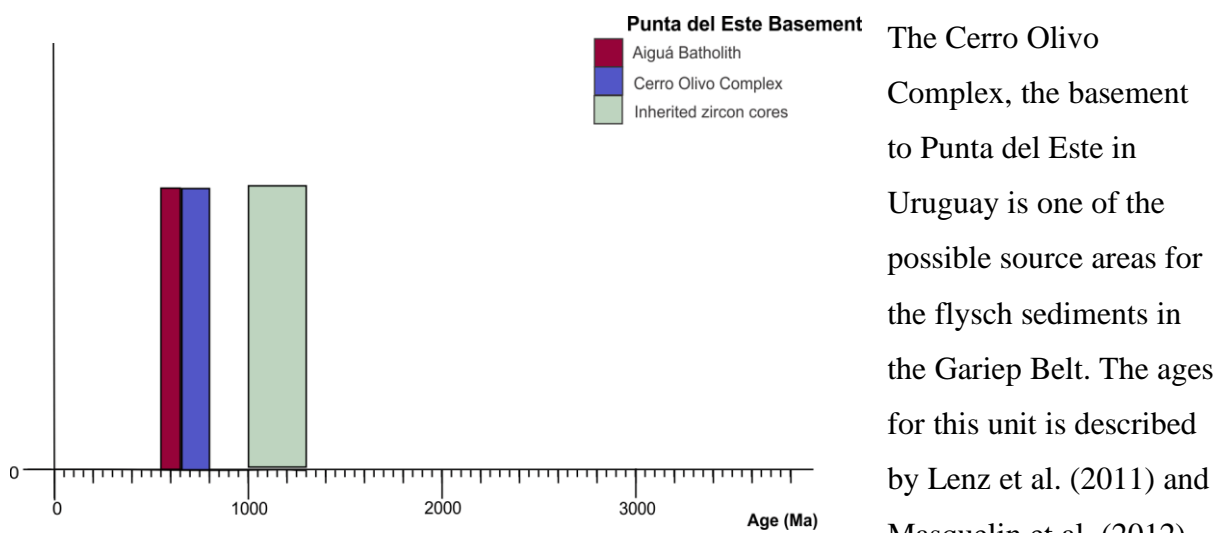
Figure 54: Kernel-density and histogram plot for the sample NS 44, showing the age spectra for this sample show several peaks at c. 650 Ma, 750 Ma, 1,0 Ga, 1.85 Ga and 2.6 Ga

4 Discussion

4.1 Potential source areas

Konopásek et al. (2017) discussed that the flysch sedimentation on the African side of the Kaoko-Dom Feliciano-Gariep orogenic system is the result of erosion of the orogenic front developing from ca. 650 Ma on the South American side of the orogen. Thus, there are three possible units that could have provided detrital material for the flysch sedimentation in the Gariep Belt - the Nico Perez Terrane, Cerro Olivo Complex and Piedra Alta Terrane. They are each presented in the following sections.

4.1.1 Cerro Olivo as potential source region for the flysch sedimentation in the Gariep Belt



inherited ages in xenocrysts from c. 800 Ma to 2165 Ma, with the majority from 1.3 – 1.0 Ga. Further they found the crystallization age to vary from c. 802 – 767 Ma and the maximum age for the metamorphic peak at 676 Ma (Figure 55).

The Agiuá Batolith shows a span of pluton ages of granites in connection with the Dom Feliciano Belt to be from 634 – 564 Ma (Lara et al., 2020).

4.1.2 Nico Perez Terrane as potential source region for the flysch sedimentation in the Gariep Belt.

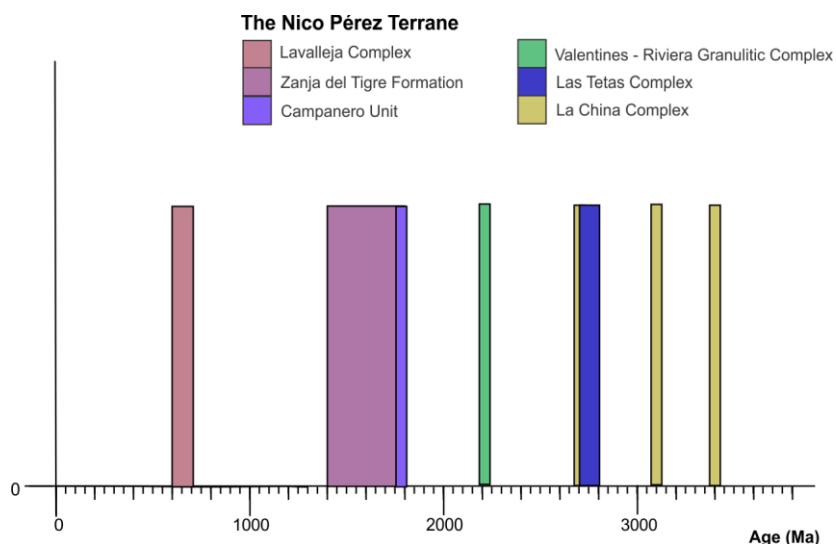


Figure 56: Histogram over protolith ages in the Nico Perez Terrane.

The Nico Perez Terrane (NPT) is divided into two blocks - the Pavas block to the south and the Cerro Chato block to the north and they are divided by a shear zone (Figure 4). The oldest rocks found in the NPT are the Archean to Paleoproterozoic basement La China complex and the

Archean to Paleoproterozoic cover of the Las Tetas Complex. The La China Complex has been dated at 2.7, 3.1 and 3.4 Ga (Oyhantçabal et al., 2018). The northern part of the NPT, the Cerro Chato block consists mainly of the Valentine Riviera Granulitic Complex, the Campanero unit and the Valentines and Vichadero formations. The Valentines – Riviera Granulitic Complex have been dated to c. 2.2 Ga (Oyhantçabal et al., 2018). Lastly the Illescas intrusion, a rapakivi-type granite, has been dated to c. 1.75 Ga (Oyhantçabal et al., 2018). The Campanero Unit is a basement inlier in the Dom Feliciano belt, it is located between the Sierra Ballena shear zone and the schist belt. The Campanero unit's supracrustal rocks and orthogneisses are interpreted as relicts of the metasedimentary rocks of the Las Tetas Complex (Oyhantçabal et al., 2018). A U-Pb zircon age of 1.7 Ga was obtained from an orthogneiss, and interpreted as the protolith age of the Campanero unit (Oyhantçabal et al., 2009). In the metasedimentary formation of Zanja del Tigre Complex, two metavolcanosedimentary sequences have been identified, both of which have been dated to c. 1.5 -1.4 Ga.

The youngest unit in the Nico Perez Terrane, the Lavalleja Group, has ages from c. 700 – 600 Ma (Figure 56).

4.1.3 Piedra Alta Terrane as potential source region

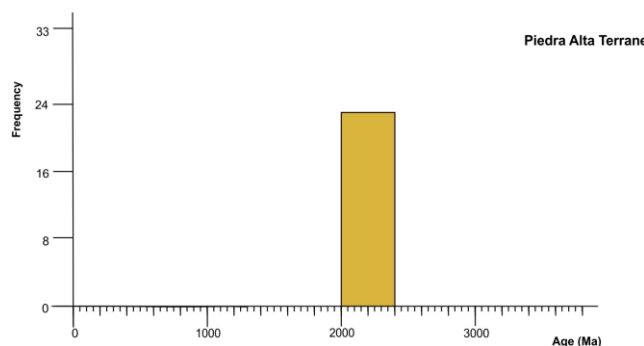


Figure 57: Histogram over protolith ages in the Rio de la Plata craton.

The Rio de la Plata craton is represented by the Piedra Alta Terrane, which lies west of the Sarandi del Yi shear zone (SYSZ), which divides it from the Nico Perez Terrane. The age of the Piedra Alta Terrane (Figure 57) is 2.4 – 2.0 Ga (Oyhantçabal et al., 2011; Preciozzi et al., 1999).

4.1.4 New Data

Samples from Uruguay were collected to complement the existing dataset of the potential source rock ages from Uruguay. The volcano-sedimentary rock sample LA 227 was collected in the Zanja del Tigre Complex. It has a major peak at 1.45 Ga, the same age found in the metavolcanic rock UF 30 (1457.2 ± 2.5 Ma).

The two studied granitic rocks (UF 22 and UF 24) have very similar protolith ages at c. 614 and 615 Ma. Lara et al. (2020) discussed a regional belt of granitic plutons from southern Brazil to Santa Catarina State in Brazil with magmatic ages between 650 – 550 Ma. The age of the two granitic rock samples collected for this thesis fit with the ages seen in other granitic intrusions. The Aiguá Batolith and the Florianópolis batolith is part of this belt of granitic plutons.

The xenocrystic population of zircons found in UF 22 appears at 700 Ma, 1.4 Ga and 2.2 Ga. This is consistent with the ages seen in the Nico Perez Terrane. The 700 Ma zircons could be xenocrysts from the Lavalleja Group, the 1.4 Ga may represent xenocrystic population from Zanja del Tigre Complex and the 2.2 Ga from the Valentines-Riviera Granulitic Complex. UF 24, which intruded into an older unit, also shows xenocrysts with older ages. It has two zircons at 1.65 and one at 2.25 and one at 3.3 Ga. The 1.65 Ga date corresponds with that of the Zanja del Tigre Complex, while the two older ages correspond with what is seen in the Valentines – Riviera Granulitic Complex and the La Chine complex. UF 30 has 4 xenocrysts, all with ages around 1.65 Ga, which is the age found in the Zanja del Tigre Complex.

The sample LA 227 has, in addition to the 1.45 Ga peak, smaller concentrations of zircons at 1.7, 2.2 and 2.9 Ga and all of these fit with the basement ages found in the Nico Perez

Terrane. The 1.7 Ga age could be either from the Campanero Unit or the Zanja del Tigre Complex. 2.2 Ga age corresponds with what is seen in The Valentines – Riviera Granulitic Complex and the cluster from 3.2 – 2.8 Ga with the La China complex. This pattern of zircon ages is the same as the one found in UF 12b, a sample from the Zanja del Tigre, however it is in a much smaller proportion than what is seen in UF 12b. Which gave the UF 30 an inherited signal close to that of the surrounding rocks it assimilated during the magmatic event.

4.1.5 The African foreland units as a potential source

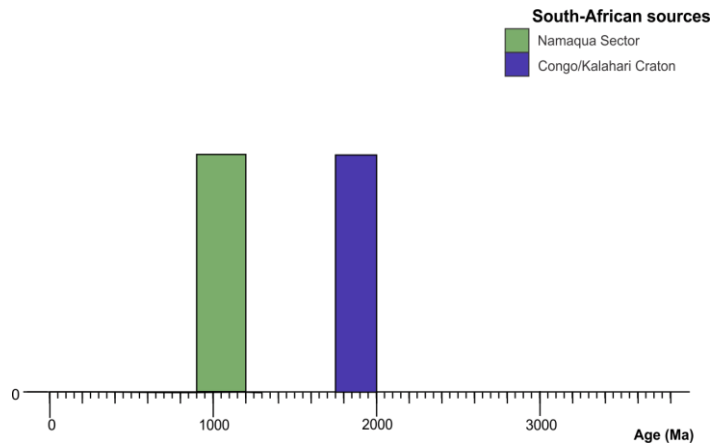


Figure 58: Histogram of protolith ages in the African foreland units.

The Namaqua metamorphic Complex includes Mesoproterozoic (1250 – 1100 Ma) rocks and a Paleoproterozoic (2000 – 1700 Ma) Basement (Becker et al., 2006). In the Sinclear-Helmeringhausen-Awasib (SHA terrane), several intrusions of c. 1.37 Ga are found (Figure 58).

4.1.6 Potential source units for metasedimentary samples of the Zanja del Tigre Complex

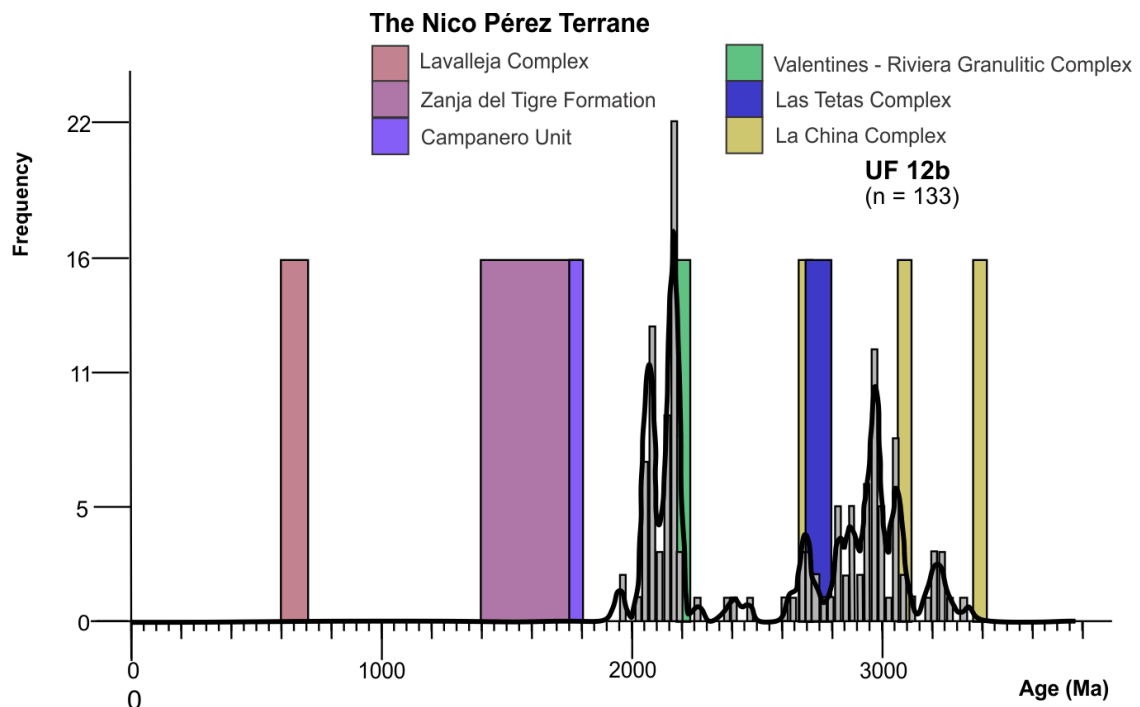


Figure 59: Histogram of detrital zircon ages in the sample UF 12b, over bars representing different geological units with protolith ages in the Nico Perez Terrane

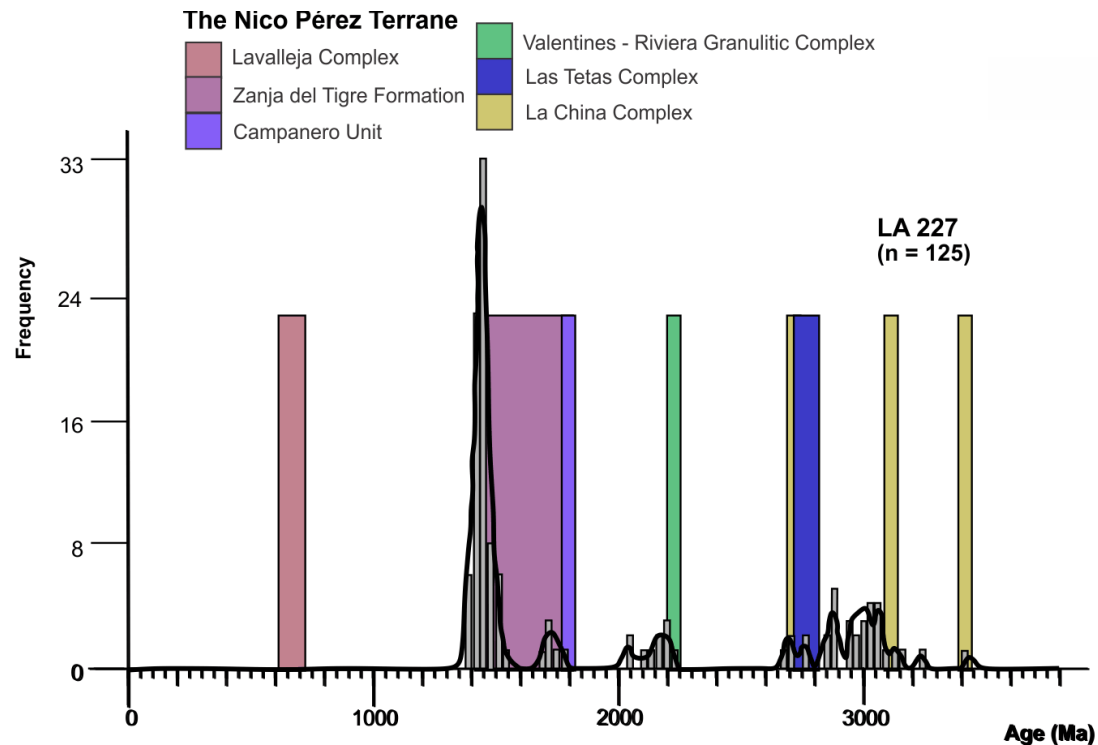


Figure 60: Histogram of detrital zircon ages in the sample LA 227, over bars representing different geological units with protolith ages in the potential source regions.

Detrital zircon population of the sample UF12 b shows Paleoproterozoic and Archean ages from c. 1.9 Ga and older (Figure 59). The peak at c. 2.20 in LA 227 (Figure 60) and at c. 2.15 Ga in UF 12b (Figure 59) fits well with the age found by Oyhantçabal et al. (2018) in the Valentines – Riviera Granulitic Complex. The rest of the population of zircons in sample UF 12b shows ages between c. 3.4 – 2.6 Ga with peaks at 2.7, 2.9, 3.05 and 3.2 Ga. The concentration of the data around 2.7 Ga fits with the ages described for the Las Tetas Complex and the 3.05 Ga peak with the La China Complex. The ages 2.9 – 2.85 Ga found in both samples UF 12b and LA 227 were never reported from rocks of the Nico Perez Terrane. An explanation could be a series of magmatic events from 3.4 – 2.8 Ga, the products of which have been eroded and now they are only seen in detrital populations of the samples. Another explanation could be an existence of still unknown terrane providing zircons of this age.

4.1.7 Interpretation of origin of the presumed flysch samples

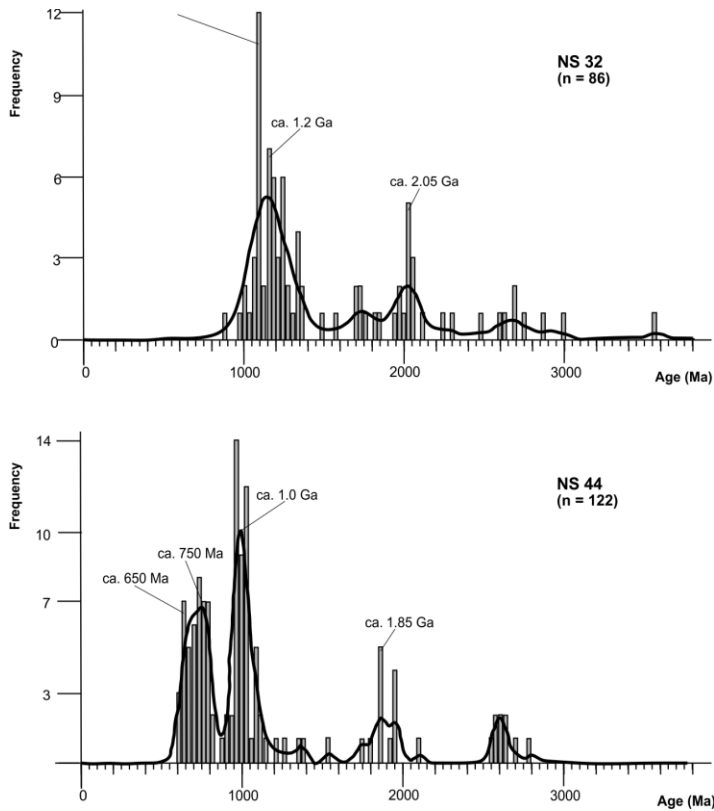


Figure 61: Kernel-density plot and histogram of the two samples thought to be flysch sediments.

The two samples from Namibia (Figure 61), which were presumed to be flysch sediments, show two different age patterns. The sample NS 32 has three peaks at c. 1.1 Ga 1.2 Ga and 2.05 Ga with individual zircons appearing from c. 3.0 Ga – 950 Ma. This sample has no data below c. 950 Ma and shows mainly Meso- and Paleoproterozoic zircons with ages from c. 3.0 Ga – 950 Ma. The pattern for a typical flysch sediment described by Konopásek et al. (2017a)

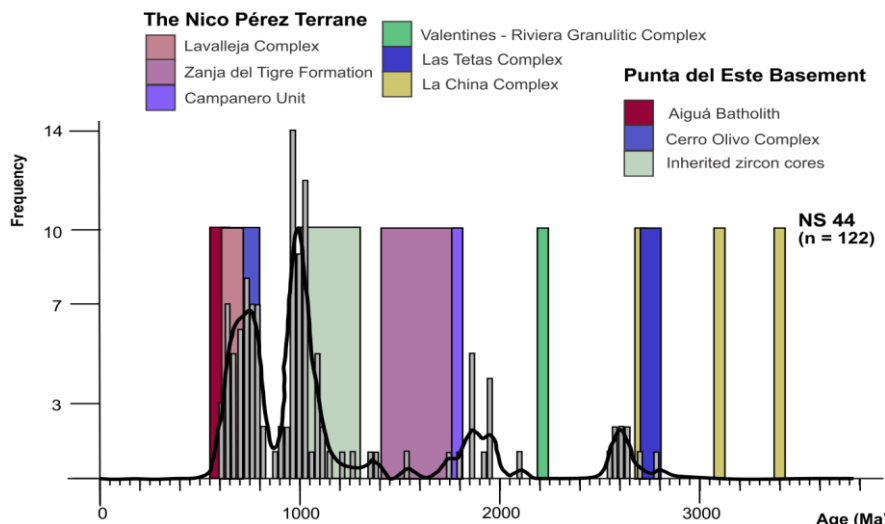


Figure 62: Histogram of sample NS 44 with bars representing the geological units in the Nico Pérez and the Punta del Este.

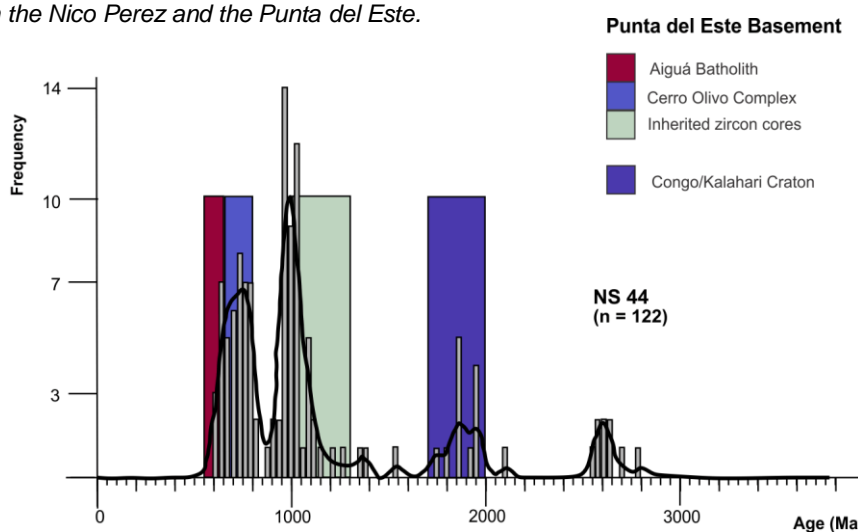


Figure 63: Histogram of the sample NS 44 overlain bars representing the Punta del Este Basement and a South-African source.

has age peaks at 650 – 630 Ma and 800 – 770 Ma. NS 32 does not have zircons younger than c. 950 Ma.

A flysch sediment is related to an orogenic evolution, and in the Dom Feliciano Belt the orogenic event started c. 650 Ma. Since

NS 32 lacks the c. 650 Ma or younger ages; it cannot be a flysch sediment. Instead, it is possibly connected with sedimentation in the rifting stage prior to the orogenic cycle.

The second sample

thought to be a flysch sediment presents the same general signal as NS 32 in zircons > c. 1.0 Ga. However, NS 44 does have a younger population of zircons and the main peaks in this sample are at 650 Ma, 750 Ma and 1.0 Ga, with two small peaks at 1.85 Ga and 2.6 Ga. Both samples present zircon ages between 1.4 – 1.0 Ga and 2.1 – 1.7 Ga, but the most abundant age groups differ somehow. A total lack of zircons between 2.6 – 2.1 Ga is only present in NS 44. The biggest difference between these two samples are the < 1.0 Ga zircon ages in NS 44, which are not present in NS 32. The first peak at 650 Ma corresponds to the migmatization in CPET described in the typical pattern of a flysch sediment, and it also has zircons in the three other age groups described by Konopásek et al. (2017a), 800 – 770 Ma, 1.85 – 1.65 and 2.05 – 1.95 Ga. Based on this article, the sample NS 44 qualifies as a flysch sediment.

Interpretation of source areas for the samples from the Gariep Belt

The flysch sample, NS 44, has 4 peaks at c. 650 Ma, 750 Ma, 1.0 Ga and 1.85 Ga. The presence of the 650 Ma peak and the presence of mostly late Mesoproterozoic ages 1.2 – 1.0 Ga makes the Kalahari and Congo cratons unlikely to be the source areas. The closest tectonic unit with c. 650 Ma felsic magmatic or high-grade metamorphic rocks together with older Neoproterozoic c. 800 – 770 Ma igneous rocks are found in the Punta del Este - Costal Terrane. Sources that could have provided zircons of these ages are not known in connection with the Kalahari and Congo cratons. The presence of late Mesoproterozoic zircons can also be explained by erosion of the Punta del Este, where inherited zircon of these ages are known (Lenz et al., 2011). When the Late Mesoproterozoic (1200 - 900 Ma) is seen together with the 650 Ma and c. 800 Ma the most probable source area for these zircons is also the Punta del Este Terrane. Samples from Konopásek et al. (2017a) and Abre et al. (2020) revealed zircons of 1.3 – 0.95 Ga in samples with 650 Ma and 800 Ma zircons. The same age intervals can be seen in sample NS 44. Figure 62 and Figure 63 shows the sample NS 44 with colored blocks representing potential source areas. The three age groups, c. 650 Ma, c. 800 Ma and 1.2 – 0.95 Ga are consistent with erosion of the Punta del Este-Coastal Terrane. The last interval described in the typical flysch pattern, c. 2.0 – 1.85 Ga, is also present in NS 44 and it is typical age pattern for erosion of the edges of the Congo/Kalahari Cratons (Figure 63).

None of the zircon ages typical for the Nico Perez Terrane are present in the flysch sample NS 44 (Figure 62). The typical pattern of a flysch sediment is not compatible with erosion of the Nico Perez Terrane, while the flysch sample has age peaks at c. 650, c. 800 – 750 Ma and the late Mesoproterozoic data between 1.2 – 0.95 Ga. The Nico Perez Terrane has rocks with ages from c. 650 – 550 Ma, 1.8 – 1.4 Ga, 2.2, c. 2.8 – 2.7, 3.1 and 3.3 Ga, but it lacks the 2.0 – 1.8 Ga and the c. 650 Ma together with c. 800 Ma and 1.2 – 0.95 Ga ages seen in the flysch sample.

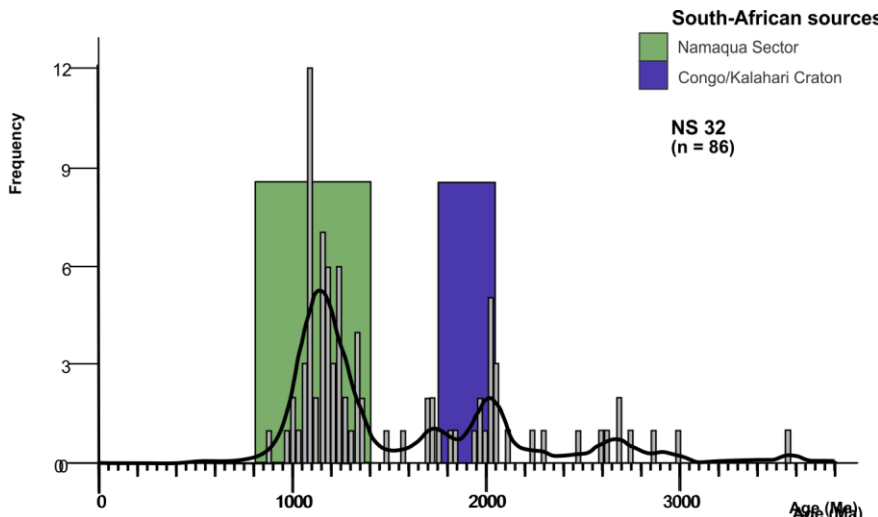


Figure 64: Histogram of the sample NS 32 overlain bars representing the South-African sources.

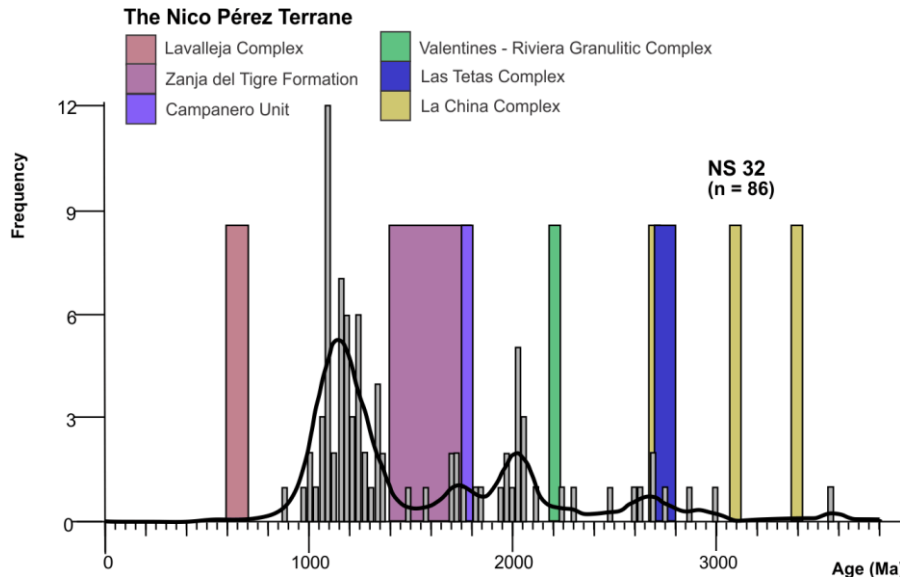


Figure 65: Histogram of the sample NS 32 overlain bars representing the Nico Pérez Terrane.

(2.05 – 1.8 Ga) found in NS 32 appear in the Congo/Kalahari craton (Figure 64). This age group is the most dominant one in the Congo Craton basement (Konopásek et al., 2017a). Even though there is an overlap around 2.0 Ga with ages of rocks of the Rio de la Plata craton, this cratonic block has an age from 2.0 Ga and older. The age pattern seen in NS 32 is also reflected in the flysch sample.

From the U-Pb dating done in this thesis and from previous works it seems clear that the two samples, NS 44 and NS 32 have a common source area for the zircons that are older than 1.0 Ga. However, the flysch sample also contains younger zircons that are not present in NS 32. The flysch sample has very little in common with the pattern seen in metasedimentary rocks

The sample NS 32, which does not qualify as a flysch sample (discussed in section 4.1.7), has a different zircon pattern (Figure 64 and Figure 65) than the metasedimentary samples from South America (LA 227 and UF12b). Compared with these two samples, NS 32 has a large concentration of zircons of late Mesoproterozoic age. The ages of 1.2 – 1.0 Ga are known from the Namaqua Sector in South Africa, and the older Paleoproterozoic dates

from the Nico Perez Terrane (UF 12b and La 227). The most likely sources for the original NS 44 sediment would be erosion of the Punta del Este Terrane.

5 Conclusions

Five samples from the Nico Perez Terrane of the southern Dom Feliciano Belt in Uruguay were dated during the work on this thesis, and they together with published results from this area provide the background for detrital zircon analysis of metasedimentary samples from the Marmora Terrane in the Gariep Belt in Namibia. The results of the dating of samples from the Nico Perez Terrane have shown the following:

- The granite sample UF 22 has a magmatic age of 611 ± 3 Ma. Xenocrystic zircons provided ages from c. 3.3 Ga - c. 700 Ma. The second granite sample UF 24 has a magmatic age of 615 ± 3 Ma, and provided xenocrystic zircons with ages from c. 3.3 Ga – 1.65 Ga.
- The felsic metavolcanic rock UF 30 has a magmatic age of 1.45 Ga, it presented with 4 xenocrystic zircons.
- The metasedimentary sample UF 12b from the Zanja del Tigre Complex presents detrital zircon spectrum with age peaks at 2.05, 2.15, 2.7, 2.9 and 3.2 Ga, with the largest peak at 2.15.
- The metamorphic volcano-sedimentary rock LA 227 has one major peak at 1.45 Ga, which is interpreted as the age of the volcanic admixture. Individual data can be seen around 1.7 Ga, 2.0 – 2.2 Ga and 2.7 – 3.2 Ga and these are interpreted as representing detrital zircon grains.

The results of the dating of samples from the Marmora Terrane suggest the following:

- Out of the two samples thought to be flysch sediments, only one (NS 44) qualifies as such.
- The other sample (NS 32) is instead interpreted as a pre-orogenic sedimentary rock, possibly connected with sedimentation in the rifting stage of the Gariep Belt evolution. The sample contains mostly Meso- and Paleoproterozoic zircons typical for the local basement represented by the Namaqua Metamorphic Complex and the western edge of the Kalahari Craton.
- As NS 32 does not represent a flysch sediment, the present mapping of the corresponding geological unit must be wrong.

- The detrital zircon pattern in the flysch sample NS 44 is consistent with erosion of the Punta del Este Terrane in the age spectrum younger than c 1.2 Ga. Even though zircons older than c. 1.2 Ga have similar pattern as seen in the Namaqua Terrane, it is more likely they come from erosion of the Punta del Este Terrane.

6 References

Uncategorized References

- Abre, P., Blanco, G., Gaucher, C., Frei, D., & Frei, R. (2020). Provenance of the Late Ediacaran Rocha Formation, Cuchilla Dionisio Terrane, Uruguay: Tectonic implications on the assembly of Gondwana. *Precambrian Research*, 342, 105704. doi:10.1016/j.precamres.2020.105704
- Allègre, C. J. (2008). *Isotope geology*: Cambridge University Press.
- Basei, M., Frimmel, H., Nutman, A., Preciozzi, F., & Jacob, J. (2005). A connection between the Neoproterozoic Dom Feliciano (Brazil/Uruguay) and Gariep (Namibia/South Africa) orogenic belts – evidence from a reconnaissance provenance study. *Precambrian Research*, 139(3-4), 195-221. doi:10.1016/j.precamres.2005.06.005
- Basei, M. A. S., Frimmel, H. E., Nutman, A. P., & Preciozzi, F. (2008). West Gondwana amalgamation based on detrital zircon ages from Neoproterozoic Ribeira and Dom Feliciano belts of South America and comparison with coeval sequences from SW Africa. *Geological Society, London, Special Publications*, 294(1), 239-256. doi:10.1144/sp294.13
- Basei, M. A. S., Peel, E., Sánchez Bettucci, L., Preciozzi, F., & Nutman, A. P. (2010). The basement of the Punta del Este Terrane (Uruguay): an African Mesoproterozoic fragment at the eastern border of the South American Río de La Plata craton. *International Journal of Earth Sciences*, 100(2-3), 289-304. doi:10.1007/s00531-010-0623-1
- Becker, T., Schreiber, U., Kampunzu, A. B., & Armstrong, R. (2006). Mesoproterozoic rocks of Namibia and their plate tectonic setting. *Journal of African Earth Sciences*, 46(1-2), 112-140. doi:10.1016/j.jafrearsci.2006.01.015
- Bogdanova, S. V., Pisarevsky, S. A., & Li, Z. X. (2009). Assembly and Breakup of Rodinia (Some results of IGCP project 440). 17(3), 259-274. doi:10.1134/s0869593809030022
- Corfu, F. (2003). Atlas of Zircon Textures. *Reviews in Mineralogy and Geochemistry*, 53(1), 469-500. doi:10.2113/0530469
- Einsele, G. (2000). *Sedimentary Basins: Evolution, Facies, and Sediment Budget*: Springer Science & Business Media.
- Evans, D. A. D., Li, Z. X., & Murphy, J. B. (2016). Four-dimensional context of Earth's supercontinents. *Geological Society, London, Special Publications*, 424(1), 1-14. doi:10.1144/sp424.12
- Faure, G. (1998). *Principles and applications of geochemistry* (R. A. McConnin Ed. 2nd ed.). Upper Saddle River, New Jersey, USA: Prentice Hall.
- Frimmel, Zartman, Robert E., & Späth, A. (2001). The Richtersveld Igneous Complex, South Africa: U - Pb Zircon and Geochemical Evidence for the Beginning of Neoproterozoic Continental Breakup. *The Journal of Geology*, 109(4), 493-508. doi:10.1086/320795
- Frimmel, H. E. (2018). The Gariep Belt. In *Geology of Southwest Gondwana* (pp. 353-386).
- Hartnady, C., Joubert, P., Stowe, C. (1985). Proterozoic Crustal Evolution in Southwestern Africa. *Episodes*, 8(4), 8.
- Hueck, M., Oyhantçabal, P., Oriolo, S., Philipp, R. P., Wemmer, K., & Siegesmund, S. (2018). The Dom Feliciano Belt in Southern Brazil and Uruguay. *Geology of Southwest Gondwana*, 34. doi:10.1007/978-3-319-68920-3_11
- Jackson, S. E., Pearson, N. J., Griffin, W. L., & Belousova, E. A. (2004). The application of laser ablation-inductively coupled plasma-mass spectrometry to in situ U-Pb zircon geochronology. *Chemical Geology*, 211(1-2), 47-69. doi:10.1016/j.chemgeo.2004.06.017
- Konopásek, J., Cavalcante, C., Fossen, H., & Janoušek, V. (2020). Adamastor – an ocean that never existed? *Earth-Science Reviews*, 205, 103201. doi:10.1016/j.earscirev.2020.103201
- Konopásek, J., Hoffmann, K.-H., Sláma, J., & Košler, J. (2017a). The onset of flysch sedimentation in the Kaoko Belt (NW Namibia) – Implications for the pre-collisional evolution of the

- Kaoko-Dom Feliciano-Gariep orogen. *Precambrian Research*, 298, 220-234. doi:10.1016/j.precamres.2017.06.017
- Konopásek, J., Janoušek, V., Oyhantçabal, P., Sláma, J., & Ulrich, S. (2017b). Did the circum-Rodinia subduction trigger the Neoproterozoic rifting along the Congo-Kalahari Craton margin? *International Journal of Earth Sciences*, 107(5), 1859-1894. doi:10.1007/s00531-017-1576-4
- Konopásek, J., Košler, J., Sláma, J., & Janoušek, V. (2014). Timing and sources of pre-collisional Neoproterozoic sedimentation along the SW margin of the Congo Craton (Kaoko Belt, NW Namibia). 26(1), 386-401. doi:10.1016/j.gr.2013.06.021
- Lara, P., Oyhantçabal, P., & Belousova, E. (2020). Two distinct crustal sources for Late Neoproterozoic granitic magmatism across the Sierra Ballena Shear Zone, Dom Feliciano Belt, Uruguay: Whole-rock geochemistry, zircon geochronology and Sr-Nd-Hf isotope evidence. *Precambrian Research*, 341, 105625. doi:10.1016/j.precamres.2020.105625
- Lenz, C., Fernandes, L. A. D., McNaughton, N. J., Porcher, C. C., & Masquelin, H. (2011). U-Pb SHRIMP ages for the Cerro Bori Orthogneisses, Dom Feliciano Belt in Uruguay: Evidences of a ~800Ma magmatic and ~650Ma metamorphic event. 185(3-4), 149-163. doi:10.1016/j.precamres.2011.01.007
- Li, Z. X., Bogdanova, S. V., Collins, A. S., Davidson, A., De Waele, B., Ernst, R. E., ... Vernikovsky, V. (2008). Assembly, configuration, and break-up history of Rodinia: A synthesis. *Precambrian Research*, 160(1-2), 179-210. doi:10.1016/j.precamres.2007.04.021
- Ludwig, K. R. (2012). Isoplot 4.15. A geochronological toolkit for Microsoft Excel: Berkeley Geochronology Center Special Publication No. 5.
- Masquelin, H., D'Avila Fernandes, L. A., Lenz, C., Porcher, C. C., & McNaughton, N. J. (2012). The Cerro Olivo Complex: a pre-collisional Neoproterozoic magmatic arc in Eastern Uruguay. 54(10), 1161-1183. doi:10.1080/00206814.2011.626597
- Oriolo, S., Oyhantçabal, P., Wemmer, K., & Siegesmund, S. (2017). Contemporaneous assembly of Western Gondwana and final Rodinia break-up: Implications for the supercontinent cycle. *Geoscience Frontiers*, 8(6), 1431-1445. doi:10.1016/j.gsf.2017.01.009
- Oyhantçabal, P., Oriolo, S., Philipp, R. P., Wemmer, K., & Siegesmund, S. (2018). The Nico Perez Terrane of Uruguay and Southeastern Brazil. doi:10.1007/978-3-319-68920-3_7
- Oyhantçabal, P., Siegesmund, S., & Wemmer, K. (2011). The Río de la Plata Craton: a review of units, boundaries, ages and isotopic signature. *International Journal of Earth Sciences*, 100(2-3), 201-220. doi:10.1007/s00531-010-0580-8
- Oyhantçabal, P., Siegesmund, S., Wemmer, K., Presnyakov, S., & Layer, P. (2009). Geochronological constraints on the evolution of the southern Dom Feliciano Belt (Uruguay). *Journal of the Geological Society*, 166(6), 1075-1084. doi:10.1144/0016-76492008-122
- Porada, H. (1979). The damara-ribeira orogen of the Pan-Africanbrasiliano cycle in Namibia (Southwest Africa) and Brazil as interpreted in terms of continental collision. 57(2-4), 237-265. doi:10.1016/0040-1951(79)90150-1
- Preciozzi, F., Basei, M. A. S., & Masquelin, H. (1999). New geochronological data from the Piedra Alta Terrane (Rio de la Plata). 2 *South American Symposium on Isotope Geology*.
- Sciences, I. o. G. o. t. C. A. o. (2019). Research reports 2018. Retrieved from [https://www.gli.cas.cz/cs/system/files/users/public/zajic 5/Research Reports/rr2018-naweb.pdf](https://www.gli.cas.cz/cs/system/files/users/public/zajic%205/Research%20Reports/rr2018-naweb.pdf)
- Sláma, J., Košler, J., Condon, D. J., Crowley, J. L., Gerdes, A., Hanchar, J. M., ... Whitehouse, M. J. (2008). Plešovice zircon — A new natural reference material for U-Pb and Hf isotopic microanalysis. *Chemical Geology*, 249(1-2), 1-35. doi:10.1016/j.chemgeo.2007.11.005
- University of Bergen, D. o. E. S. (2019). Mineral separation laboratory. Retrieved from <https://www.uib.no/en/geo/111549/mineral-separation-laboratory>,
- Uwe, J. M. J. (1994). *Sedimentology and Structural Geology of the Gariep Belt in Southern Namibia*: University of the Witwatersrand.
- Vermeesch, P. (2012). On the visualisation of detrital age distribution. *Chemical Geology*, 312, pp. 190-194.

- White, W. M. (2013). *Geochemistry* (Vol. John Wiley & Sons Inc.). New York, United States.
- Wiedenbeck, M., Alle, P., Corfu, F., W.L., G., Meier, M., Oberli, F., . . . Speigel, W. (1995). 3 natural zircon standards for U-Th-Pb, Lu-Hf, trace-element and REE analysis. *Geostandards Newsletter* 19, 23.
- Will, T. M., Frimmel, H. E., Gaucher, C., & Bossi, J. (2014). Geochemical and isotopic composition of Pan-African metabasalts from southwestern Gondwana: Evidence of Cretaceous South Atlantic opening along a Neoproterozoic back-arc. 202-203, 363-381.
doi:10.1016/j.lithos.2014.05.034

7 Appendix A

* Dis. (6/38/7/6) = discordance of ($^{206}\text{Pb} / ^{238}\text{U}$) / ($^{207}\text{Pb}/^{206}\text{Pb}$)

* Dis. (6/38/7/35) = discordance of ($^{206}\text{Pb} / ^{238}\text{U}$) / ($^{207}\text{Pb}/^{235}\text{Pb}$)

Sample	ISOTOPIC AND ELEMENT RATIOS						CONCENTRATIONS ppm						CALCULATED AGES Ma						Dis. (6/38/7/35)
	$^{207}\text{Pb}/^{235}\text{U}$	± 2 sigma	$^{206}\text{Pb}/^{238}\text{U}$	± 2 sigma	Rho	$^{207}\text{Pb}/^{206}\text{Pb}$	± 2 sigma	U	Th	Pb	$^{207}\text{Pb}/^{235}\text{U}$	± 2 sigma	$^{206}\text{Pb}/^{238}\text{U}$	± 2 sigma	$^{207}\text{Pb}/^{206}\text{Pb}$	± 2 sigma	Dis.(6/38/7/6)		
UF12b_1	13.62	0.15	0.5255	0.0087	0.52944	0.1882	0.0024	57.86	81.4	968	2722.2	11	2722	36	2723	21	0.0	0.0	
UF12b_2	10.6	0.13	0.401	0.0071	0.64484	0.1922	0.0026	354.1	169.8	1461	2487.5	44	2173	32	2758	22	21.2	12.6	
UF12b_3	19.51	0.3	0.6059	0.012	0.79883	0.2339	0.0029	101.1	29.6	421	3064	45	3048	47	3075	20	0.9	0.5	
UF12b_4	6.816	0.083	0.3816	0.0065	0.74319	0.12964	0.0016	127.3	147.7	1274	2086	11	2082	31	2091	22	0.4	0.2	
UF12b_5	7.024	0.081	0.3924	0.0067	0.60539	0.12939	0.0016	201.7	157.9	1430	2112.2	10	2134	31	2086	23	-2.3	-1.0	
UF12b_6	15.96	0.18	0.5653	0.0097	0.71883	0.2049	0.0025	101.5	201	2480	2873.4	11	2886	40	2863	20	-0.8	-0.4	
UF12b_7	17.92	0.24	0.5799	0.011	0.69536	0.2236	0.003	74.3	67.01	877	2983	13	2949	42	3003	22	1.8	1.1	
UF12b_8	22.27	0.69	0.613	0.024	0.78596	0.2646	0.0065	135.9	139	1850	3191	31	3075	97	3269	40	5.9	3.6	
UF12b_9	7.074	0.075	0.3959	0.0067	0.63684	0.12971	0.0016	167.7	160.3	1473	2119.2	94	2154	30	2091	22	-2.9	-1.5	
UF12b_10	20.26	0.23	0.5854	0.011	0.66259	0.2524	0.0034	152	122.7	853	3103	11	2969	44	3198	21	7.2	4.3	
UF12b_11	7.538	0.096	0.3939	0.007	0.69224	0.1384	0.0018	106.6	152.2	1404	2176.6	11	2139	32	2204	23	2.9	1.7	
UF12b_12	18.77	0.23	0.6086	0.011	0.6392	0.2234	0.0029	57.8	159.5	2184	3029.1	12	3064	42	3001	21	-2.1	-1.2	
UF12b_13	8.637	0.11	0.4296	0.0075	0.66022	0.1453	0.002	52.17	98.5	971	2298	12	2304	34	2289	24	-0.7	-0.3	
UF12b_14	8.493	0.11	0.4502	0.0078	0.62141	0.1364	0.0019	47.56	64.78	667.6	2283	12	2394	35	2177	24	-10.0	-4.9	
UF12b_15	18.13	0.34	0.591	0.013	0.78834	0.2206	0.0033	80.9	115.8	1509	2995	18	2986	54	2979	25	-0.2	0.3	
UF12b_16	7.849	0.11	0.416	0.0073	0.60672	0.1374	0.0019	46.31	51.31	494	2242	42	2240	33	2189	25	-2.3	-1.3	
UF12b_17	6.937	0.083	0.3853	0.0065	0.6537	0.13033	0.0016	152.9	86.9	747	2101.7	11	2099	30	2100	22	0.0	0.1	
UF12b_18	7.777	0.079	0.4072	0.0066	0.5876	0.13838	0.0017	126	256.3	2447	2204	94	2204	30	2203	24	0.1	0.1	
UF12b_19	6.707	0.072	0.3726	0.006	0.6138	0.1296	0.0016	281.9	183.7	1558	2071.8	9.5	2041	28	2091	22	2.4	1.5	
UF12b_20	7.51	0.12	0.3959	0.008	0.70881	0.1379	0.0021	195.4	46.2	338	2173	44	2148	37	2196	26	2.2	1.2	
UF12b_21	17.64	0.23	0.5659	0.01	0.708	0.2245	0.003	222.8	80	994	2969	42	2889	43	3012	22	4.1	2.7	
UF12b_22	18.86	0.24	0.5936	0.011	0.70386	0.2291	0.003	228.4	226.8	2968	3032	12	3002	43	3042	21	1.3	1.0	
UF12b_23	5.524	0.063	0.3298	0.0056	0.74117	0.12121	0.0015	343.2	265.8	1686	1902.2	9.9	1836	27	1970	22	6.8	3.5	
UF12b_24	5.704	0.069	0.3383	0.0056	0.49449	0.1222	0.0017	63.8	206.3	1789	1930.4	40	1878	27	1984	24	5.3	2.7	
UF12b_25	17.21	0.2	0.5327	0.009	0.64067	0.2321	0.003	291.7	386.9	3885	2945.2	11	2752	38	3064	20	10.2	6.6	
UF12b_26	8.103	0.099	0.4244	0.0071	0.52483	0.1384	0.0018	78.7	87.5	844	2239.8	11	2279	32	2203	22	-3.4	-1.8	
UF12b_27	7.287	0.092	0.4066	0.0071	0.6425	0.1298	0.0017	83.9	60.16	571.1	2145.4	44	2199	32	2089	23	-5.3	-2.5	
UF12b_28	20.52	0.24	0.6265	0.011	0.69517	0.2362	0.0029	100.7	228.4	3163	3144.4	44	3135	42	3094	20	-1.4	-0.7	
UF12b_29	7.79	0.15	0.3252	0.0082	0.7145	0.1724	0.0031	599	139.7	929	2206	47	1814	40	2577	30	29.6	17.8	
UF12b_30	11.31	0.16	0.4979	0.0094	0.63451	0.1638	0.0025	73.3	68.9	795	2547	43	2605	40	2488	25	-4.7	-2.3	
UF12b_31	7.804	0.092	0.4102	0.007	0.58921	0.1373	0.0017	169.8	236.3	2273	2208.2	40	2214	32	2189	22	-1.1	-0.3	
UF12b_32	6.866	0.097	0.3768	0.0068	0.65633	0.131	0.0019	136.8	119.3	965	2094	12	2060	32	2107	25	2.2	1.6	
UF12b_33	7.896	0.086	0.4202	0.007	0.60236	0.1357	0.0017	75.8	120.34	1128	2218	9.7	2260	32	2168	22	-4.2	-1.9	
UF12b_34	14.02	0.15	0.5406	0.0088	0.64022	0.1871	0.0023	89.8	214.2	2586	2749	9.8	2784	37	2715	21	-2.5	-1.3	
UF12b_35	18.52	0.2	0.601	0.01	0.64749	0.2233	0.0028	64.02	38.49	507.6	3016.4	10	3033	41	3001	20	-1.1	-0.6	

UF12b_36	6.381	0.096	0.3615	0.0066	0.54846	0.1271	0.0019	80.7	76.34	638.1	2029	43	1988	34	2057	26	3.4	2.0
UF12b_37	4.968	0.07	0.2778	0.0049	0.75938	0.1291	0.0017	321.6	638	3560	4812	42	1582	26	2083	23	24.1	12.7
UF12b_38	7.022	0.079	0.3844	0.0064	0.631580135	0.13221	0.0016	181.4	291.5	2494	2112.2	40	2095	30	2125	24	1.4	0.8
UF12b_39	7.709	0.11	0.403	0.0069	0.630203272	0.1385	0.002	28.83	37.39	343	2195	13	2181	32	2202	26	1.0	0.6
UF12b_40	17.85	0.24	0.5859	0.011	0.628826408	0.2206	0.0031	161.3	133.5	1651	2981	14	2969	45	2980	23	0.4	0.4
UF12b_41	17.98	0.2	0.584	0.0096	0.627449545	0.2234	0.0027	122.8	197.2	2388	2987.1	44	2963	39	3003	49	1.3	0.8
UF12b_42	15.47	0.18	0.5496	0.0091	0.626072681	0.2028	0.0025	81.1	77.35	920	2842	11	2823	38	2846	20	0.8	0.7
UF12b_43	7.76	0.097	0.407	0.0073	0.624695818	0.1377	0.0019	49.8	130.8	1237	2202.6	11	2199	33	2191	24	-0.4	0.2
UF12b_44	8.053	0.09	0.4207	0.0069	0.623318954	0.1382	0.0018	100.2	89.19	847.9	2234.9	10	2262	31	2203	23	-2.7	-1.2
UF12b_45	7.912	0.098	0.4201	0.0073	0.621942091	0.1361	0.0018	61.3	151.2	1407	2219.1	11	2259	33	2173	23	-4.0	-1.8
UF12b_46	5.79	0.12	0.2262	0.0047	0.620565228	0.1847	0.0024	691	1326	3819	1935	19	1313	25	2693	22	51.2	32.1
UF12b_47	24.37	0.31	0.6636	0.012	0.619188364	0.2663	0.0034	82.4	67.06	966	3281	12	3279	46	3281	20	0.1	0.1
UF12b_48	16.45	0.36	0.548	0.014	0.617811501	0.2159	0.0043	220.2	124.2	1048	2900	21	2816	58	2946	32	4.4	2.9
UF12b_49	8.266	0.099	0.4288	0.0072	0.616434637	0.1394	0.0018	116	107.9	1063	2258.9	44	2302	33	2220	24	-3.7	-1.9
UF12b_50	15.39	0.27	0.5174	0.012	0.615057774	0.2139	0.0032	328	104.2	1114	2837	47	2692	48	2932	25	8.2	5.1
UF12b_51	21.21	0.24	0.6322	0.011	0.61368091	0.2424	0.0029	90.7	107.2	1447	3146.7	11	3155	42	3134	20	-0.7	-0.3
UF12b_52	12.73	0.16	0.5042	0.0087	0.612304047	0.1828	0.0022	218.1	80.66	915	2657.6	42	2632	37	2673	49	1.5	1.0
UF12b_53	7.362	0.091	0.3977	0.0068	0.610927183	0.1337	0.0017	128.6	115.8	1024	2153.6	11	2160	32	2145	23	-0.7	-0.3
UF12b_54	17.58	0.32	0.5809	0.013	0.60955032	0.2192	0.0029	74.26	75.8	896	2961	19	2953	52	2971	21	0.6	0.3
UF12b_55	8.111	0.091	0.4246	0.0074	0.608173457	0.1384	0.0019	73.3	82.37	798	2242.3	10	2281	33	2208	24	-3.3	-1.7
UF12b_56	7.886	0.088	0.4157	0.0069	0.606796593	0.1372	0.0018	46.8	62.2	598	2216.8	10	2239	32	2187	24	-2.4	-1.0
UF12b_57	12.41	0.25	0.4287	0.01	0.60541973	0.2086	0.003	451.7	227.5	752	2632	19	2297	45	2891	23	20.5	12.7
UF12b_58	14.63	0.18	0.5474	0.0096	0.604042866	0.1928	0.0025	109	118	1502	2789.3	12	2811	40	2764	21	-1.7	-0.8
UF12b_59	8.09	0.13	0.4274	0.0084	0.602666003	0.1358	0.0021	115.5	411.6	3873	2238	15	2296	39	2175	27	-5.6	-2.6
UF12b_60	8.23	0.14	0.3068	0.0061	0.601289139	0.1943	0.0025	400	464	2216	2250	45	1722	30	2774	24	37.9	23.5
UF12b_61	7.595	0.1	0.4018	0.0071	0.599942276	0.1365	0.0018	160.8	130	1290	2183	42	2184	32	2180	22	0.0	0.1
UF12b_62	12.66	0.16	0.5096	0.009	0.598535413	0.1799	0.0024	139.5	371	4110	2656.1	11	2657	40	2649	22	-0.3	0.0
UF12b_63	22.45	0.41	0.6206	0.013	0.597158549	0.2612	0.0041	163.9	127.9	1826	3198	48	3108	52	3248	25	4.3	2.8
UF12b_64	17.43	0.18	0.5751	0.0097	0.595781686	0.2199	0.0027	148	91.2	1156	2957.7	10	2926	39	2976	20	1.7	1.1
UF12b_65	7.39	0.12	0.3843	0.0072	0.594404822	0.1386	0.0024	225.2	232	2319	2158	44	2094	33	2204	34	5.0	3.0
UF12b_66	10.06	0.14	0.4644	0.0082	0.593027959	0.1564	0.002	89.7	46.72	496	2437	13	2457	36	2415	21	-1.7	-0.8
UF12b_67	6.605	0.083	0.3677	0.0065	0.591651095	0.1299	0.0017	214.3	165.5	1313	2059.1	11	2017	31	2094	24	3.7	2.0
UF12b_68	6.776	0.088	0.376	0.0066	0.590274232	0.1308	0.0017	278.4	245	2174	2079.5	11	2056	31	2101	20	2.1	1.1
UF12b_69	17.16	0.2	0.5904	0.011	0.588897368	0.2102	0.0027	78.9	47.81	612.2	2941.8	44	2990	42	2905	24	-2.9	-1.6
UF12b_70	13.91	0.4	0.498	0.014	0.587520505	0.204	0.0048	31.2	147.4	1598	2740	27	2605	60	2854	37	8.7	4.9
UF12b_71	7.233	0.09	0.4031	0.0069	0.586143642	0.1299	0.0018	58.15	34.33	332.1	2138.1	11	2182	32	2092	24	-4.3	-2.1
UF12b_72	17.64	0.21	0.567	0.01	0.584766778	0.2251	0.0028	85.4	100.4	1250	2968.5	11	2898	40	3015	20	3.9	2.4
UF12b_73	7.782	0.097	0.4135	0.0073	0.583389915	0.1362	0.0018	101.2	77.74	762.5	2206.4	11	2229	33	2175	24	-2.5	-1.0
UF12b_74	19.43	0.27	0.5935	0.011	0.582013051	0.236	0.0031	101.9	255	3330	3060	44	3008	43	3092	24	2.7	1.7
UF12b_75	16.75	0.23	0.5825	0.04	0.580636188	0.2087	0.0028	94.7	152.6	2130	2917	43	2958	42	2894	24	-2.2	-1.4
UF12b_76	14.25	0.22	0.492	0.01	0.579259324	0.2099	0.0031	267.1	369	3746	2765	15	2578	44	2902	24	11.2	6.8
UF12b_77	18.01	0.3	0.5775	0.011	0.577882461	0.2256	0.0031	140.1	94.1	1158	2987	15	2938	45	3017	21	2.6	1.6
UF12b_78	6.367	0.075	0.3614	0.0062	0.576505597	0.12773	0.0015	391.6	143.2	1194	2026.3	40	1988	29	2064	24	3.7	1.9
UF12b_79	7.21	0.13	0.3996	0.0086	0.575128734	0.1302	0.0021	44.5	65.2	635	2132	46	2164	40	2094	29	-3.3	-1.5
UF12b_80	8.033	0.1	0.4191	0.0074	0.573751871	0.1394	0.0019	136.6	119.7	1209	2232.6	44	2256	33	2216	22	-4.8	-1.0
UF12b_81	23.26	0.3	0.6563	0.012	0.572375007	0.257	0.0033	71.2	69.69	1005	3236	13	3248	46	3224	20	-0.7	-0.4
UF12b_82	7.395	0.097	0.41	0.0074	0.570998144	0.1308	0.0018	53.41	49.67	494.7	2157	42	2213	34	2105	24	-5.4	-2.6
UF12b_83	16.57	0.22	0.5624	0.01	0.56962128	0.2126	0.0029	94.2	57.7	718.9	2907	12	2879	43	2923	21	1.5	1.0
UF12b_84	13.59	0.17	0.5193	0.0092	0.568244417	0.1896	0.0025	135.7	287.9	3525	2719	12	2693	39	2734	22	1.5	1.0
UF12b_85	20.29	0.27	0.6273	0.014	0.566867553	0.236	0.0033	102.2	90	4264	3106	13	3135	45	3087	21	-1.6	-0.9

UF12b_86	7.832	0.11	0.4126	0.0073	0.56549069	0.1377	0.0019	74.6	59.34	587	2208	12	2225	33	2193	24	-1.5	-0.8
UF12b_87	16.09	0.24	0.5732	0.04	0.564113826	0.2035	0.0027	93.6	454.7	4958	2879	13	2917	43	2853	20	-2.2	-1.3
UF12b_88	7.209	0.11	0.3985	0.0075	0.562736963	0.1307	0.0018	74.8	72.11	701	2136	13	2162	35	2108	23	-2.6	-1.2
UF12b_89	8.337	0.11	0.4379	0.0073	0.5613601	0.1376	0.0019	52.2	57.52	570	2266	12	2340	33	2192	24	-6.8	-3.3
UF12b_90	17.93	0.23	0.5796	0.01	0.559983236	0.2243	0.0028	122.7	134.4	1754	2983	13	2943	43	3009	21	2.2	1.3
UF12b_91	19.79	0.22	0.6299	0.011	0.558606373	0.2282	0.0028	167.8	279.7	3947	3079.8	11	3146	43	3036	20	-3.6	-2.1
UF12b_92	7.633	0.096	0.4041	0.007	0.557229509	0.1373	0.0018	96.9	473.1	4673	2188	11	2188	31	2189	24	0.0	0.0
UF12b_93	20.67	0.28	0.6321	0.012	0.555852646	0.237	0.0032	122.1	34.1	493	3120	43	3156	48	3094	24	-2.0	-1.2
UF12b_94	19.12	0.27	0.6185	0.012	0.554475782	0.2241	0.0031	60.9	24.68	363.5	3046	13	3102	46	3007	22	-3.2	-1.8
UF12b_95	17.34	0.23	0.6002	0.011	0.553098919	0.2111	0.0028	71.31	20.35	271.2	2956	14	3028	46	2911	22	-4.0	-2.4
UF12b_96	8.04	0.12	0.4246	0.0079	0.551722055	0.1364	0.002	47.6	64.1	671	2233	13	2281	35	2180	27	-4.6	-2.1
UF12b_97	14.12	0.21	0.5425	0.01	0.550345192	0.1885	0.0027	39.3	74.7	974	2753	14	2793	43	2725	24	-2.5	-1.5
UF12b_98	18.19	0.24	0.5873	0.011	0.548968329	0.2241	0.0032	41.4	54.39	753	2996	13	2973	46	3005	22	1.1	0.8
UF12b_99	24.39	0.47	0.677	0.017	0.547591465	0.2646	0.0049	14.07	8.02	124.2	3279	19	3328	62	3263	30	-2.0	-1.5
UF12b_100	20.99	0.38	0.641	0.014	0.546214602	0.2351	0.0039	51.2	1.583	23.6	3141	17	3198	56	3088	26	-3.6	-1.8
UF12b_101	13.58	0.19	0.5301	0.0096	0.544837738	0.1861	0.0028	46.27	86.6	1113	2719	13	2738	40	2706	24	-1.2	-0.7
UF12b_102	7.091	0.09	0.3945	0.0071	0.543460875	0.1302	0.0018	121.8	106.1	1016	2120	11	2141	33	2097	24	-2.1	-1.0
UF12b_103	14.24	0.22	0.4911	0.0094	0.542084011	0.2095	0.0031	264.6	419	4340	2765	45	2574	44	2898	24	11.2	6.9
UF12b_104	2.999	0.072	0.1699	0.004	0.540707148	0.134	0.0048	954	1267	3750	1398	19	1013	21	2087	30	51.5	27.5
UF12b_105	17.05	0.27	0.5717	0.012	0.539330284	0.2178	0.0034	169.6	18.54	256.6	2933	15	2920	46	2955	24	1.2	0.4
UF12b_106	21.79	0.41	0.606	0.014	0.537953421	0.2595	0.0043	159.2	114.5	1598	3170	18	3059	55	3239	25	5.6	3.5
UF12b_107	6.791	0.086	0.3836	0.007	0.536576558	0.1294	0.0021	228.2	237	2238	2081.7	11	2091	33	2073	24	-0.9	-0.4
UF12b_108	7.884	0.11	0.4139	0.0079	0.535199694	0.1383	0.0021	36.8	36.56	371	2215	42	2230	36	2199	26	-4.4	-0.7
UF12b_109	7.852	0.11	0.4184	0.0078	0.533822831	0.1351	0.0019	81.6	70.2	692	2210	13	2256	34	2160	24	-4.4	-2.1
UF12b_110	21.15	0.27	0.6332	0.012	0.532445967	0.2431	0.0042	197.7	324	4660	3143	13	3165	47	3123	20	-1.3	-0.7
UF12b_111	7.913	0.1	0.418	0.0074	0.531069104	0.1371	0.0018	93.9	76.55	789.2	2219.1	12	2254	34	2185	24	-3.2	-1.6
UF12b_112	13.64	0.19	0.5113	0.0091	0.52969224	0.1933	0.0027	200.7	144.4	1656	2723	13	2660	39	2771	23	4.0	2.3
UF12b_113	14.54	0.17	0.5305	0.0095	0.528315377	0.1995	0.0029	158.6	38.2	520	2784	44	2743	39	2843	23	2.5	1.5
UF12b_114	14.98	0.18	0.5228	0.0093	0.526938514	0.2077	0.0026	258.8	152.7	1274	2812.1	12	2709	39	2884	21	6.1	3.7
UF12b_115	20.95	0.31	0.6474	0.013	0.52556165	0.2338	0.0038	42.1	36.67	521	3135	14	3214	51	3075	26	-4.5	-2.5
UF12b_116	20.6	0.29	0.624	0.012	0.524184787	0.2395	0.0032	164.4	216.1	3011	3119	13	3122	47	3112	21	-0.3	-0.1
UF12b_117	18.87	0.26	0.6111	0.012	0.522807923	0.2258	0.0034	115.3	124.4	4783	3035	13	3069	48	3014	22	-1.8	-1.1
UF12b_118	7.7	0.12	0.4066	0.0079	0.52143106	0.1372	0.0024	25.19	52.04	519.4	2192	14	2196	36	2185	30	-0.5	-0.2
UF12b_119	18.12	0.31	0.5842	0.013	0.520054196	0.2253	0.0037	117.4	85.4	1188	2992	47	2969	54	3011	26	1.4	0.8
UF12b_120	6.702	0.089	0.3778	0.0069	0.518677333	0.129	0.0018	194.1	136.4	988	2070.7	42	2064	33	2077	25	0.6	0.3
UF12b_121	24.8	0.33	0.6659	0.012	0.517300469	0.2714	0.0037	197.9	263	3369	3299	13	3288	47	3311	22	0.7	0.3
UF12b_122	8.013	0.11	0.4241	0.0075	0.515923606	0.1375	0.002	102.8	127.6	1314	2232	12	2277	34	2190	24	-4.0	-2.0
UF12b_123	18.48	0.23	0.613	0.011	0.514546743	0.2189	0.0029	109.3	118.3	1628	3013	42	3078	44	2969	22	-3.7	-2.2
UF12b_124	7.582	0.1	0.4086	0.0072	0.513169879	0.1343	0.002	62.2	73.61	764	2181	43	2208	34	2148	26	-2.8	-1.2
UF12b_125	7.71	0.1	0.4099	0.0077	0.511793016	0.1364	0.0019	122.2	93.81	936	2198	42	2242	35	2177	24	-4.6	-0.6
UF12b_126	6.977	0.098	0.3884	0.0073	0.510416152	0.1297	0.0019	63.6	33.69	308.2	2105	13	2113	34	2091	26	-1.1	-0.4
UF12b_127	15.83	0.23	0.5664	0.014	0.509039289	0.2031	0.0029	75.59	25.6	322.6	2864	14	2890	45	2846	23	-1.5	-0.9
UF12b_128	7.54	0.4	0.4077	0.0075	0.507662425	0.1343	0.0019	147.7	107.7	986	2175	12	2204	35	2149	25	-2.6	-1.3
UF12b_129	7.946	0.11	0.4161	0.0077	0.506285562	0.1387	0.0019	115.6	137.5	1361	2225	14	2240	35	2210	23	-1.4	-0.7
UF12b_130	18.31	0.23	0.5967	0.011	0.504908698	0.2232	0.0032	85.9	97.4	1345	3004	12	3012	46	3000	22	-0.4	-0.3
UF12b_131	20.74	0.25	0.6377	0.011	0.503531835	0.2356	0.003	174.2	184.7	2587	3124.4	12	3180	44	3089	20	-2.9	-1.8
UF12b_132	25.85	0.5	0.664	0.015	0.502154972	0.2823	0.0048	60.6	52.3	843	3339	19	3276	57	3371	27	2.8	1.9
UF12b_133	10.34	0.15	0.4723	0.0086	0.500778108	0.1589	0.0022	118.1	148.6	1667	2464	13	2491	38	2442	23	-2.0	-1.1
UF12b_134	18.67	0.26	0.6134	0.013	0.499401245	0.2227	0.0035	17.81	25.09	355.6	3024	13	3081	49	2995	25	-2.9	-1.9
UF12b_135	13.03	0.27	0.4993	0.012	0.498024381	0.1874	0.0036	63.9	106.9	919	2674	19	2610	52	2707	31	3.6	2.4

UF12b_136	7.553	0.11	0.4027	0.0076	0.496647518	0.1361	0.0019	155.6	131.2	1275	2180	13	2181	34	2173	24	-0.4	0.0
UF12b_137	6.858	0.098	0.3883	0.0075	0.495270654	0.1283	0.0019	109.1	75.2	693	2090	12	2112	34	2070	27	-2.0	-1.1
UF12b_138	6.859	0.092	0.3886	0.0071	0.493893791	0.1278	0.0017	84.5	99.6	916	2094	12	2114	33	2065	24	-2.4	-1.0
UF12b_139	18.99	0.33	0.618	0.015	0.492516927	0.2222	0.0039	74.1	49.8	714	3044	18	3095	59	2988	28	-3.6	-1.7
UF12b_140	7.92	0.12	0.4162	0.0077	0.491140064	0.1378	0.002	124	144.2	1418	2220	13	2243	36	2192	25	-2.3	-1.0

Sample	ISOTOPIC AND ELEMENT RATIOS						CONCENTRATIONS ppm						CALCULATED AGES Ma					
	$^{207}\text{Pb}/^{235}\text{U}$	± 2 sigma	$^{206}\text{Pb}/^{238}\text{U}$	± 2 sigma	Rho	$^{207}\text{Pb}/^{206}\text{Pb}$	± 2 sigma	U	Th	Pb	$^{207}\text{Pb}/^{235}\text{U}$	± 2 sigma	$^{206}\text{Pb}/^{238}\text{U}$	± 2 sigma	$^{207}\text{Pb}/^{206}\text{Pb}$	± 2 sigma	Dis.(6/38/7/6)	Dis.(6/38/7/35)
UF22_1	3.136	0.059	0.2559	0.0051	0.70861	0.0894	0.0013	96.4	89.1	62.8	1439	15	1466	26	1402	27	-4.6	-1.9
UF22_2	7.607	0.093	0.4035	0.0054	0.69864	0.1366	0.0011	116.5	58.4	62.6	2184.9	44	2183	25	2182	45	0.0	0.1
UF22_3	7.381	0.092	0.3942	0.0052	0.6469	0.1353	0.0012	163.5	97.5	101.6	2156.3	44	2144	24	2162	45	1.0	0.7
UF22_4	4.994	0.077	0.3	0.0046	0.68336	0.1206	0.0013	312.1	413.9	301.3	1816	13	1691	23	1960	19	13.7	6.9
UF22_5	25.77	0.3	0.679	0.0096	0.71572	0.2761	0.0022	165.6	134.6	238	3335.3	11	3336	37	3338	12	0.1	0.0
UF22_6	16.62	0.32	0.5124	0.0093	0.69745	0.2354	0.0031	101.3	15.9	15.2	2907	19	2667	39	3082	21	13.5	8.3
UF22_7	3.261	0.057	0.2422	0.0039	0.50619	0.0978	0.0014	77.5	118	82.3	1469	14	1397	20	1573	28	11.2	4.9
UF22_8	2.408	0.029	0.1997	0.0027	0.79174	0.08733	0.00068	472.8	346.3	229.2	1244.4	9	1175	15	1362	15	13.7	5.6
UF22_9	12.14	0.16	0.4695	0.0063	0.7474	0.1858	0.0015	498	62.4	78.1	2613	43	2480	28	2703	43	8.3	5.1
UF22_10	6.832	0.1	0.3715	0.0054	0.47691	0.1332	0.0016	178.7	239.3	251.2	2086	13	2036	26	2130	21	4.4	2.4
UF22_11	1.085	0.031	0.0853	0.0023	0.046482	0.0939	0.0034	1158	461	137.3	743	15	528	14	1464	69	63.9	28.9
UF22_12	5.528	0.085	0.3199	0.0055	0.70926	0.1252	0.0014	586	254.1	214.7	1903	13	1788	27	2030	19	11.9	6.0
UF22_13	3.487	0.097	0.2525	0.0059	0.43845	0.1012	0.0027	23.85	26.34	15.72	1517	22	1449	30	1624	50	10.8	4.5
UF22_14	1.05	0.036	0.0976	0.0021	0.53019	0.0781	0.002	842	322	54.2	724	18	600	12	1128	53	46.8	17.1
UF22_15	0.823	0.017	0.0992	0.0022	0.69191	0.06039	0.00096	631	10.8	2.46	608.4	9.2	609	13	606	35	-0.5	-0.1
UF22_16	1.02	0.016	0.0967	0.0016	0.707	0.0764	0.00081	706	185.3	61.8	712.7	7.9	594.8	9.2	1099	24	45.9	16.5
UF22_17	7.518	0.089	0.3982	0.0053	0.66135	0.13681	0.00099	253.8	134.7	142.7	2173.5	11	2159	24	2183	13	1.1	0.7
UF22_18	0.981	0.012	0.1054	0.0014	0.49359	0.0677	0.00067	1139	276.5	89.9	693.5	6.2	645.8	8.3	858	20	24.7	6.9
UF22_19	14.3	0.21	0.5161	0.0077	0.52952	0.2005	0.0024	177.2	89.7	124.8	2769	14	2681	33	2827	20	5.2	3.2
UF22_20	0.897	0.02	0.099	0.0019	0.14311	0.0661	0.0014	846	16.4	17.1	649	44	608	44	790	44	23.0	6.3
UF22_21	0.851	0.014	0.0991	0.0016	0.65688	0.06261	0.00078	670	82.1	27.9	624	7.8	610.2	9.9	686	26	11.0	2.2
UF22_22	0.886	0.013	0.099	0.0014	0.092409	0.06464	0.00068	1053	274.1	95.1	643.8	7	608.6	8.2	757	22	19.6	5.5
UF22_23	13.68	0.26	0.4585	0.0086	0.29385	0.216	0.0026	140.9	60.7	83.3	2723	18	2430	38	2946	20	17.5	10.8
UF22_24	1.057	0.051	0.0979	0.002	0.16981	0.0794	0.0039	694	63.3	43.4	726	25	602	42	1118	92	46.2	17.1
UF22_25	10.66	0.16	0.3888	0.0055	0.61912	0.1997	0.0023	77.8	23.61	26	2491	14	2115	25	2819	19	25.0	15.1
UF22_26	0.834	0.019	0.1011	0.0021	0.64671	0.0604	0.0011	616	27.5	7.77	615	11	620	12	611	37	-1.5	-0.8
UF22_27	0.829	0.013	0.0986	0.0014	0.67259	0.06117	0.00065	566	40.46	12.67	611.8	7.1	606.2	8.4	635	22	4.5	0.9
UF22_28	2.909	0.044	0.239	0.0035	0.81717	0.0884	0.00071	348	182.9	127.4	1381	42	1382	48	1390	45	0.6	-0.1
UF22_29	12.63	0.17	0.01089	0.00066	0.043244	9.07	0.47	2695	134.7	165.6	2643	47	69.7	4.2	23600	1100	99.7	97.4
UF22_30	0.837	0.021	0.0993	0.0028	0.56461	0.0624	0.0012	836	144.9	40.4	616	42	610	47	674	43	9.5	1.0
UF22_31	2.946	0.04	0.2364	0.0034	0.60407	0.09016	0.00096	206.6	176.8	118.4	1391.7	40	1367	48	1422	24	3.9	1.8
UF22_32	5.369	0.067	0.3193	0.0043	0.51711	0.1224	0.001	539.7	132.8	113.5	1877.4	11	1787	21	1985	14	10.0	4.8
UF22_33	0.882	0.017	0.0995	0.0017	0.73722	0.06426	0.00072	1302	443	128.3	640.9	9	611.2	10	748	24	18.3	4.6
UF22_34	0.948	0.02	0.0995	0.0019	0.37925	0.0695	0.0012	1745	608	176.4	675.6	10	611	11	898	36	32.0	9.6
UF22_35	0.856	0.022	0.1	0.0029	0.68174	0.0629	0.0013	729	35.2	8.69	627	12	614	17	692	46	11.3	2.1
UF22_36	2.541	0.061	0.1838	0.0039	0.049302	0.1008	0.0021	67.7	150.1	35.59	1278	47	1087	24	1619	38	32.9	14.9
UF22_37	0.959	0.017	0.0989	0.0016	0.49143	0.0706	0.0012	1899	280	94.6	681.3	8.5	607.7	9.5	936	33	35.1	10.8
UF22_38	1.307	0.039	0.0861	0.0025	0.45516	0.1116	0.0034	1230	579	226.8	847	47	532	45	1813	56	70.7	37.2
UF22_39	15.7	0.23	0.5268	0.0083	0.84852	0.2172	0.0019	229	65.1	85	2861	15	2724	34	2955	14	7.8	4.8
UF22_40	0.84	0.025	0.0995	0.0034	0.21469	0.0621	0.0016	915	73.1	21.7	618	13	611	20	662	55	7.7	1.1
UF22_41	0.823	0.018	0.0985	0.0026	0.7723	0.0612	0.0011	625	31.6	9.59	608	40	605	45	629	44	3.8	0.5
UF22_42	5.11	0.11	0.289	0.0058	0.92275	0.1279	0.0011	243.1	194	114.1	1828	20	1633	29	2065	14	20.9	10.7
UF22_43	1.087	0.015	0.08186	0.0012	0.61932	0.09588	0.00097	813	344.1	133	746.7	7.3	507.1	6.9	1539	19	67.1	32.1
UF22_44	1.152	0.03	0.115	0.003	0.18884	0.0735	0.0017	734	156.7	45.2	777	14	701	17	1013	47	30.8	9.8
UF22_45	1.198	0.043	0.0986	0.0022	0.53821	0.088	0.0026	747	115.6	67.2	793	21	606	13	1368	58	55.7	23.6

UF22_46	1.135	0.059	0.1139	0.003	0.49221	0.0724	0.0025	449	37.7	14.6	763	26	695	17	947	69	26.6	8.9
UF22_47	2.43	0.19	0.1454	0.0069	0.82518	0.1208	0.0054	591	143.2	39.6	1230	53	873	39	1932	80	54.8	29.0
UF22_48	0.823	0.015	0.0993	0.0018	0.5922	0.06052	0.00093	828	121	34.95	609.1	8.4	609.8	11	611	33	0.2	-0.1
UF22_49	0.838	0.03	0.0992	0.0048	0.67205	0.0624	0.0022	1091	131.6	43.8	617	46	609	28	672	79	9.4	1.3
UF22_50	6.71	0.2	0.3632	0.0094	0.92972	0.1323	0.0016	107.8	38.71	36.67	2047	32	1994	46	2120	22	6.1	2.7
UF22_51	0.849	0.015	0.0999	0.0022	0.66473	0.06214	0.00094	609	53.8	14.34	623.1	8.3	613	13	675	32	9.2	1.6
UF22_52	0.885	0.015	0.0984	0.0015	0.55497	0.06513	0.00084	564	42.9	16.24	642.4	8.2	604.8	8.7	774	27	21.6	5.9
UF22_53	0.834	0.019	0.1005	0.0025	0.58522	0.0608	0.0012	728	112.5	19.1	614.4	10	617	14	612	44	-0.8	-0.4
UF22_54	0.916	0.033	0.0998	0.0035	0.67118	0.0673	0.0019	728	81.8	22.7	658	18	613	20	830	61	26.1	6.8
UF22_55	1.241	0.048	0.0984	0.0047	0.75154	0.0911	0.0026	515	350	39.5	817	22	604	27	1438	56	58.0	26.1
UF22_56	0.976	0.023	0.1007	0.0024	0.64408	0.0704	0.0013	433.2	75	21.8	691	11	618	14	932	38	33.7	10.6
UF22_57	0.796	0.025	0.0879	0.0025	0.74796	0.0662	0.0014	611	95.4	30.5	595	15	543	15	798	45	32.0	8.7
UF22_58	1.973	0.085	0.1544	0.005	0.7459	0.0927	0.0026	709	208.8	64.7	1098	29	924	28	1461	54	36.8	15.8
UF22_59	0.98	0.022	0.1131	0.002	0.4408	0.06263	0.00086	325	50.6	21.38	690	11	690	11	686	27	-0.6	0.0
UF22_60	0.819	0.018	0.0988	0.0025	0.5746	0.0609	0.0011	2006	765	223.3	609	44	607	45	624	44	2.7	0.3
UF22_61	0.837	0.035	0.1	0.0043	0.62751	0.0614	0.0017	2012	864	242.5	646	49	614	25	642	60	4.4	0.3
UF22_62	3.132	0.049	0.2496	0.0037	0.54386	0.0915	0.0012	72.6	101.3	70.7	1440	12	1435	19	1444	25	0.6	0.3
UF22_63	0.847	0.02	0.0984	0.0023	0.83932	0.0623	0.0012	645	32	10.92	622	44	605	44	687	39	11.9	2.7
UF22_64	14.27	0.4	0.399	0.017	0.48726	0.304	0.029	780	502	435.3	2741	31	2129	84	3285	82	35.2	22.3
UF22_65	0.895	0.016	0.0994	0.0017	0.2468	0.06501	0.00073	1218	313	90.9	647.4	8.7	610.8	40	765	24	20.2	5.7
UF22_66	3.28	0.18	0.1647	0.0063	0.77611	0.145	0.0054	533	130.6	38.3	1460	45	981	35	2262	64	56.6	32.8
UF22_67	1.059	0.034	0.0974	0.0021	0.36006	0.0804	0.0013	696.5	164.2	37.89	738	14	599	12	1194	33	49.8	18.8
UF22_68	0.842	0.02	0.0994	0.0026	0.63959	0.0614	0.0011	971	262.6	85.2	620	11	611	15	647	39	5.6	1.5
UF22_69	1.61	0.12	0.1268	0.0075	0.26889	0.0939	0.0046	822	160.2	63.9	968	46	769	43	1490	100	48.4	20.6
UF22_70	17.47	0.27	0.558	0.0085	0.75781	0.2272	0.0023	48.2	32.82	46.3	2958	15	2854	35	3027	16	5.7	3.5

Sample	ISOTOPIC AND ELEMENT RATIOS						CONCENTRATIONS ppm						CALCULATED AGES Ma					
	$^{207}\text{Pb}/^{235}\text{U}$	\pm 2 sigma	$^{206}\text{Pb}/^{238}\text{U}$	\pm 2 sigma	Rho	$^{207}\text{Pb}/^{206}\text{Pb}$	\pm 2 sigma	U	Th	Pb	$^{207}\text{Pb}/^{235}\text{U}$	\pm 2 sigma	$^{206}\text{Pb}/^{238}\text{U}$	\pm 2 sigma	$^{207}\text{Pb}/^{206}\text{Pb}$	\pm 2 sigma	Dis.(6/38/7/6)	Dis.(6/38/7/35)
UF24_1	1.267	0.038	0.099	0.003	0.476	0.093	0.003	326	29.9	471	829	17	611	18	1481	53	58.7	26.3
UF24_2	1.461	0.036	0.045	0.003	0.643	0.242	0.011	1105	146.5	3910	912	45	285	45	3101	70	90.8	68.8
UF24_3	1.061	0.016	0.109	0.002	0.562	0.071	0.001	537	122.7	570	732.5	7.9	664.4	42	943	32	29.6	9.3
UF24_4	1.342	0.020	0.100	0.002	0.443	0.099	0.002	2063	76.6	3300	862.2	8.6	611.2	11	1579	29	61.3	29.1
UF24_5	1.134	0.025	0.099	0.002	0.028	0.082	0.002	1228	54	1204	768	12	608	11	1246	51	51.2	20.8
UF24_6	2.260	0.120	0.056	0.002	0.637	0.322	0.022	1221	382	8290	1144	42	348.7	9	3220	130	89.2	69.5
UF24_7	0.891	0.026	0.100	0.003	0.504	0.065	0.002	417	123.7	374	646	14	613	17	754	53	18.7	5.1
UF24_8	1.484	0.023	0.098	0.002	0.085	0.110	0.002	327	68.3	822	922.2	9.6	603.4	11	1791	39	66.3	34.6
UF24_9	0.847	0.010	0.099	0.002	0.562	0.062	0.001	1140	50.6	163.1	622.3	5.7	609.6	9.9	657	28	7.2	2.0
UF24_10	1.046	0.021	0.101	0.002	0.688	0.075	0.001	735	39.6	549	724	10	619.1	11	1053	33	41.2	14.5
UF24_11	0.834	0.010	0.100	0.002	0.565	0.060	0.001	396.2	39.1	95.7	615.2	5.7	615.3	9.9	610	29	-0.9	0.0
UF24_12	0.836	0.011	0.100	0.002	0.614	0.060	0.001	405	39.2	97.6	616.4	5.9	614.9	9.9	618	28	0.5	0.2
UF24_13	0.832	0.010	0.100	0.002	0.526	0.060	0.001	368.7	34.02	82.4	614.4	5.6	612.5	9.6	613	29	0.1	0.3
UF24_14	0.867	0.011	0.099	0.002	0.750	0.063	0.001	1569	34.37	169.2	633.3	6	610.3	9.9	706	27	13.6	3.6
UF24_15	0.869	0.018	0.100	0.002	0.592	0.063	0.001	361	82.9	237.4	633.3	10	616.7	12	701	39	12.0	2.6
UF24_16	1.880	0.180	0.105	0.004	0.076	0.136	0.015	2.991	0.0363	8.7	4026	69	644	26	4830	230	64.8	37.2
UF24_17	0.993	0.029	0.121	0.003	0.737	0.060	0.001	443	137.7	400	700	15	737	17	606	49	-21.6	-5.3
UF24_18	0.908	0.020	0.101	0.002	0.712	0.065	0.001	682	207	609	655	44	619	42	780	36	20.6	5.5
UF24_19	4.370	0.120	0.303	0.007	0.184	0.106	0.003	5.766	10.34	74.6	1692	23	1705	32	1672	53	-2.0	-0.8
UF24_20	1.067	0.041	0.084	0.004	0.640	0.117	0.012	2840	156	1890	732	49	549	26	4560	440	66.7	29.1
UF24_21	3.161	0.036	0.054	0.002	0.216	0.452	0.015	1580	185	13000	1447.6	8.8	338	42	4042	54	91.6	76.7
UF24_22	3.920	0.150	0.064	0.004	0.911	0.475	0.018	1520	107	13100	1603	29	396	24	4131	54	90.4	75.3
UF24_23	0.941	0.013	0.101	0.002	0.574	0.067	0.001	822	252.3	815	672.8	7	619.7	11	837	32	26.0	7.9
UF24_24	0.840	0.009	0.100	0.002	0.531	0.061	0.001	1180	469.9	1208	618.8	4.9	613	9.6	643	27	4.7	0.9
UF24_25	0.889	0.036	0.101	0.004	0.653	0.065	0.002	576	157.7	532	643	20	618	20	742	67	16.7	3.9
UF24_26	8.070	0.130	0.417	0.008	0.626	0.141	0.002	29.1	55.43	547.4	2235	15	2245	37	2235	27	-0.4	-0.4
UF24_27	23.840	0.370	0.642	0.013	0.657	0.269	0.004	214.6	288.5	3901	3261	45	3194	54	3294	23	3.0	2.1
UF24_28	3.860	0.130	0.270	0.006	0.090	0.104	0.004	6.48	20.68	136.3	4592	27	4540	32	4648	65	6.6	3.3

Sample	ISOTOPIC AND ELEMENT RATIOS					CONCENTRATIONS ppm					CALCULATED AGES Ma							
	$^{207}\text{Pb}/^{235}\text{U}$	± 2 sigma	$^{206}\text{Pb}/^{238}\text{U}$	± 2 sigma	Rho	$^{207}\text{Pb}/^{206}\text{Pb}$	± 2 sigma	U	Th	Pb	$^{207}\text{Pb}/^{235}\text{U}$	± 2 sigma	$^{206}\text{Pb}/^{238}\text{U}$	± 2 sigma	$^{207}\text{Pb}/^{206}\text{Pb}$	± 2 sigma	Dis.(6/38/7/6)	Dis. (6/38/7/35)
LA227_1	35.820	1.100	0.548	0.010	0.408	0.225	0.007	300	86.2	746	3653	30	2814	41	3015	50	6.7	23.0
LA227_2	20.100	1.700	0.312	0.012	0.040	0.262	0.023	58.5	78.1	345	2952	71	1734	54	2960	140	41.4	41.3
LA227_3	8.240	0.450	0.260	0.006	0.028	0.148	0.009	123.4	101.1	342	2215	47	1484	29	2197	95	32.5	33.0
LA227_4	6.340	0.340	0.257	0.005	0.142	0.125	0.006	118.5	165.7	458	1975	39	1470	27	1912	77	23.1	25.6
LA227_5	25.670	0.660	0.596	0.009	0.520	0.242	0.006	166.8	150.4	804	3330	25	3011	38	3129	43	3.8	9.6
LA227_6	4.020	0.160	0.246	0.008	0.516	0.098	0.004	443	363.7	881	1629	31	1413	40	1561	65	9.5	13.3
LA227_7	3.860	0.210	0.255	0.007	0.150	0.098	0.007	89.1	99.5	283	1596	39	1461	33	1516	80	3.6	8.5
LA227_8	3.390	0.100	0.244	0.005	0.547	0.092	0.003	452.1	330.1	728	1498	23	1407	27	1456	57	3.4	6.1
LA227_9	7.520	0.180	0.379	0.006	0.463	0.135	0.003	227.7	125.3	433	2173	21	2071	28	2154	43	3.9	4.7
LA227_10	13.480	0.330	0.508	0.009	0.518	0.186	0.005	315.3	194.8	855	2710	22	2642	37	2691	42	1.8	2.5
LA227_11	3.200	0.130	0.237	0.007	0.456	0.096	0.004	87.6	92.8	193.8	1445	31	1367	37	1506	69	9.2	5.4
LA227_12	3.126	0.094	0.243	0.005	0.151	0.093	0.003	59.7	59.63	135.2	1430	22	1398	26	1458	53	4.1	2.2
LA227_13	18.500	0.470	0.588	0.012	0.569	0.230	0.006	353.2	95.6	468	3013	25	2981	50	3027	35	1.5	1.1
LA227_14	3.107	0.110	0.240	0.008	0.730	0.095	0.003	541	447	976	1430	27	1381	39	1506	58	8.3	3.4
LA227_15	3.053	0.089	0.241	0.005	0.646	0.091	0.003	38.98	24.75	54.8	1415	23	1387	24	1421	56	2.4	2.0
LA227_16	14.060	0.350	0.519	0.010	0.620	0.195	0.005	117.7	6.85	30.38	2750	23	2690	43	2773	43	3.0	2.2
LA227_17	3.143	0.110	0.235	0.006	0.433	0.096	0.004	18.29	24.29	53.4	1433	28	1356	32	1507	72	10.0	5.4
LA227_18	3.343	0.094	0.258	0.006	0.625	0.093	0.003	359	266	645	1486	22	1476	32	1469	54	-0.5	0.7
LA227_19	5.440	0.290	0.302	0.017	0.774	0.128	0.006	530	343	1113	1886	46	1698	86	2060	76	17.6	10.0
LA227_20	3.104	0.088	0.240	0.005	0.595	0.091	0.003	76.7	78.7	178.4	1426	22	1386	26	1443	54	4.0	2.8
LA227_21	3.125	0.083	0.244	0.005	0.654	0.092	0.002	153.1	105	244.5	1434	20	1403	25	1451	50	3.3	2.2
LA227_22	3.121	0.089	0.241	0.005	0.685	0.091	0.003	107.1	103.1	236.7	1431	21	1391	27	1442	52	3.5	2.8
LA227_23	3.280	0.120	0.251	0.009	0.611	0.094	0.004	187.8	267	569	1476	30	1437	46	1479	72	2.8	2.6
LA227_24	3.063	0.085	0.244	0.004	0.670	0.089	0.002	107.1	86	196.8	1418	21	1404	23	1384	51	-1.4	1.0
LA227_25	3.058	0.084	0.235	0.005	0.577	0.093	0.003	91	87.6	195.5	1418	22	1361	24	1461	53	6.8	4.0
LA227_26	3.073	0.083	0.238	0.005	0.572	0.093	0.003	88.5	109.4	243.1	1421	21	1375	25	1456	53	5.6	3.2
LA227_27	2.993	0.077	0.232	0.005	0.577	0.092	0.003	269.3	175.2	395	1403	20	1343	23	1460	52	8.0	4.3
LA227_28	2.569	0.093	0.185	0.006	0.642	0.099	0.003	570	464	918	1286	26	1095	35	1591	69	31.2	14.9
LA227_29	3.074	0.085	0.247	0.005	0.500	0.091	0.002	135.5	131.9	299.5	1420	21	1422	26	1422	51	0.0	-0.1
LA227_30	20.340	0.590	0.610	0.014	0.801	0.245	0.006	198.8	112.9	587	3100	28	3065	57	3149	40	2.7	1.1
LA227_31	2.931	0.084	0.237	0.005	0.672	0.091	0.003	79.6	77.4	176.2	1383	21	1368	27	1440	51	5.0	1.1
LA227_32	2.962	0.082	0.241	0.005	0.700	0.092	0.003	169.7	128.5	293.7	1395	22	1388	27	1444	52	3.9	0.5
LA227_33	2.994	0.091	0.239	0.005	0.615	0.093	0.003	51.7	62.65	142.9	1396	23	1376	27	1469	54	6.3	1.4
LA227_34	2.959	0.082	0.238	0.005	0.554	0.092	0.003	145.7	128.6	291.2	1391	20	1379	25	1454	50	5.2	0.9
LA227_35	2.766	0.071	0.224	0.005	0.721	0.092	0.002	702	452.7	1067	1345	19	1304	25	1462	50	10.8	3.0
LA227_36	2.986	0.079	0.244	0.005	0.757	0.091	0.002	324	395.1	929	1403	21	1409	25	1457	49	3.3	-0.4
LA227_37	2.971	0.088	0.247	0.006	0.164	0.090	0.003	136.6	301	701	1392	21	1418	30	1401	51	-1.2	-1.9
LA227_38	15.130	0.420	0.548	0.011	0.726	0.207	0.005	194	37.39	174.3	2817	27	2812	48	2880	41	2.4	0.2
LA227_39	2.882	0.081	0.241	0.005	0.646	0.091	0.003	106.7	103.5	240.8	1373	22	1393	28	1423	54	2.1	-1.5
LA227_40	4.362	0.120	0.302	0.007	0.720	0.109	0.003	90.6	105.5	300.2	1703	24	1696	35	1762	49	3.7	0.4
LA227_41	2.980	0.086	0.249	0.005	0.661	0.089	0.002	117.3	174.9	411.4	1396	22	1432	28	1399	54	-2.4	-2.6
LA227_42	3.086	0.085	0.2514	0.0057	0.63955	0.0922	0.0025	219.7	185.1	444	1426	21	1442	29	1457	53	1.0	-1.1
LA227_43	2.996	0.081	0.2428	0.0054	0.65937	0.0909	0.0025	99.2	68	153.8	1401	21	1398	28	1428	52	2.1	0.2
LA227_44	7.42	0.2	0.396	0.0086	0.69611	0.1395	0.0039	142.6	52.7	174.9	2157	25	2122	41	2209	47	3.9	1.6
LA227_45	3.091	0.083	0.2455	0.005	0.72531	0.0918	0.0024	262.4	167	392.3	1424	21	1412	26	1452	50	2.8	0.8
LA227_46	3.26	0.13	0.2481	0.0077	0.61751	0.096	0.0035	52.7	60	131.7	1465	30	1430	41	1514	68	5.5	2.4
LA227_47	4.394	0.12	0.3036	0.0068	0.57214	0.1057	0.003	102.6	116.3	318	1704	23	1704	33	1716	52	0.7	0.0
LA227_48	3.075	0.086	0.2438	0.0049	0.72835	0.0914	0.0024	130	91.6	207.3	1420	21	1403	25	1441	50	2.6	1.2
LA227_49	17.36	0.42	0.5633	0.01	0.69276	0.2236	0.0056	327.6	110.1	505	2952	23	2876	42	3001	40	4.2	2.6
LA227_50	3.067	0.084	0.2345	0.0041	0.62277	0.0945	0.0025	154.1	90.9	196.2	1421	21	1356	21	1503	50	9.8	4.6
LA227_51	2.973	0.079	0.2355	0.0045	0.61366	0.0913	0.0023	116.9	94.5	208.4	1395	20	1361	23	1444	47	5.7	2.4
LA227_52	17.19	0.56	0.529	0.017	0.70976	0.2361	0.0071	153.1	118	513	2935	32	2732	68	3079	48	11.3	6.9
LA227_53	2.981	0.088	0.2583	0.0051	0.60576	0.0907	0.0026	64.3	52.42	118.6	1397	22	1375	26	1423	56	3.4	1.6
LA227_54	3.072	0.083	0.2451	0.0056	0.66174	0.091	0.0025	112	90.4	206.8	1421	21	1412	29	1438	52	1.8	0.6
LA227_55	15.27	0.4	0.53	0.011	0.57918	0.209	0.0055	362	50.3	151.4	2833	25	2738	46	2891	42	5.3	3.4

LA227_56	2.969	0.083	0.2363	0.0052	0.7234	0.0907	0.0024	284.7	324.8	724	1393	21	1364	27	1439	51	5.2	2.1
LA227_57	3.002	0.09	0.2398	0.0055	0.71593	0.0906	0.0025	76.4	54.51	127.2	1402	23	1388	29	1418	52	2.1	1.0
LA227_58	13.25	0.35	0.5125	0.01	0.73027	0.1865	0.0047	129.2	132.2	585.9	2693	26	2663	44	2709	44	1.7	1.1
LA227_59	3.088	0.093	0.2441	0.0056	0.63819	0.0917	0.0026	61.3	64.13	145.6	1421	23	1404	29	1446	55	2.9	1.2
LA227_60	17.6	0.46	0.578	0.011	0.57592	0.2215	0.0059	238.4	57.9	294	2964	26	2945	46	2976	44	1.0	0.6
LA227_61	18.33	0.43	0.5729	0.01	0.74261	0.2324	0.0057	324.3	125.9	617	3007	24	2916	43	3064	39	4.8	3.0
LA227_62	3.06	0.086	0.2397	0.0047	0.67168	0.092	0.0025	102.5	75.7	171.4	1415	21	1382	24	1452	50	4.8	2.3
LA227_63	3.125	0.077	0.2456	0.0042	0.67448	0.0919	0.0023	429	256.3	580	1436	19	1416	22	1458	48	2.9	1.4
LA227_64	2.966	0.077	0.2372	0.0045	0.5968	0.0905	0.0024	84	55.81	123.1	1394	19	1372	23	1419	52	3.3	1.6
LA227_65	21.96	0.65	0.615	0.014	0.81062	0.2581	0.0066	451.5	361.6	1856	3178	28	3085	56	3235	39	4.6	2.9
LA227_66	7.5	0.2	0.3881	0.0073	0.44384	0.1394	0.0035	160.8	69.03	237.6	2166	23	2109	34	2211	43	4.6	2.6
LA227_67	3.13	0.12	0.2438	0.008	0.71338	0.0929	0.0029	417	388	841	1429	29	1408	42	1465	59	3.9	1.5
LA227_68	3.163	0.084	0.2509	0.0053	0.69537	0.0912	0.0024	216.8	230.9	535.1	1446	20	1440	27	1443	53	0.2	0.4
LA227_69	3.027	0.083	0.2455	0.0054	0.58756	0.0896	0.0025	79.6	50.36	114.1	1409	21	1414	28	1397	56	-1.2	-0.4
LA227_70	3.04	0.082	0.2394	0.0048	0.65626	0.0919	0.0025	121.4	91.1	203.4	1413	20	1383	25	1451	50	4.7	2.1
LA227_71	6.32	0.16	0.3586	0.0067	0.69586	0.1277	0.0032	147.3	75.2	245	2018	23	1974	32	2056	45	4.0	2.2
LA227_72	3.047	0.088	0.2386	0.0066	0.66759	0.0922	0.0027	169.1	133.8	300	1416	21	1380	35	1462	57	5.6	2.5
LA227_73	3.151	0.078	0.2448	0.0043	0.66583	0.0932	0.0024	278.4	202.7	428.5	1445	20	1409	22	1482	48	4.9	2.5
LA227_74	7.56	0.19	0.4033	0.0076	0.64523	0.1363	0.0035	168	73.4	265	2178	23	2179	35	2167	45	-0.6	0.0
LA227_75	16.18	0.41	0.5547	0.011	0.77995	0.2098	0.0051	206.8	246	1128	2882	23	2840	44	2899	40	2.0	1.5
LA227_76	2.975	0.078	0.2376	0.0045	0.62278	0.0903	0.0024	110.9	97.9	212	1399	19	1376	24	1427	49	3.6	1.6
LA227_77	3.113	0.086	0.2419	0.0045	0.39168	0.0916	0.0024	202.9	212.7	469	1427	20	1394	23	1442	49	3.3	2.3
LA227_78	15.48	0.38	0.537	0.0089	0.70265	0.2073	0.0051	153.6	128.9	582	2846	24	2768	38	2881	40	3.9	2.7
LA227_79	3.078	0.08	0.2393	0.0045	0.59475	0.0926	0.0025	149	127.1	289	1424	20	1384	24	1467	50	5.7	2.8
LA227_80	3.125	0.089	0.2423	0.0049	0.26459	0.0922	0.0024	141	135.2	304.6	1431	21	1398	25	1454	49	3.9	2.3
LA227_81	16.71	0.42	0.5481	0.01	0.6693	0.2185	0.0056	301.1	49.9	228.3	2915	24	2813	43	2963	41	5.1	3.5
LA227_82	4.848	0.13	0.3181	0.0069	0.70806	0.1096	0.0029	212.4	120.5	342	1790	23	1779	34	1784	48	0.3	0.6
LA227_83	3.13	0.088	0.2435	0.0046	0.16081	0.0917	0.0024	126.3	107.3	239.7	1433	21	1402	24	1443	50	2.8	2.2
LA227_84	3.035	0.083	0.2405	0.0049	0.58151	0.0905	0.0025	64.7	49.9	110.5	1411	21	1386	25	1422	55	2.5	1.8
LA227_85	3.202	0.093	0.2492	0.0052	0.68105	0.0941	0.0026	117.9	72.6	166.4	1451	22	1431	27	1491	51	4.0	1.4
LA227_86	18.31	0.47	0.575	0.012	0.71505	0.2317	0.0059	297	23.85	109.1	2999	25	2929	47	3051	38	4.0	2.3
LA227_87	17.39	0.52	0.57	0.015	0.66198	0.2233	0.0065	151.7	42.8	197.8	2949	28	2895	60	2988	47	3.1	1.8
LA227_88	4.544	0.13	0.3118	0.0072	0.32245	0.1077	0.003	30.81	60.4	171	1730	23	1744	35	1736	52	-0.5	-0.8
LA227_89	7.04	0.2	0.3914	0.0087	0.71088	0.1317	0.0034	186.3	76.4	270.4	2108	25	2122	40	2108	46	-0.7	-0.7
LA227_90	3.158	0.09	0.2484	0.0052	0.13553	0.093	0.0025	135.2	96.2	223.8	1439	21	1427	27	1465	51	2.6	0.8
LA227_91	3.04	0.085	0.2399	0.0054	0.60447	0.0928	0.0026	115.9	62.84	147.9	1410	21	1383	28	1465	54	5.6	1.9
LA227_92	18.58	0.54	0.6	0.014	0.78817	0.2281	0.0059	122.9	26.65	136.1	3007	27	3015	56	3026	42	0.4	-0.3
LA227_93	16.5	0.51	0.552	0.018	0.6657	0.2214	0.0076	250.4	27.5	125.5	2901	31	2827	76	2960	47	4.5	2.6
LA227_94	19.91	0.53	0.622	0.014	0.7258	0.2356	0.0062	188	139.3	733	3079	26	3115	53	3078	41	-1.2	-1.2
LA227_95	3.015	0.085	0.2435	0.0058	0.46375	0.0922	0.0026	92	67.3	148.8	1408	22	1401	30	1451	53	3.4	0.5
LA227_96	3.19	0.088	0.2554	0.006	0.69	0.0917	0.0025	193.4	283.3	666	1448	21	1462	31	1453	51	-0.6	-1.0
LA227_97	3.101	0.094	0.2452	0.0058	0.66579	0.0921	0.0026	38.68	25.07	60.6	1423	23	1409	30	1452	56	3.0	1.0
LA227_98	3.101	0.096	0.2478	0.0056	0.0092777	0.0918	0.0027	60.8	41.26	95.1	1422	23	1423	29	1440	53	1.2	-0.1
LA227_99	4.341	0.13	0.3019	0.0072	0.62962	0.1059	0.003	88.3	68.8	193.2	1693	24	1695	35	1707	53	0.7	-0.1
LA227_100	3.051	0.083	0.2297	0.0051	0.65826	0.0978	0.0026	493.7	436	1124	1417	21	1330	27	1567	52	15.1	6.1
LA227_101	15.85	0.48	0.559	0.014	0.74536	0.2064	0.0056	65.8	65.4	328.9	2854	29	2850	55	2860	45	0.3	0.1
LA227_102	3.021	0.086	0.2465	0.0054	0.6525	0.0898	0.0025	87.9	63.43	146.9	1407	22	1420	28	1399	52	-1.5	-0.9
LA227_103	3.081	0.1	0.2415	0.0061	0.72538	0.0921	0.0027	59	37.5	87.7	1422	24	1393	32	1443	57	3.5	2.0
LA227_104	3.21	0.16	0.243	0.011	0.78174	0.0959	0.0038	407	261.5	675	1443	37	1406	61	1510	74	6.9	2.6
LA227_105	27.55	0.92	0.68	0.021	0.60159	0.2968	0.01	179.3	89.9	577	3397	33	3337	81	3440	55	3.0	1.8

LA227_106	17.57	0.58	0.583	0.016	0.69695	0.219	0.0063	142.8	46.5	239.5	2955	32	2950	66	2957	48	0.2	0.2
LA227_107	4.63	0.15	0.311	0.0084	0.17663	0.1082	0.0032	73.4	38.51	113.2	1740	26	1738	41	1738	55	0.0	0.1
LA227_108	7.38	0.3	0.309	0.018	0.38751	0.202	0.02	491	86.1	329.5	2144	37	1710	90	2620	110	34.7	20.2
LA227_109	3.217	0.1	0.2544	0.0071	0.2707	0.092	0.0028	112.9	88	212.7	1449	24	1455	36	1431	58	-1.7	-0.4
LA227_110	15.98	0.73	0.461	0.035	0.3857	0.264	0.034	347	36	389	2871	46	2480	140	3180	120	22.0	13.6
LA227_111	7.57	0.26	0.403	0.012	0.69833	0.138	0.0043	41.9	34.23	134.3	2168	31	2167	55	2178	54	0.5	0.0
LA227_112	6.38	0.2	0.3626	0.01	0.77645	0.1279	0.0037	261	123.6	426	2017	27	1984	47	2045	49	3.0	1.6
LA227_113	3.133	0.1	0.246	0.0071	0.67001	0.0936	0.0029	73.1	41.92	103.7	1431	26	1411	37	1467	61	3.8	1.4
LA227_114	3.223	0.097	0.2503	0.006	0.32011	0.0937	0.0027	228.3	244.5	603	1451	22	1436	31	1475	55	2.6	1.0
LA227_115	3.001	0.1	0.2432	0.0075	0.63096	0.0916	0.003	45.2	23.32	60	1395	26	1396	38	1424	63	2.0	-0.1
LA227_116	16.46	0.51	0.575	0.016	0.67247	0.2087	0.0062	76.1	32.5	169.6	2887	30	2920	66	2889	50	-1.1	-1.1
LA227_117	19.5	0.66	0.607	0.018	0.71112	0.2355	0.0072	84.7	26.84	152.6	3059	33	3042	70	3075	50	1.1	0.6
LA227_118	3.011	0.12	0.2381	0.009	0.4187	0.0946	0.0033	72.9	59.8	132.9	1402	30	1370	46	1478	68	7.3	2.3
LA227_119	3.155	0.098	0.2541	0.0066	0.69813	0.0913	0.0026	98.5	57	137.8	1439	24	1460	35	1427	55	-2.3	-1.5
LA227_120	3.252	0.099	0.2492	0.0055	0.58839	0.0946	0.0028	173.3	225.4	548	1461	23	1431	28	1497	54	4.4	2.1
LA227_121	3.119	0.096	0.2457	0.0064	0.63151	0.093	0.0028	84	48.13	114.5	1428	24	1411	33	1455	59	3.0	1.2
LA227_122	3.19	0.1	0.25	0.0068	0.59175	0.0933	0.0029	54.9	54.14	133.6	1444	25	1433	34	1460	60	1.8	0.8
LA227_123	3.131	0.098	0.2479	0.0061	0.71373	0.0922	0.0026	73	51.49	117.6	1431	24	1423	31	1446	54	1.6	0.6
LA227_124	19.2	0.92	0.582	0.03	0.55254	0.24	0.012	219.6	31.9	165	3034	46	2980	110	3085	72	3.4	1.8
LA227_125	13.44	0.41	0.502	0.012	0.70009	0.1937	0.0053	183.5	131.2	621	2702	28	2621	55	2763	47	5.1	3.0
LA227_126	13.47	0.53	0.211	0.018	0.037591	0.835	0.1	642	161.8	693	2694	34	1192	93	4800	250	75.2	55.8
LA227_127	17.93	0.58	0.576	0.017	0.5504	0.2283	0.0071	204.1	33.5	175.8	2978	32	2917	70	3024	48	3.5	2.0
LA227_128	17.22	0.47	0.537	0.012	0.53492	0.2343	0.0067	301.8	124.6	537	2941	26	2771	53	3070	45	9.7	5.8
LA227_129	3.088	0.098	0.2554	0.0079	0.72425	0.0897	0.0027	180.8	231.4	555	1428	25	1461	40	1403	59	-4.1	-2.3
LA227_130	2.994	0.1	0.2321	0.0063	0.63076	0.0942	0.0032	79	52.7	126	1402	27	1343	33	1486	65	9.6	4.2
LA227_131	13.49	0.39	0.529	0.013	0.70507	0.1874	0.0052	140.5	107.7	510.8	2704	27	2725	54	2702	45	-0.9	-0.8
LA227_132	3.051	0.094	0.2409	0.0071	0.47952	0.0933	0.0029	392	173.3	437	1415	23	1393	35	1472	57	5.4	1.6
LA227_133	15.04	0.45	0.541	0.014	0.68924	0.2055	0.0059	93.3	72.2	354.1	2810	29	2780	60	2847	47	2.4	1.1
LA227_134	7.27	0.2	0.3824	0.0081	0.6787	0.1385	0.0037	249.9	70.5	213.5	2142	24	2083	37	2201	46	5.4	2.8
LA227_135	8.84	0.27	0.375	0.016	0.37711	0.191	0.018	441.2	49.8	131	2313	28	2058	74	2608	90	21.1	11.0
LA227_136	16.1	0.45	0.523	0.013	0.68089	0.2285	0.0083	372.3	172.3	775	2880	28	2706	55	3015	30	10.2	6.0
LA227_137	3.061	0.081	0.243	0.005	0.37951	0.0929	0.0026	96.5	72.6	164.8	1417	20	1399	26	1463	52	4.4	1.3
LA227_138	2.806	0.073	0.2158	0.0041	0.56361	0.0944	0.0025	484	552	1202	1354	20	1258	21	1506	49	16.5	7.1
LA227_139	16.72	0.49	0.543	0.014	0.74594	0.2234	0.006	224.8	83.8	430.2	2913	28	2796	58	2998	43	6.7	4.0
LA227_140	2.228	0.07	0.1583	0.0042	0.5994	0.1024	0.0031	218	215	322.5	1184	22	946	23	1652	54	42.7	20.1

ISOTOPIC AND ELEMENT RATIOS				CONCENTRATIONS ppm						CALCULATED AGES Ma								
Sample	$^{207}\text{Pb}/^{235}\text{U}$	\pm 2 sigma	$^{206}\text{Pb}/^{238}\text{U}$	\pm 2 sigma	Rho	$^{207}\text{Pb}/^{206}\text{Pb}$	\pm 2 sigma	U	Th	Pb	$^{207}\text{Pb}/^{235}\text{U}$	\pm 2 sigma	$^{206}\text{Pb}/^{238}\text{U}$	\pm 2 sigma	$^{207}\text{Pb}/^{206}\text{Pb}$	\pm 2 sigma	Dis.(6/38/7/6)	Dis.(6/38/7/35)

UF30_1	3.156	0.043	0.254	0.004	0.444	0.090	0.001	54.5	80.51	489.8	1443.6	11	1460	23	1430	31	-2.1	-1.1
UF30_2	1.574	0.037	0.161	0.003	0.234	0.071	0.002	30.48	70.9	281.2	954	15	963	17	919	54	-4.8	-0.9
UF30_3	3.135	0.043	0.252	0.005	0.481	0.090	0.001	54.3	69.6	419.5	1441.9	11	1448	23	1419	30	-2.0	-0.4
UF30_4	3.128	0.047	0.251	0.005	0.261	0.091	0.002	52.39	76.29	456.8	1438	11	1441	24	1448	36	0.5	-0.2
UF30_5	3.142	0.048	0.253	0.005	0.373	0.090	0.002	39.39	47.9	280.2	1440	12	1453	23	1414	34	-2.8	-0.9
UF30_6	4.752	0.091	0.323	0.007	0.399	0.107	0.002	12.81	47.46	361.1	1771	16	1801	32	1738	38	-3.6	-1.7
UF30_7	3.159	0.049	0.254	0.005	0.446	0.091	0.002	225.4	281.4	1694	1446	12	1459	26	1446	31	-0.9	-0.9
UF30_8	3.114	0.066	0.249	0.005	0.435	0.092	0.002	54.3	63.5	383.6	1434	16	1430	27	1450	41	1.4	0.3
UF30_9	3.193	0.066	0.252	0.005	0.424	0.092	0.002	36.46	54.5	261.1	1452	16	1448	26	1457	41	0.6	0.3
UF30_10	3.231	0.048	0.256	0.005	0.260	0.093	0.002	203.7	299.7	1775	1464	11	1471	27	1475	37	0.3	-0.5
UF30_11	3.220	0.070	0.252	0.006	0.559	0.093	0.002	49.3	50.72	317.7	1459	17	1448	30	1474	39	1.8	0.8
UF30_12	3.199	0.040	0.252	0.005	0.418	0.093	0.001	417	664	4230	1454.7	9.6	1448	23	1472	23	1.6	0.5
UF30_13	3.213	0.046	0.256	0.005	0.420	0.091	0.001	94.3	116.1	706	1457.9	11	1470	24	1436	30	-2.4	-0.8
UF30_14	3.262	0.044	0.256	0.005	0.601	0.092	0.001	281.6	376.2	2375	1470	11	1472	24	1463	27	-0.6	-0.1
UF30_15	3.195	0.051	0.255	0.005	0.513	0.091	0.002	54.79	56.64	349.1	1453	12	1465	25	1443	31	-1.5	-0.8
UF30_16	3.176	0.052	0.256	0.005	0.410	0.090	0.002	59.46	63.69	387.6	1450	13	1469	24	1414	33	-3.9	-1.3
UF30_17	3.162	0.048	0.254	0.005	0.618	0.090	0.001	68.6	99.1	624.6	1447	12	1459	24	1429	29	-2.1	-0.8
UF30_18	3.206	0.042	0.255	0.005	0.517	0.092	0.001	191	294.8	1663	1457	10	1463	23	1459	26	-0.3	-0.4
UF30_19	3.246	0.043	0.257	0.004	0.572	0.092	0.001	134.7	162.3	1027	1465.7	10	1474	23	1458	27	-1.1	-0.6
UF30_20	1.840	0.027	0.182	0.003	0.348	0.074	0.001	82.3	57.3	254.2	1058.4	9.4	1079	18	1019	34	-5.9	-1.9
UF30_21	3.209	0.043	0.256	0.005	0.619	0.091	0.001	136.5	168.2	1023	1458.7	11	1470	23	1446	27	-1.7	-0.8
UF30_22	3.243	0.061	0.259	0.005	0.462	0.091	0.002	61.1	150.4	543	1464	15	1481	27	1432	35	-3.4	-1.2
UF30_23	3.180	0.046	0.252	0.004	0.528	0.092	0.001	59.4	97.5	564.5	1451.2	11	1450	22	1457	28	0.5	0.1
UF30_24	3.213	0.041	0.256	0.005	0.589	0.091	0.001	121.5	119.5	765	1458.1	9.7	1470	23	1446	25	-1.7	-0.8
UF30_25	4.043	0.062	0.295	0.006	0.665	0.100	0.002	98.2	166.2	1061	1641	13	1663	30	1612	29	-3.2	-1.3
UF30_26	3.238	0.046	0.254	0.004	0.398	0.093	0.001	56.61	75.1	464.1	1463.4	11	1456	22	1472	29	1.1	0.5
UF30_27	3.180	0.044	0.253	0.004	0.458	0.091	0.001	51.69	63.39	384.1	1451.4	10	1450	23	1447	30	-0.2	0.1
UF30_28	3.248	0.041	0.259	0.005	0.644	0.091	0.001	215.5	354.2	2219	1468	10	1482	24	1447	26	-2.4	-1.0
UF30_29	2.181	0.028	0.203	0.004	0.512	0.078	0.001	128.2	88.2	440	1173.3	8.8	1194	19	1138	29	-4.7	-1.5
UF30_30	3.234	0.047	0.258	0.005	0.488	0.091	0.001	61.8	92.2	574	1463	12	1479	24	1442	30	-2.6	-1.1
UF30_31	2.140	0.033	0.197	0.003	0.276	0.079	0.001	67.57	104.18	500	1159	11	1464	19	1148	32	-1.1	-0.2
UF30_32	3.192	0.044	0.252	0.005	0.549	0.092	0.002	70.6	108	656.7	1453.3	11	1449	24	1459	28	0.7	0.3
UF30_33	3.276	0.061	0.259	0.005	0.364	0.092	0.002	99.4	128.1	791	1474	14	1486	24	1460	38	-1.8	-0.8
UF30_34	1.852	0.023	0.184	0.003	0.516	0.073	0.001	147	125.2	577.7	1062.5	8.1	1088	17	1015	28	-7.2	-2.4
UF30_35	3.260	0.073	0.256	0.006	0.623	0.093	0.002	129.4	149.4	901	1469	17	1471	30	1476	35	0.3	-0.1

UF30_36	3.175	0.045	0.256	0.004	0.523	0.090	0.001	64.47	96.83	590.5	+448.6	+4	+467	+22	+448	+29	-3.5	-1.3
UF30_37	0.553	0.009	0.069	0.001	0.487	0.058	0.001	1013	641	1147	+447.5	+5.8	+432.1	+8.4	+520	+37	16.9	3.4
UF30_38	3.621	0.065	0.261	0.005	0.507	0.101	0.002	201.4	298.9	2120	+455.1	+44	+449.5	+23	+462.8	+33	8.2	3.6
UF30_39	3.472	0.047	0.274	0.005	0.670	0.092	0.001	88.6	155.9	1029	1518.9	+11	1558	+25	1463	+26	-6.5	-2.6
UF30_40	3.276	0.043	0.257	0.004	0.563	0.092	0.001	132.7	162.9	1041	1473.6	+10	1474	+22	1468	+26	-0.4	0.0
UF30_41	3.286	0.081	0.257	0.006	0.580	0.093	0.002	60	95	634	+476	+49	+470	+32	+479	+37	0.6	0.4

Sample	ISOTOPIC AND ELEMENT RATIOS				CONCENTRATIONS ppm						CALCULATED AGES Ma						Dis.(6/38/7/	Dis.(6/38/7/35)
	$^{207}\text{Pb}/^{235}\text{U}$	± 2	$^{206}\text{Pb}/^{238}\text{U}$	± 2	Rho	$^{207}\text{Pb}/^{206}\text{Pb}$	± 2	U	Th	Pb	$^{207}\text{Pb}/^{23$	± 2	$^{206}\text{Pb}/^{238}$	± 2 sigma	$^{207}\text{Pb}/^{206}$	± 2	sigma	6)
NS32_1	1.606	0.046	0.146	0.0024	0.18954	0.079	0.0017	97.3	152.9	42.97	970	18	878	14	1159	44	24.2	9.5
NS32_2	3.677	0.072	0.1971	0.0023	0.22716	0.1346	0.002	348.8	290.8	228.8	+4562	+45	+4459.2	+43	+2449	+25	46.1	25.8
NS32_3	2.336	0.029	0.2103	0.0023	-0.0041335	0.07985	0.00092	101.4	110.8	64.08	+4221.6	+9	+4230.2	+12	+1189	+24	-3.5	-0.7
NS32_4	2.772	0.047	0.2319	0.0026	0.025713	0.086	0.0014	65.7	80.3	50.31	1341.6	9.6	1344.1	14	1322	22	-1.7	-0.2
NS32_5	2.089	0.035	0.1921	0.0025	0.04396	0.0781	0.0013	72.9	140.8	73.5	1141	12	1132	13	1141	30	0.8	0.8
NS32_6	2.314	0.028	0.2088	0.0022	0.17749	0.07983	0.00077	134.8	41.04	23.45	1214.8	8.5	1221.9	12	1184	18	-3.2	-0.6
NS32_7	2.065	0.025	0.1935	0.0021	0.06037	0.07667	0.00094	128.9	140.4	74.87	1135.8	8.2	1140	11	1113	20	-2.4	-0.4
NS32_8	4.512	0.069	0.2906	0.0037	0.017647	0.1109	0.002	117.9	115.5	74	1732	13	1644	18	1820	24	9.7	5.1
NS32_9	4.523	0.078	0.2606	0.0044	0.7124	0.12484	0.00071	382	152.3	14.32	+4734	+45	+4494	+23	+2023	+40	26.1	13.7
NS32_10	2.018	0.025	0.1898	0.002	0.12334	0.07659	0.0007	130	78.6	41.73	1119.8	8.4	1120.1	11	1102	19	-1.6	0.0
NS32_11	6.017	0.075	0.3444	0.0043	0.51582	0.1269	0.0012	305	302.8	248.1	1977.1	11	1907	21	2052	16	7.1	3.5
NS32_12	1.803	0.041	0.1758	0.0023	0.102	0.0739	0.0017	30.59	33.76	16.83	1042	15	1043	13	1008	46	-3.5	-0.1
NS32_13	2.373	0.029	0.2117	0.0025	0.25129	0.08068	0.00077	235.6	130.4	77.6	1234.3	8.8	1237.7	13	1208	19	-2.5	-0.3
NS32_14	6.765	0.1	0.3881	0.0045	0.14656	0.1267	0.0014	37.93	13.6	13.54	2081	12	2113	21	2042	20	-3.5	-1.5
NS32_15	6.005	0.061	0.358	0.0038	0.51582	0.12126	0.00065	308	409.7	382.3	1975.2	8.9	1972	18	1972	9.6	0.0	0.2
NS32_16	1.972	0.028	0.1606	0.0023	0.013956	0.0887	0.0013	116.2	136.2	74.3	+4403.6	+9.6	+960	+13	+4393	+25	31.1	13.0
NS32_17	2.488	0.035	0.2191	0.0026	0.16964	0.08229	0.00089	171	99	57.7	1266.8	10	1276.8	14	1244	22	-2.6	-0.8
NS32_18	2.646	0.035	0.2253	0.0025	-0.0082417	0.0842	0.0013	69.4	42	25.03	+4311.2	+9.9	+4309.4	+13	+4303	+22	-0.5	0.1
NS32_19	4.103	0.061	0.285	0.0046	0.77128	0.1042	0.001	651	772	522	1654	12	1616	23	1696	18	4.7	2.3
NS32_20	2.189	0.083	0.1993	0.0022	-0.004489	0.0797	0.0029	83.5	89.1	48.9	+4462	+40	+4471.4	+42	+4427	+26	-3.9	-0.8
NS32_21	2.049	0.03	0.193	0.0021	-0.018828	0.07687	0.0009	141.8	317.1	171.4	+4429.5	+9.5	+4437.1	+44	+4406	+22	-2.8	-0.7
NS32_22	2.057	0.031	0.1893	0.0024	0.092413	0.07901	0.00098	229.8	147.3	71.3	1133.5	10	1117	13	1166	24	4.2	1.5
NS32_23	13.83	0.16	0.5358	0.0063	0.75356	0.1866	0.0019	108.4	52.88	74.3	2737.1	11	2765	26	2709	16	-2.1	-1.0
NS32_24	2.447	0.052	0.2136	0.0031	-0.0055018	0.0831	0.0017	26.2	30.1	17.18	+4250	+45	+4247	+46	+4234	+45	-1.1	0.2
NS32_25	1.855	0.042	0.1783	0.0024	0.23821	0.0756	0.0016	26.64	17.1	8.49	1060	15	1057	13	1049	44	-0.8	0.3
NS32_26	1.991	0.026	0.1893	0.0021	0.11142	0.07637	0.00083	120.7	125.2	65.5	1111.3	8.8	1117.3	11	1094	22	-2.1	-0.5
NS32_27	2.182	0.03	0.2023	0.0022	-0.027802	0.07818	0.00094	125.3	67.9	37.46	+4473.5	+9.3	+4487.2	+42	+4439	+24	-4.2	-1.2
NS32_28	4.14	0.11	0.233	0.0043	0.28945	0.1271	0.0022	165.6	320	178.4	+4650	+24	+4348	+22	+2053	+22	34.3	18.3
NS32_29	1.615	0.026	0.1456	0.0024	0.90921	0.08019	0.0005	731	377	29.38	973.3	9.9	875	+43	+4499	+43	27.0	10.1
NS32_30	2.936	0.083	0.1906	0.0046	-0.018332	0.1118	0.0027	50.75	109	56.6	+4384	+24	+4423	+25	+4808	+44	37.9	18.9
NS32_31	2.028	0.036	0.1911	0.0023	-0.01103	0.0764	0.0011	88.3	67.3	38.5	+4423	+42	+4427.2	+42	+4095	+28	-2.9	-0.4

NS32_32	3.014	0.034	0.2481	0.0026	0.075423	0.08799	0.00074	125.3	77.4	52.4	1409.6	8.5	1428.3	13	1376	16	-3.8	-1.3
NS32_33	1.805	0.024	0.1632	0.002	0.67759	0.07981	0.00067	456.5	369	61.7	1046.1	8.7	974.3	11	1188	17	18.0	6.9
NS32_34	6.593	0.061	0.3791	0.0038	0.68176	0.12583	0.0006	406.9	376.4	367.9	2057.9	8.3	2072	18	2038.9	8.6	-1.6	-0.7
NS32_35	6.454	0.063	0.3716	0.0038	0.065319	0.12593	0.00068	184.5	60.6	47.8	2038.5	8.6	2036	18	2039	9.5	0.1	0.1
NS32_36	4.923	0.053	0.3159	0.0034	-0.0074051	0.11285	0.00086	129.7	144.5	88.7	1804.7	9.1	1769	16	1844	14	3.9	2.0
NS32_37	7.737	0.096	0.3091	0.0039	0.54825	0.18109	0.00091	256	334.4	292.5	2198.1	14	1735	19	2660.5	8.3	34.8	21.1
NS32_38	2.005	0.024	0.19	0.002	-0.0061275	0.07632	0.00084	121.8	50.78	26.82	1145.5	8.3	1120.9	14	1098	20	-2.1	-0.5
NS32_39	2.212	0.028	0.2024	0.0021	0.058154	0.07929	0.00083	97.8	102.7	58.25	1183.8	8.7	1188.1	12	1169	21	-1.6	-0.4
NS32_40	2.345	0.025	0.2082	0.0021	0.12205	0.0815	0.00058	308.4	49.7	32.2	1225	7.6	1219.1	11	1229	14	0.8	0.5
NS32_41	10.53	0.27	0.4099	0.0085	0.8062	0.188	0.0024	593	561	279.3	2480	24	2243	39	2722	22	18.7	10.8
NS32_42	1.997	0.034	0.1914	0.0022	0.11171	0.0757	0.0012	43.74	64	33.99	1111	11	1128.7	12	1064	32	-6.1	-1.6
NS32_43	2.16	0.026	0.199	0.0022	0.039792	0.07822	0.00084	168.3	70.7	38.85	1166.8	8.3	1169.7	12	1155	17	-1.3	-0.2
NS32_44	12.731	0.13	0.5173	0.0058	0.38343	0.1783	0.0012	77.3	88.2	118.2	2659.7	9.6	2686	25	2634	11	-2.0	-1.0
NS32_45	2.856	0.039	0.2393	0.0028	0.17817	0.08653	0.00094	130.3	64.4	41.56	1368.4	10	1383	15	1342	21	-3.1	-1.1
NS32_46	2.487	0.037	0.2177	0.0034	0.52605	0.0831	0.001	278.3	282.7	160.2	1267.2	11	1269	18	1267	24	-0.2	-0.1
NS32_47	5.445	0.083	0.3286	0.0046	0.043042	0.1202	0.0015	238.9	117	82.8	1890	13	1831	22	1954	21	6.3	3.1
NS32_48	10.627	0.11	0.4723	0.0057	0.62733	0.1634	0.0013	268.9	80.9	91.7	2490.1	9.8	2493	25	2488	13	-0.2	-0.1
NS32_49	6.406	0.077	0.344	0.0041	0.53944	0.1343	0.0012	141.9	239	148.1	2031.9	14	1905	20	2151	16	114	6.2
NS32_50	2.866	0.049	0.2364	0.0029	-0.014632	0.0876	0.0016	27.1	32.9	21.66	1368	13	1367	15	1344	40	-1.7	0.1
NS32_51	2.578	0.034	0.2225	0.0024	0.0026139	0.0834	0.0012	63	33.67	20.73	1292.3	9.6	1294.8	13	1277	22	-1.4	-0.2
NS32_52	4.073	0.051	0.2489	0.003	0.24199	0.11797	0.00078	368.5	152.1	74.1	1646.5	10	1432	15	1920	10	25.4	13.0
NS32_53	2.4	0.051	0.2114	0.0037	0.22767	0.083	0.0019	199.2	79.9	43.8	1241	15	1236	20	1261	44	2.0	0.4
NS32_54	1.789	0.025	0.176	0.002	0.089142	0.0735	0.00092	77.6	59.96	30.21	1039.2	9.2	1045	11	1013	26	-3.2	-0.6
NS32_55	4.526	0.056	0.3101	0.0034	0.17978	0.1055	0.0011	75.5	60.7	52.21	1733.5	10	1740	17	1715	19	-1.5	-0.4
NS32_56	5.392	0.081	0.344	0.004	0.01355	0.1136	0.0015	27.52	5.43	5.12	1879	13	1905	19	1845	24	-3.3	-1.4
NS32_57	6.638	0.07	0.3803	0.0043	0.62347	0.1266	0.00084	256.6	206.2	204.8	2063.4	9.3	2077	20	2049	12	-1.4	-0.7
NS32_58	14.436	0.13	0.542	0.0053	0.45179	0.19236	0.00089	218.3	138.2	190.9	2777.8	8.6	2791	22	2760.4	7.6	-1.1	-0.5
NS32_59	2.101	0.037	0.1895	0.0028	0.62478	0.0807	0.001	177.9	105.1	24.19	1148	12	1118	15	1208	26	7.5	2.6
NS32_60	5.79	0.37	0.2457	0.0063	0.90088	0.1672	0.0058	250.4	218.3	140	1894	39	1411	32	2495	50	43.4	25.5
NS32_61	1.889	0.025	0.1798	0.002	-0.0716	0.07582	0.0009	100.7	129.1	67.24	1075.4	9	1065.6	14	1082	23	1.5	0.9
NS32_62	2.008	0.022	0.1892	0.002	0.50753	0.07677	0.00056	216.5	259.9	136.9	1117	7.4	1116.8	11	1111	15	-0.5	0.0
NS32_63	2.002	0.028	0.1897	0.0021	-0.046111	0.07643	0.00096	78.6	97.5	51.57	1114.1	9.5	1119.3	14	1092	26	-2.5	-0.5
NS32_64	2.066	0.027	0.1953	0.0021	0.16088	0.07653	0.00088	92.9	53	29.21	1135.5	9.1	1149.5	11	1097	23	-4.8	-1.2
NS32_65	2.046	0.036	0.1925	0.0021	-0.071385	0.077	0.0012	84.1	72.9	38.63	1127.6	10	1134.5	14	1105	26	-2.7	-0.6
NS32_66	2.009	0.045	0.1893	0.0026	0.31909	0.0774	0.0016	63.23	48.89	25.38	1117	15	1117	14	1112	41	-0.4	0.0
NS32_67	1.974	0.025	0.1857	0.0021	0.14729	0.07711	0.00085	121	125.8	65.73	1104.8	8.7	1097.9	11	1113	22	1.4	0.6
NS32_68	6.584	0.064	0.3787	0.0038	0.64924	0.12592	0.00069	266.1	64.9	63.8	2056.1	8.6	2070	18	2038.8	9.7	-1.5	-0.7
NS32_69	2.371	0.059	0.2099	0.003	-0.03378	0.082	0.002	16.76	8.14	4.67	1224	48	1229	16	1194	50	-2.9	-0.4
NS32_70	2.172	0.027	0.2001	0.0021	0.10446	0.07858	0.0008	119.6	74.19	40.86	1170.4	8.7	1175.9	11	1152	20	-2.1	-0.5
NS32_74	2.408	0.039	0.20992	0.0032	0.19509	0.0843	0.001	405.7	339.2	68.2	1244	12	1224	17	1295	24	5.5	1.6
NS32_72	4.566	0.055	0.3101	0.0035	0.20636	0.1071	0.00095	85.7	85.5	70.6	1740.9	10	1741	17	1744	16	0.2	0.0
NS32_73	2.194	0.031	0.2015	0.0021	0.054572	0.07946	0.00078	134.8	70.3	38.38	1180.1	7.9	1182.9	12	1174	19	-0.8	-0.2
NS32_74	2.387	0.033	0.161	0.0023	0.70609	0.10754	0.00099	716	390.7	162.4	1237.4	10	962	13	1756	16	45.2	22.3
NS32_75	4.416	0.052	0.2853	0.0035	0.48956	0.1125	0.0011	123.6	93.46	74.78	1713.9	9.8	1617	18	1835	18	41.9	5.7
NS32_76	2.388	0.06	0.2116	0.0024	0.014885	0.0819	0.002	96.5	113.3	64.3	1229.2	8.6	1237	13	1216	22	-1.7	-0.6
NS32_77	2.495	0.048	0.2172	0.0027	0.0071112	0.0831	0.0017	108.2	84.3	48.1	1263.1	10	1266	14	1254	22	-1.0	-0.2
NS32_78	1.845	0.021	0.1802	0.0019	-0.003111	0.07395	0.00094	164.5	124.7	60.72	1060.6	7.5	1067.7	10	1048	18	-4.9	-0.7
NS32_79	2.389	0.047	0.213	0.0027	-0.014958	0.0812	0.0017	64.22	72.2	40.29	1235	13	1244	14	1221	33	-1.9	-0.7
NS32_80	4.429	0.05	0.2843	0.0036	0.60638	0.1137	0.001	328.7	219.5	163	1716.9	9.4	1613	18	1856	16	43.4	6.1
NS32_81	2.348	0.046	0.2077	0.0029	0.15462	0.0825	0.0015	72.9	57.8	31.73	1224	14	1217	16	1240	35	1.9	0.6
NS32_82	2.152	0.028	0.1842	0.0021	0.54803	0.08501	0.00084	200.7	197.7	82.9	1163.9	9.1	1089.5	11	1310	19	16.8	6.4
NS32_83	16.1	0.17	0.5666	0.0064	0.40077	0.2067	0.0014	89.8	39.56	55.51	2881.1	10	2894	26	2877	11	-0.6	-0.4
NS32_84	2.611	0.089	0.2257	0.0081	0.2681	0.0859	0.0021	417	269	107	1302	25	1311	43	1329	48	1.4	-0.7

NS32_85	6.733	0.069	0.3843	0.0042	0.63311	0.12773	0.00083	164.5	401.6	403.2	2076.2	8.8	2096	20	2063	11	-1.6	-1.0
NS32_86	2.271	0.026	0.2098	0.0022	0.074127	0.07868	0.00063	194.6	49.1	27.1	1202	8.1	1227.5	12	1158	16	-6.0	-2.1
NS32_87	2.019	0.025	0.1909	0.002	0.074264	0.07694	0.00073	160.5	89.5	43	1120.4	8.5	1126.1	11	1111	19	-1.4	-0.5
NS32_88	2.772	0.036	0.234	0.0027	0.064354	0.0862	0.001	96.5	23.6	14.86	1346.5	9.8	1355	14	1334	23	-1.6	-0.6
NS32_89	4.618	0.05	0.3154	0.0034	0.51461	0.10665	0.00082	171.6	175.1	149.3	1751	9.1	1767	17	1739	14	-1.6	-0.9
NS32_90	6.654	0.076	0.3799	0.0043	0.78759	0.1275	0.00091	97.9	83.66	83.12	2064.5	9.9	2075	20	2062	12	-0.6	-0.5
NS32_91	13.37	0.15	0.5242	0.0062	0.68974	0.1856	0.0013	112.3	56.31	76.5	2704.2	10	2719	27	2702	11	-0.6	-0.5
NS32_92	3.19	0.048	0.2464	0.0031	0.49745	0.0943	0.0012	72.13	78.2	44.4	1453	12	1421	16	1506	23	5.6	2.2
NS32_93	2.644	0.069	0.2316	0.0034	-0.0038407	0.0843	0.0022	14.9	11.39	7.35	1306	48	14342	48	1244	54	-8.4	-2.8
NS32_94	2.034	0.03	0.1917	0.0022	0.40042	0.07747	0.00093	67.9	58.25	32	1126	10	1130.8	12	1122	24	-0.8	-0.4
NS32_95	2.4	0.032	0.2171	0.0024	0.39498	0.08073	0.00089	82.2	95.6	58.6	1241.3	9.6	1266	13	1204	22	-5.1	-2.0
NS32_96	2.863	0.038	0.239	0.0028	0.4995	0.08708	0.00091	88.1	67.5	46.2	1369.8	10	1382	15	1352	21	-2.2	-0.9
NS32_97	4.741	0.065	0.3168	0.0041	0.12032	0.1089	0.0011	148.9	189.8	158.3	1769.7	10	1773	20	1769	14	-0.2	-0.2
NS32_98	6.08	0.11	0.3631	0.006	0.70105	0.1216	0.0015	117.8	147	143.6	1986	16	1996	29	1975	22	-1.1	-0.5
NS32_99	1.955	0.024	0.1861	0.0021	0.16269	0.07616	0.00079	168.2	119	63.68	1099.2	8.2	1100.1	12	1092	21	-0.7	-0.1
NS32_100	2.235	0.026	0.2035	0.0025	0.64334	0.07994	0.00057	333.5	244.8	134	1190.9	8	1193.5	13	1190	14	-0.3	-0.2
NS32_101	11.89	0.15	0.489	0.006	0.61414	0.1765	0.0015	39.4	71.7	93.1	2593	12	2565	26	2617	14	2.0	1.1
NS32_102	2.009	0.044	0.1899	0.0025	0.059989	0.077	0.0015	29.9	11.28	6.28	1112	15	1120	14	1085	40	-3.2	-0.7
NS32_103	1.928	0.03	0.1753	0.0022	0.059287	0.0801	0.0012	61.9	179.8	25.41	1087.9	44	1040.9	42	1182	29	41.9	4.3
NS32_104	2.39	0.028	0.2144	0.0024	0.38261	0.08098	0.00077	125.8	26.31	16.25	1238.1	8.4	1251.8	13	1214	19	-3.1	-1.1
NS32_105	8.995	0.091	0.4434	0.0049	0.51807	0.14744	0.00092	150.9	58.97	69.51	2336	9.2	2366	22	2313	11	-2.3	-1.3
NS32_106	2.14	0.033	0.1961	0.0032	0.46951	0.0797	0.0011	151.5	127.7	68.5	1160.5	11	1154	17	1180	28	2.2	0.6
NS32_107	6.483	0.065	0.3813	0.0043	0.66204	0.12316	0.0007	176	120.5	122.9	2044.1	8.5	2081	20	2000	11	-4.1	-1.8
NS32_108	1.85	0.048	0.1701	0.0046	0.63698	0.0787	0.0017	227	79	27.39	1062	47	1042	25	1157	44	42.5	4.7
NS32_109	8.05	0.081	0.4132	0.0045	0.61835	0.14127	0.00094	123.1	69.09	60.27	2235.2	9.1	2229	21	2240	11	0.5	0.3
NS32_110	1.977	0.033	0.187	0.0024	0.5421	0.0768	0.0011	51.29	69.2	35.54	1106	11	1105	13	1103	29	-0.2	0.1
NS32_111	2.587	0.044	0.2279	0.003	0.46439	0.0825	0.0012	37.98	21.31	13.27	1294	12	1323	16	1243	27	-6.4	-2.2
NS32_112	2.213	0.029	0.203	0.0026	0.55153	0.07927	0.00084	229.7	140.5	75.5	1184	9.2	1191	14	1175	22	-1.4	-0.6
NS32_113	1.937	0.035	0.1854	0.0026	-0.010436	0.0758	0.0014	60	22.65	11.18	1092	42	4096	44	1072	37	-2.2	-0.4
NS32_114	2.078	0.028	0.1954	0.0024	0.6916	0.07695	0.00075	149.5	122.4	65.5	1139.5	9.1	1150.3	13	1114	19	-3.3	-0.9
NS32_115	7.292	0.071	0.3987	0.0043	0.61934	0.13229	0.0008	273.5	153	159.4	2146.6	8.7	2162	20	2125	11	-1.7	-0.7
NS32_116	3.729	0.044	0.2739	0.0028	0.43021	0.09832	0.00089	143.9	99.9	74.3	1576.5	9.5	1560.3	14	1586	17	1.6	1.0
NS32_117	2.857	0.042	0.2347	0.0027	0.61184	0.0877	0.00089	133.4	67.5	47.65	1368.7	11	1358.5	14	1370	19	0.8	0.7
NS32_118	33.46	0.56	0.7442	0.011	0.77129	0.3234	0.0032	191.4	87.7	156.5	3591	17	3584	40	3584	15	0.0	0.2
NS32_119	0.997	0.032	0.1021	0.0022	0.52601	0.0713	0.0018	168.2	46	7.2	701	46	627	43	954	52	34.3	10.6
NS32_120	2.358	0.079	0.1409	0.002	0.39499	0.1243	0.0043	491	348.2	149	1226	24	849.2	42	1988	59	57.3	30.7
NS32_121	17.87	0.25	0.5888	0.009	0.7957	0.2209	0.0018	109.1	75.5	101.6	2982	14	2982	36	2984	13	0.1	0.0
NS32_122	1.999	0.022	0.1898	0.002	0.50745	0.07602	0.00058	266.5	185.8	97.9	1114.2	7.3	1119.9	11	1091	15	-2.6	-0.5
NS32_123	2.838	0.038	0.2371	0.0026	-0.039087	0.08681	0.00093	84.2	108	68	1363.6	40	1371.1	43	1347	24	-4.8	-0.6
NS32_124	4.574	0.034	0.1315	0.0025	0.93046	0.08614	0.00062	635	738	31.84	954	43	795	44	1337	44	40.5	16.7
NS32_125	1.839	0.045	0.1583	0.0033	0.79461	0.0836	0.0012	287	377.1	161.9	1057	46	947	48	1277	28	25.8	10.4
NS32_126	1.856	0.034	0.1758	0.0023	0.28584	0.0767	0.0013	41	70.8	22.43	1062	12	1043.6	13	1086	35	3.9	1.7

ISOTOPIC AND ELEMENT RATIOS						CONCENTRATIONS ppm						CALCULATED AGES Ma						
Sample	$^{207}\text{Pb}/^{235}\text{U}$	\pm 2 sigma	$^{206}\text{Pb}/^{238}\text{U}$	\pm 2 sigma	Rho	$^{207}\text{Pb}/^{206}\text{Pb}$	\pm 2 sigma	U	Th	Pb	$^{207}\text{Pb}/^{235}\text{U}$	\pm 2 sigma	$^{206}\text{Pb}/^{238}\text{U}$	\pm 2 sigma	$^{207}\text{Pb}/^{206}\text{Pb}$	\pm 2 sigma	Dis.(6/38/7/6)	Dis.(6/38/7/35)
NS44_1	1.234	0.019	0.1173	0.0015	0.62404	0.07603	0.00078	546	427	122	814.8	8.4	714.9	8.5	1089	21	34.4	12.3
NS44_2	0.955	0.019	0.03566	0.00077	0.96243	0.19526	0.00099	4040	4520	619	677.7	9.7	225.8	4.8	2785.4	8.4	91.9	66.7
NS44_3	1.718	0.018	0.1718	0.0018	0.50182	0.0726	0.00053	437	47.8	22.71	1014.6	6.6	4022	9.9	4000	44	-2.2	-0.7
NS44_4	4.688	0.052	0.3041	0.0036	0.74013	0.11206	0.00071	631	320	259.8	1765.7	9.2	1711	18	1830	12	6.5	3.1

NS44_5	0.9166	0.011	0.1098	0.0012	0.3978	0.06092	0.00058	313.1	140.3	43.2	659.8	5.8	671.9	6.8	628	21	-7.0	-1.8
NS44_6	5.97	0.063	0.3566	0.0039	0.72462	0.12195	0.0007	417	175	169.2	1970.5	9.1	1965	19	1982	10	0.9	0.3
NS44_7	1.07	0.019	0.1227	0.0015	0.14722	0.0637	0.0012	75.3	49.1	16.83	737.1	9.6	745.6	8.7	704	38	-5.9	-1.2
NS44_8	1.682	0.02	0.1694	0.0019	0.46108	0.07222	0.00065	183	116.2	54.9	1001	7.6	1008.4	10	984	18	-2.5	-0.7
NS44_9	1.702	0.019	0.1708	0.0018	0.50889	0.07264	0.00058	211.5	95.4	44.5	1008.3	7.4	1016.3	9.8	1000	46	-1.6	-0.8
NS44_10	1.118	0.014	0.12659	0.0014	0.26779	0.06428	0.00068	181.5	58.9	21.1	761	6.8	768.2	7.9	739	22	-4.0	-0.9
NS44_11	1.106	0.018	0.12568	0.0014	0.21441	0.06422	0.00098	102.3	58.6	19.99	754.8	8.8	763	7.9	728	32	-4.8	-1.1
NS44_12	1.822	0.022	0.0862	0.0017	0.56496	0.1557	0.0022	1788	2566	545.6	1052	7.8	532.8	10	2395	24	77.8	49.4
NS44_13	1.514	0.02	0.1535	0.0017	0.48888	0.07156	0.00069	234.2	244.7	108.8	934.9	8	920.4	9.6	967	20	4.8	1.6
NS44_14	1.122	0.019	0.1251	0.0021	0.6019	0.06573	0.00089	551	344	109.9	763	9.3	759	12	795	27	4.5	0.5
NS44_15	1.336	0.021	0.1134	0.002	0.37238	0.0865	0.0015	1217	817	214.2	861.8	9.5	692	12	1343	35	48.5	19.7
NS44_16	5.65	0.06	0.3428	0.0038	0.66448	0.11921	0.00075	532.8	140.7	131.6	1922.9	9.2	1899	48	1942	44	2.2	1.2
NS44_17	1.1382	0.012	0.12681	0.0013	0.47744	0.06516	0.0051	525	95.8	23.9	771	5.9	769.5	7.5	773	16	0.5	0.2
NS44_18	1.856	0.026	0.1808	0.002	0.23844	0.07477	0.00094	124	53.6	26.8	1063.6	9.2	1070.9	14	1050	25	-2.0	-0.7
NS44_19	1.76	0.029	0.1746	0.0031	0.72733	0.07359	0.00084	549	182.9	85.4	1029.6	11	1037	17	1027	24	-1.0	-0.7
NS44_20	1.634	0.023	0.1648	0.0018	0.25146	0.07207	0.00089	103.4	46.5	21.33	983	8.9	983.2	10	978	25	-0.5	0.0
NS44_21	0.935	0.017	0.1076	0.0015	0.5049	0.06334	0.00094	337	132.5	33.38	670.4	8.4	658.4	9	710	34	7.3	1.8
NS44_22	1.863	0.026	0.1817	0.0021	0.34868	0.07426	0.00084	105.3	99.4	50.4	1066.6	9	1075.7	11	1038	23	-3.6	-0.9
NS44_23	12.45	0.16	0.5046	0.0072	0.87312	0.1784	0.001	276	326	331	2637	12	2632	31	2636.9	9.3	0.2	0.2
NS44_24	2.023	0.037	0.1903	0.0025	0.23967	0.0775	0.0014	46.8	33.31	17.35	1123	42	1122	43	1117	36	-0.4	0.1
NS44_25	1.253	0.014	0.1373	0.0015	0.52803	0.06617	0.00054	333.4	146.9	56.3	823.8	6.4	829.4	8.7	804	17	-3.2	-0.7
NS44_26	0.874	0.011	0.10318	0.0012	0.58208	0.06142	0.00054	435	170.9	41.7	637	5.9	632.9	7.2	648	19	2.3	0.6
NS44_27	5.244	0.054	0.3323	0.0035	0.6456	0.11478	0.00071	221.5	336	284.6	1859.7	8.5	1849	47	1873	44	1.3	0.6
NS44_28	1.282	0.015	0.1317	0.0015	0.47215	0.07079	0.00064	438	158.5	59.73	837.3	6.7	797.2	8.4	945	49	15.6	4.8
NS44_29	1.162	0.023	0.1277	0.0019	0.29531	0.0666	0.0013	104	28.1	9.13	781.4	44	774.3	44	814	42	4.5	0.9
NS44_30	1.801	0.022	0.1764	0.002	0.37488	0.07397	0.00071	153.2	57.68	29.39	1044.4	7.9	1047.8	14	1037	29	-1.0	-0.3
NS44_31	1.586	0.03	0.1595	0.003	0.76877	0.0728	0.00087	579	316.9	127.9	963	42	953	47	1003	24	5.0	1.0
NS44_32	0.998	0.016	0.1144	0.0015	0.42296	0.06348	0.00081	218.4	50.23	16.64	702.2	8.1	698.2	8.4	712	28	1.9	0.6
NS44_33	0.938	0.018	0.11058	0.0013	0.27585	0.0616	0.0011	73.59	69.67	22.22	670.9	9.4	675.9	7.8	629	39	-7.5	-0.7
NS44_34	0.861	0.012	0.09945	0.0012	0.2027	0.06276	0.00082	165.5	65.83	16.91	629.9	6.5	611.1	6.8	687	28	11.0	3.0
NS44_35	1.168	0.014	0.1128	0.0014	0.67893	0.07518	0.00058	1264	325	82.8	784.9	6.4	688.8	7.9	1067	15	35.4	12.2
NS44_36	1.955	0.031	0.1857	0.0022	0.17946	0.0764	0.0011	61.5	28.57	14.81	1097.9	44	1097.5	42	1094	29	-0.3	0.0
NS44_37	5.292	0.054	0.3356	0.0037	0.57598	0.1141	0.00073	388.1	381.3	314.1	1866.7	8.7	1865	48	1866	42	0.1	0.1
NS44_38	1.233	0.021	0.1352	0.002	0.30559	0.0661	0.0011	228.4	176.1	72.5	816.4	40	817.1	44	804	36	-2.0	-0.1
NS44_39	0.925	0.022	0.0974	0.0022	0.69421	0.0693	0.0011	568	563	74.8	664	11	599	13	899	34	33.4	9.8
NS44_40	0.978	0.018	0.1147	0.0014	0.31568	0.06186	0.00099	79.6	68.8	22.42	693.3	9	699.7	8.3	650	35	-7.6	-0.9
NS44_41	1.044	0.015	0.1204	0.0014	0.44884	0.06267	0.00072	469.7	295.6	102	725.1	7.3	733	8.3	690	24	-6.2	-1.1
NS44_42	2.395	0.027	0.2143	0.0024	0.5578	0.08098	0.00062	275.6	154.3	90.8	1240.1	8	1251.5	13	1217	15	-2.8	-0.9
NS44_43	0.98	0.018	0.1143	0.0021	0.70771	0.06236	0.00076	1081	336	102.9	692.8	9.2	698	12	681	26	-2.5	-0.8
NS44_44	0.9064	0.01	0.10701	0.0011	0.38792	0.06138	0.00057	349	225.1	69.7	654.5	5.6	655.2	6.7	643	20	-1.9	-0.1
NS44_45	1.873	0.028	0.1824	0.0022	0.13201	0.0742	0.0011	169	87.7	46.3	1070.4	10	1080	12	1036	31	-4.2	-0.9
NS44_46	1.116	0.017	0.12641	0.0014	0.24785	0.06383	0.00086	189	82.9	29.7	759.8	8.2	767.3	7.8	724	29	-6.0	-1.0
NS44_47	1.022	0.014	0.11754	0.0013	0.31865	0.06326	0.00072	182.6	101.2	31.02	713.8	7.1	716.2	7.6	704	25	-1.7	-0.3
NS44_48	1.12	0.013	0.1254	0.0015	0.65519	0.06486	0.00051	516	183.2	63.2	762.2	6.3	761.4	8.5	763	16	0.2	0.1
NS44_49	1.202	0.014	0.1335	0.0015	0.59608	0.06534	0.00053	463.2	87.3	32.13	890.6	6.5	897.5	8.8	784	47	-3.4	-0.9
NS44_50	1.178	0.017	0.1315	0.0018	0.65608	0.06507	0.0006	723	51.88	19.24	789.4	7.8	796	10	776	24	-2.6	-0.8
NS44_51	0.8927	0.011	0.10669	0.0012	0.17477	0.06086	0.00065	345.6	125.1	36.91	647.9	6.1	653.4	7.1	622	23	-5.0	-0.8
NS44_52	6.187	0.066	0.3709	0.0042	0.63403	0.12103	0.00083	189.8	130	121.6	2004	9.3	2033	20	1968	42	-3.3	-1.6
NS44_53	1.431	0.017	0.147	0.0016	0.40756	0.07037	0.00069	259	113.5	22.3	900.9	7.1	883.9	9.2	931	21	5.1	1.9
NS44_54	0.9754	0.011	0.11238	0.0013	0.54614	0.06306	0.00053	942	94.9	28.16	690.7	5.6	686.4	7.8	705	18	2.6	0.6
NS44_55	1.052	0.013	0.1214	0.0016	0.65376	0.06297	0.00054	507	200.8	66.1	728.7	6.7	738.4	9	701	19	-5.3	-1.3
NS44_56	0.9012	0.011	0.10697	0.0011	0.47948	0.0612	0.00053	532	171.2	50.5	651.7	5.8	655.1	6.7	641	19	-2.2	-0.5

NS44_57	1.744	0.032	0.1746	0.0022	0.39722	0.0725	0.0012	63.71	50.18	23.69	1023	12	1037.2	12	986	34	-5.2	-1.4
NS44_58	0.992	0.012	0.11408	0.0013	0.57937	0.06336	0.00054	713	93.3	28.22	699	6	696.3	7.5	714	18	2.5	0.4
NS44_59	1.654	0.019	0.1661	0.0018	0.48103	0.07229	0.00063	249.5	166.3	77.1	990.1	7.3	990.3	10	986	18	-0.4	0.0
NS44_60	13.65	0.15	0.529	0.0064	0.60622	0.1866	0.0015	83	115.5	156.4	2724.6	44	2736	27	2709	43	-1.0	-0.4
NS44_61	1.396	0.018	0.072	0.0013	0.44037	0.1418	0.002	1650	3610	444	885.7	7.6	448.1	7.8	2234	26	79.9	49.4
NS44_62	1.459	0.021	0.07329	0.00092	0.15999	0.1452	0.0021	2095	2660	478.3	913.1	8.8	455.8	5.5	2276	25	80.0	50.1
NS44_63	1.996	0.033	0.1917	0.0028	0.67903	0.07601	0.00081	524	117.5	56.1	4443	44	4430	45	4090	22	-3.7	-1.5
NS44_64	1.766	0.025	0.1739	0.002	0.2395	0.07359	0.00094	101.6	50.63	24.62	1030.8	9.1	1034	11	1017	26	-1.7	-0.3
NS44_65	12.96	0.17	0.5259	0.0072	0.6572	0.1804	0.0016	220.4	125.4	159.9	2675	42	2722	30	2652	44	-2.6	-1.8
NS44_66	1.05	0.017	0.1187	0.0016	0.51936	0.06387	0.0008	537	252.6	87.9	728.2	8.4	722.9	9	731	27	1.1	0.7
NS44_67	11.11	0.21	0.46	0.011	0.81224	0.1751	0.0022	835	999	805	2531	18	2437	48	2604	21	6.4	3.7
NS44_68	1.691	0.018	0.1697	0.0019	0.63582	0.0722	0.00049	590	226.2	108.7	1004.1	6.9	1010.2	11	986	14	-2.5	-0.6
NS44_69	1.599	0.022	0.1628	0.0019	0.40085	0.07118	0.00075	184.8	140.8	66	967.9	8.5	972.2	44	952	22	-2.1	-0.4
NS44_70	1.209	0.016	0.1336	0.0015	0.4888	0.06562	0.00065	259.9	266.3	99.9	803.3	7.3	808.4	8.5	784	21	-3.1	-0.6
NS44_71	4.068	0.018	0.0853	0.0019	-0.29507	0.0944	0.0028	741	514	433	735.6	8.8	527	11	1439	56	63.4	28.4
NS44_72	0.897	0.017	0.1063	0.0017	0.60462	0.06168	0.00088	470	91.4	27.89	649	9.2	651.2	10	652	31	0.1	-0.3
NS44_73	1.638	0.02	0.1657	0.0019	0.54915	0.07152	0.00064	361.3	278.2	132	983.6	7.7	988.4	10	969	18	-2.0	-0.5
NS44_74	1.158	0.013	0.1296	0.0015	0.53701	0.06464	0.00054	423	218.2	81	780.3	6.3	785.6	8.3	757	47	-3.8	-0.7
NS44_75	4.322	0.023	0.0976	0.0015	-0.04449	0.0994	0.0024	1238	906	496	852.7	40	599.9	8.6	4572	39	64.8	29.6
NS44_76	0.971	0.025	0.1136	0.0016	0.10952	0.0622	0.0016	27.42	22.78	7.37	686	13	693.1	9.4	633	58	-9.5	-1.0
NS44_77	1.844	0.031	0.1808	0.0024	0.23988	0.0737	0.0011	67.2	32	16.09	1058	11	1071	13	1025	32	-4.5	-1.2
NS44_78	1.922	0.03	0.1857	0.0023	0.29062	0.075	0.0011	54.2	81.5	42.86	1085.7	44	1097.8	42	1050	29	-4.6	-1.1
NS44_79	1.64	0.02	0.1661	0.0019	0.50892	0.07131	0.00067	252	306	140.3	984.5	7.8	990.8	44	957	49	-3.5	-0.6
NS44_80	1.94	0.026	0.1881	0.0021	0.42944	0.07464	0.0008	113.8	104.4	56.2	1093.1	8.9	1110.8	42	1050	22	-5.8	-1.6
NS44_81	1.066	0.014	0.12241	0.0013	0.34992	0.06311	0.00068	188.3	79.95	28.53	736.5	6.7	744.3	7.6	700	23	-6.3	-1.1
NS44_82	12.66	0.18	0.513	0.0072	0.76956	0.1795	0.0015	460	141.3	181.5	2653	44	2668	34	2646	44	-0.8	-0.6
NS44_83	1.829	0.02	0.1788	0.0019	0.37557	0.074	0.00061	238.5	99.6	49.8	1055.3	7	1060	10	1036	16	-2.3	-0.4
NS44_84	6.154	0.061	0.366	0.0038	0.62168	0.1215	0.00073	177.2	119.9	118.8	1996.7	8.7	2010	18	1976	11	-1.7	-0.7
NS44_85	0.696	0.014	0.0658	0.0012	0.44423	0.0775	0.0015	227	191.4	47.03	536.3	8.4	410.6	7.3	1117	39	63.2	23.4
NS44_86	0.9405	0.012	0.11125	0.0012	0.24333	0.06117	0.00066	275.8	102.5	32.46	672.3	6.1	679.9	6.8	634	23	-7.2	-1.1
NS44_87	4.01	0.29	0.1253	0.0027	0.90456	0.223	0.0143	546	350	433	1570	67	760	15	2860	120	73.4	51.6
NS44_88	15.48	0.15	0.5589	0.006	0.49956	0.2	0.0014	59.4	42.9	60.7	2844.7	9.1	2862	25	2824	11	-1.3	-0.6
NS44_89	1.704	0.025	0.1717	0.0019	0.16546	0.07169	0.00099	67.4	50.92	24.33	1008.4	9.6	1021	11	967	29	-5.6	-1.2
NS44_90	1.1721	0.013	0.13014	0.0014	0.54322	0.06505	0.00047	360.3	196.3	72.7	787.4	5.9	788.5	7.9	771	15	-2.3	-0.1
NS44_91	1.615	0.017	0.16432	0.0016	0.48512	0.07097	0.0005	323.6	177.3	83.5	975.3	6.6	980.6	9.1	951	14	-3.1	-0.5
NS44_92	4.265	0.03	0.0717	0.0017	-0.49776	0.1327	0.0046	653	859	462	825	13	446.2	10	2035	69	78.1	45.9
NS44_93	1.687	0.022	0.1669	0.002	0.58325	0.07317	0.00066	263	121.5	46.8	1003.4	8.2	995.4	44	1011	49	4.5	0.8
NS44_94	2.093	0.028	0.1939	0.0022	0.46738	0.07803	0.00082	106.3	41.7	22.48	1145.2	9.1	1142.2	12	1139	21	-0.3	0.3
NS44_95	1.647	0.023	0.1659	0.002	0.46851	0.07195	0.00078	242.6	76.6	34.11	987.1	8.8	989.2	11	982	22	-0.7	-0.2
NS44_96	0.817	0.013	0.09905	0.0011	0.15679	0.05978	0.00086	176.1	102.1	28.2	605.7	7.2	608.8	6.4	578	32	-5.3	-0.5
NS44_97	1.657	0.019	0.1661	0.0018	0.60728	0.07186	0.00053	436	187	76.6	991.5	7.1	990.5	10	977	15	-1.4	0.1
NS44_98	1.97	0.022	0.1878	0.0019	0.41246	0.07593	0.00066	195.7	56.4	28.5	1104.8	7.8	1109.3	11	1086	18	-2.1	-0.4
NS44_99	11.055	0.12	0.4608	0.0054	0.81554	0.17281	0.00086	888	30.2	43.9	2527.3	9.6	2442	24	2583.2	8.3	5.5	3.4
NS44_100	1.972	0.02	0.1872	0.0019	0.45994	0.07618	0.00055	311.4	117	56.61	1106	6.8	1106	10	1096	14	-0.9	0.0
NS44_101	1.723	0.019	0.1724	0.0018	0.47205	0.07225	0.00056	274.9	204.8	96.8	1016.8	7.1	1025.2	9.7	987	16	-3.9	-0.8
NS44_102	0.953	0.027	0.1125	0.0016	0.19103	0.0617	0.0017	28.48	14.27	4.41	674	14	687	9.2	601	59	-14.3	-1.9
NS44_103	6.022	0.061	0.3589	0.0039	0.69726	0.12116	0.0006	531	29.6	28.2	1977.7	8.9	1976	49	1970.8	8.9	-0.3	0.1
NS44_104	1.696	0.027	0.1702	0.002	0.2952	0.0723	0.0011	75.3	46.3	21.3	1004.2	10	1013.6	11	977	31	-3.7	-0.9
NS44_105	4.902	0.05	0.3065	0.0033	0.49575	0.1153	0.00083	245.1	133.3	106.6	1802.4	8.7	1723	16	1883	13	8.5	4.4
NS44_106	0.874	0.012	0.1046	0.0011	0.21543	0.06067	0.00075	457.1	116.4	32.64	637.7	6.5	641.3	6.6	618	27	-3.8	-0.6
NS44_107	6.805	0.11	0.3717	0.0058	0.59199	0.1326	0.0017	64.5	23.18	15.78	2083	14	2036	28	2124	23	4.1	2.3
NS44_108	2.225	0.033	0.206	0.0029	0.41258	0.0787	0.001	285.5	196	102.1	1188.1	44	1207	45	1158	26	4.2	-1.6

NS44_109	5.303	0.062	0.3321	0.0039	0.64646	0.11573	0.00085	359.2	502	422.6	1868.3	10	1848	19	1890	14	2.2	1.1
NS44_110	2.614	0.024	0.2254	0.0022	0.51427	0.08375	0.00048	284.1	85.5	51.81	1304.3	6.7	1310.1	12	1283	11	-2.1	-0.4
NS44_111	5.47	0.058	0.3433	0.0037	0.68142	0.11516	0.00069	375	302.4	263.8	1894.9	9.1	1903	18	1882	11	-1.1	-0.4
NS44_112	1.68	0.03	0.1667	0.002	0.19019	0.0728	0.0012	74.8	43.31	20.61	1002	11	993.6	11	997	34	0.3	0.8
NS44_113	1.735	0.02	0.1709	0.0019	0.53894	0.07345	0.00063	511.2	220.9	83.1	1021.7	7.5	1016.9	11	1022	17	0.5	0.5
NS44_114	1.617	0.019	0.1643	0.0018	0.56643	0.07142	0.0006	443.2	228.6	90.6	976.1	7.2	980.7	9.9	965	17	-1.6	-0.5
NS44_115	3.708	0.04	0.2789	0.0031	0.52082	0.09663	0.00076	254.1	220.3	158.4	1572.4	8.6	1586	15	1557	15	-1.9	-0.9
NS44_116	1.069	0.02	0.1209	0.0019	0.56085	0.06462	0.00099	402.1	157.6	47	739.2	10	735.4	11	761	31	3.4	0.5
NS44_117	4.108	0.019	0.0995	0.0014	0.0046756	0.0813	0.0017	729	584	141.8	755.9	9.1	611.4	8.5	1193	39	48.8	19.1
NS44_118	11.03	0.16	0.4613	0.0072	0.84149	0.1739	0.0013	849	177.3	88.4	2525	14	2444	32	2594	12	5.8	3.2
NS44_119	12.385	0.12	0.502	0.005	0.67674	0.1773	0.00093	385	625	705	2633.3	8.9	2622	22	2626	8.7	0.2	0.4
NS44_120	1.84	0.02	0.1781	0.0019	0.42651	0.07422	0.00063	370	70.3	35.5	1059.2	7.3	1056.6	10	1043	17	-1.3	0.2
NS44_121	1.213	0.013	0.13324	0.0013	0.30989	0.06577	0.00055	264.8	145.6	55.68	806.5	6.1	806.3	7.4	792	18	-1.8	0.0
NS44_122	2.655	0.043	0.2171	0.0028	0.52899	0.0887	0.0011	82.4	32.1	15.54	1314	12	1266	15	1388	24	8.8	3.7
NS44_123	1.832	0.026	0.1769	0.002	0.25665	0.07487	0.00098	80.4	46.8	23.34	1054.8	9.4	1050	11	1054	26	0.4	0.5
NS44_124	4.142	0.023	0.04959	0.0017	0.68463	0.0753	0.001	831	334	74.5	758	11	648.5	9.7	1074	27	39.4	14.4
NS44_125	1.623	0.02	0.1599	0.0018	0.52551	0.07324	0.00065	392.7	447.8	187.9	978.4	7.6	955.8	10	1015	18	5.8	2.3
NS44_126	1.69	0.028	0.1548	0.002	0.58189	0.07875	0.00091	845	480	129.1	1003.3	11	927.4	11	1162	23	20.2	7.6
NS44_127	4.12	0.016	0.1035	0.0018	0.61683	0.0787	0.0011	1014	947	244.8	762.6	7.8	634.6	10	1159	26	45.2	16.8
NS44_128	1.46	0.16	0.0976	0.0016	0.49557	0.106	0.01	304.3	184.9	73.9	860	57	600.2	9.3	1450	160	58.6	30.2
NS44_129	2.007	0.025	0.1904	0.0021	0.40339	0.07589	0.00072	143.5	56.6	30.78	1116.9	8.7	1123.4	11	1083	19	-3.7	-0.6
NS44_130	1.719	0.023	0.1719	0.0019	0.42467	0.07223	0.00076	121.5	20.67	10.49	1013.8	8.7	1022.5	11	984	21	-3.9	-0.9
NS44_131	1.677	0.018	0.1673	0.0018	0.5891	0.07217	0.00051	418.3	343.8	166.4	998.9	7	997.3	9.7	985	14	-1.2	0.2
NS44_132	4.244	0.024	0.11335	0.0019	0.30053	0.0785	0.0021	865	1040	185	819	11	692.6	11	1150	51	39.8	15.4
NS44_133	1.097	0.013	0.1221	0.0014	0.53291	0.06475	0.00057	375	202.9	71.2	751.4	6.5	742.3	8.2	763	19	2.7	1.2
NS44_134	4.511	0.053	0.3026	0.0033	0.62946	0.10713	0.00076	139.4	126.5	106.7	1730.9	9.9	1704	16	1749	13	2.6	1.6
NS44_135	4.623	0.069	0.308	0.0043	0.40367	0.1087	0.0014	165.2	155.5	106.9	1752	12	1730	21	1777	23	2.6	1.3
NS44_136	1.083	0.013	0.12267	0.0013	0.18892	0.06363	0.00061	263.3	93.9	32.74	744.4	6.4	745.8	7.3	720	20	-3.6	-0.2
NS44_137	1.908	0.029	0.1847	0.0023	0.25056	0.0742	0.0011	111.9	49.93	27.56	1082.6	10	1092.5	12	1044	27	-4.6	-0.9
NS44_138	2.969	0.029	0.2437	0.0024	0.54104	0.08779	0.00055	306.6	88.3	60.4	1398.8	7.5	1405.6	13	1374	12	-2.3	-0.5
NS44_139	1.611	0.017	0.1645	0.0017	0.51938	0.07067	0.00053	308	105.3	48.5	974.5	6.8	981.7	9.3	945	15	-3.9	-0.7

